FLASH

Flexible Laser-Based Manufacturing

Precision Surface Metrology Workshop

Dr Shan Lou

Reader in Precision Metrology

Future Metrology Hub, Centre for Precision Technologies, University of Huddersfield

04/09/2024

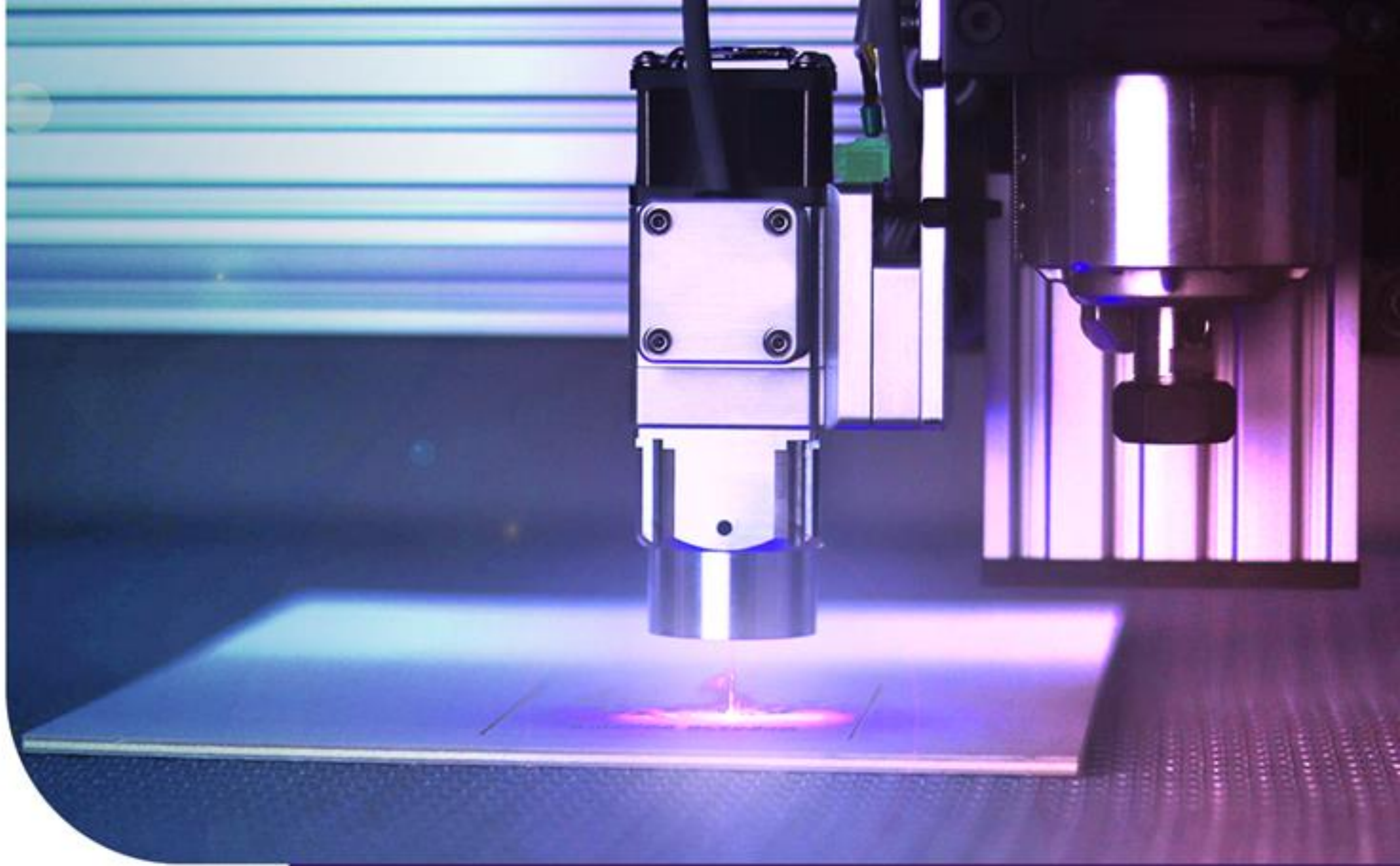

Co-funded by the European Union

Funded by the European Union. Views and opinions expressed are however those of the author(s) only and do not necessarily reflect those of the European Union or the European Health and Digital Executive Agency. Neither the European Union nor the granting authority can be held responsible for them. **HORIZON-CL4-2023-TWIN-TRANSITION-01-02.**

INDEX

Co-funded by the European Union

Surface Metrology

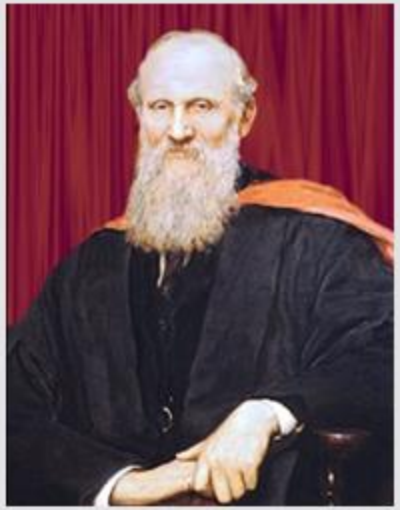

Lord Kelvin (1824-1907)

“When you can measure what are you speaking about, and express it in numbers, you know something about it; but when you cannot express it in numbers, your knowledge is of a meagre and unsatisfactory kind”

"If you can't measure it, you can't make it"

Jane Jiang, David Whitehouse et al. (2007)

“the science of measuring small-scale geometrical features on surfaces: the topography of the surface”

FLASH

Co-funded by the European Union

1. Historical Development

- First Period: Before 1920s
- Second Period: 1920s - 1980s
- Third Period: 1990s - Present

Co-funded by
the European Union

First period: before 1920s

- 2500BC Surface measurement in ancient Egypt


Great Pyramid of Giza and its casting stone

- 15c L. da Vinci: friction is independent of the “area of contact”


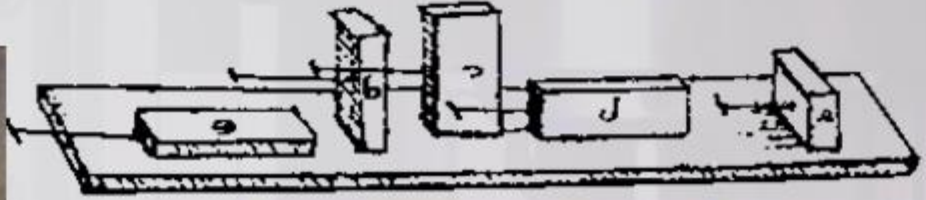
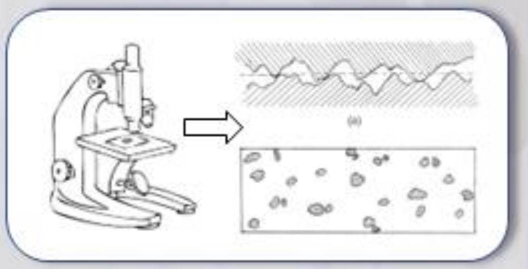

- 16-17c Royal Navy of England: accurate cannon


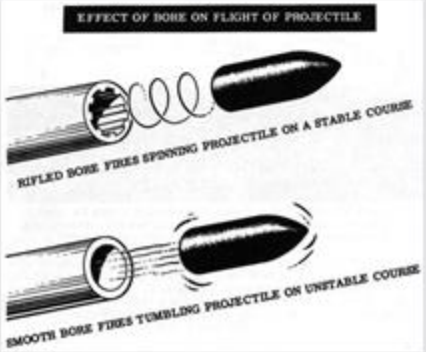

Rifling

- 1668 Isaac Newton: reflecting telescope



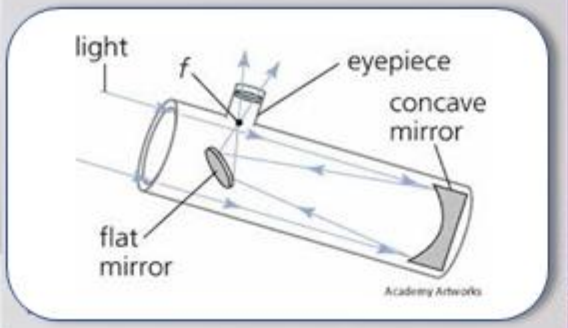

Second period: 1920s - 1980s

- 1920s~1930s: Recognition of the importance of surface texture

Surface: the smoother, the better?

BENTLEY

24 Hours of Le Mans

Second period: early surface metrology concepts

- 1940-1950 Establishment of surface metrology

  Surface texture: roughness, waviness and form error

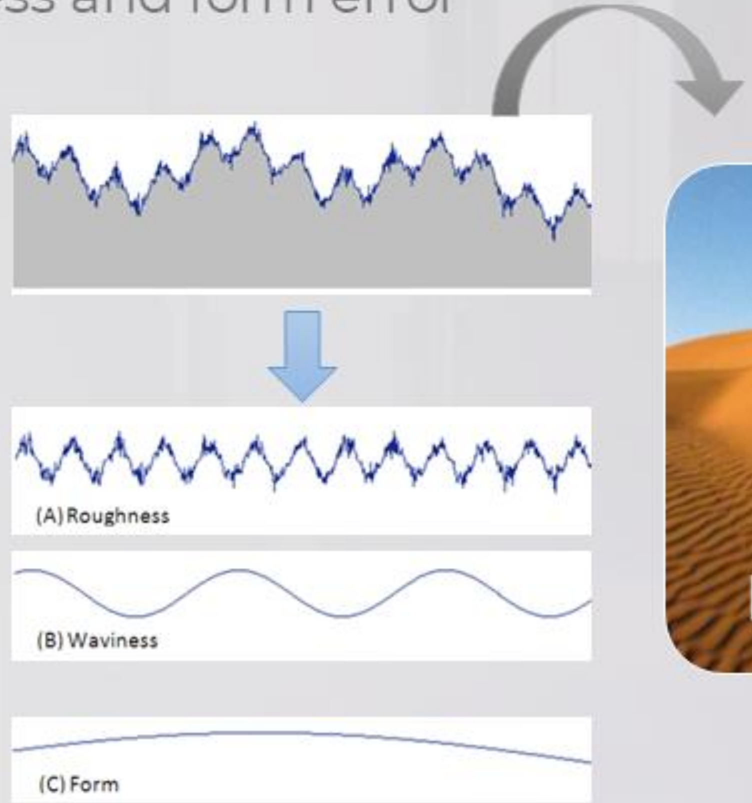

Reason, R. E. et al. 1944 Report on the measurement of surface finish by stylus methods. Leicester, UK: Rank Taylor Hobson.

Perthen, J. 1949 Prufen und messen der oberflachengeatalt. Munchen, Germany: Carl Hanser Verlag.

Schorsch, H. 1958 Gutebestummung an technischen oberfiachen, wissenschagtliche, Verlagsgesellschaft, Stuttgart.

Co-funded by the European Union

Second period: early instruments

- Early instruments

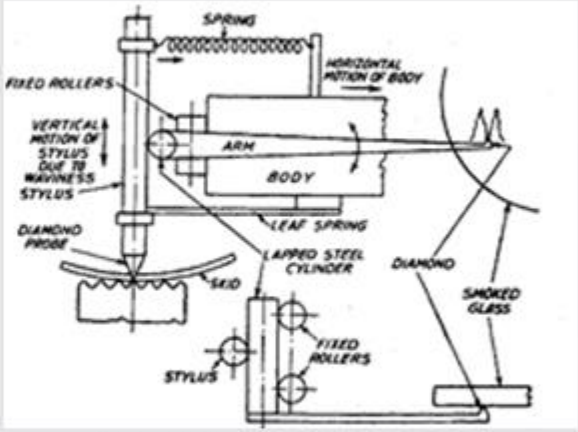

1919 NPL: W. Tomlinson

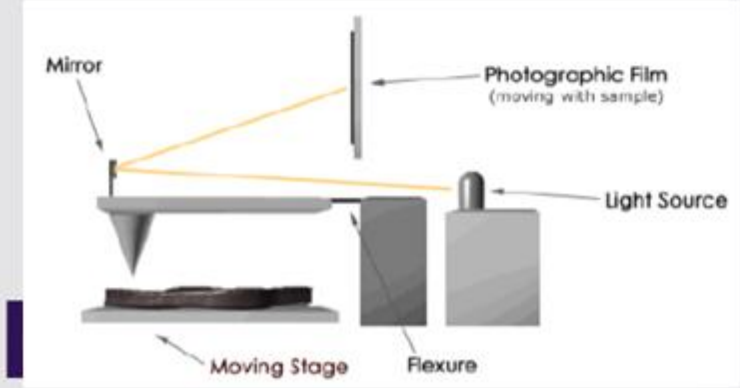

1929 Carl Zeiss: G. Schmalz

- First commercial instrument

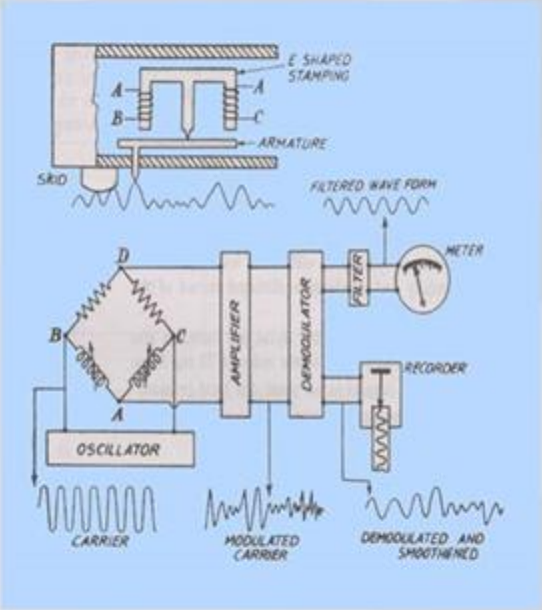

1941 Taylor Hobson: Talysurf 1 invented by Richard Reason

Co-funded by
the European Union

Second period: surface texture characterisation

Measurement → Filtration → Parameterisation

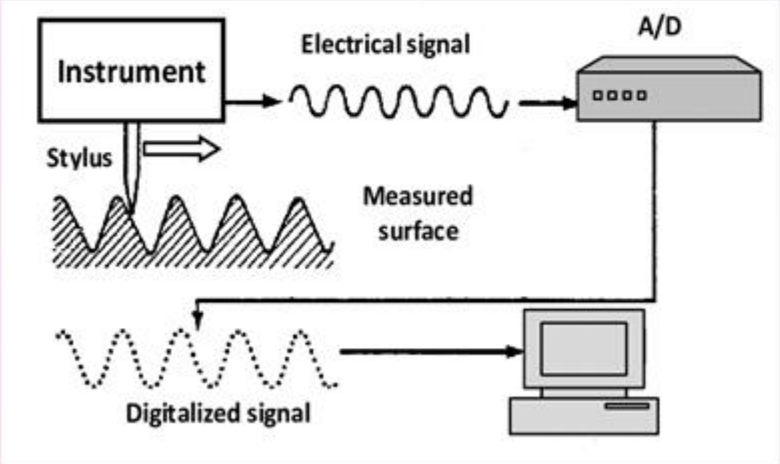

(src: Daniel Schlegel et al. 2011)

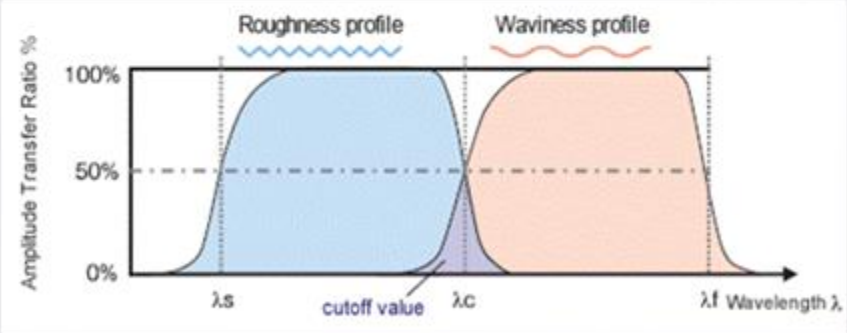

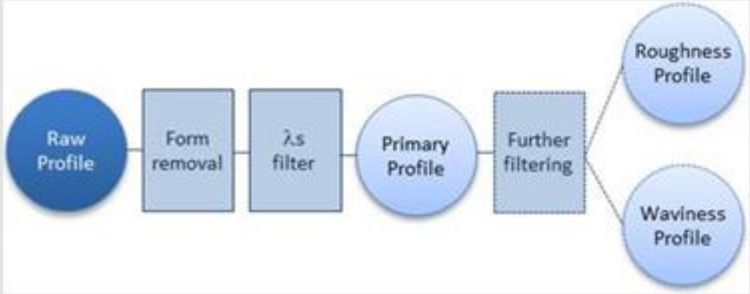

(src: Digital Surf)

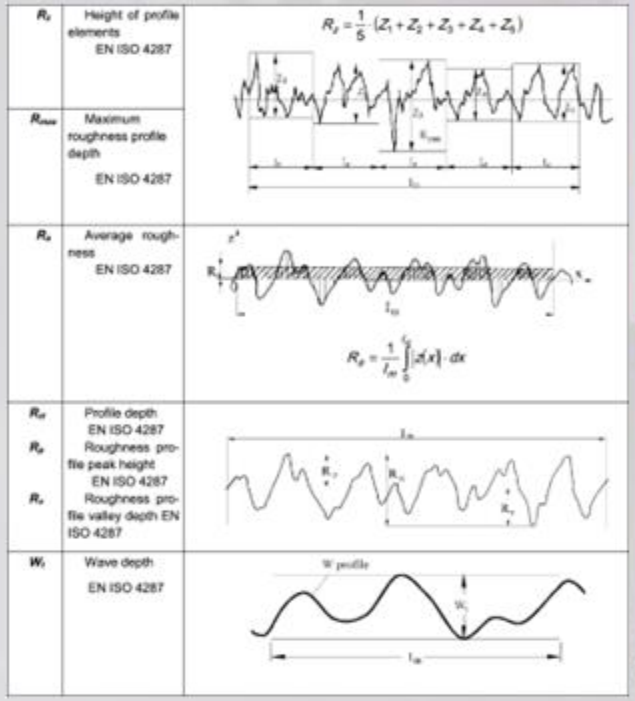

(src: ISO 4287)

FLASH

Second period: two early competing filtration system

- Mean-line system (M-system)

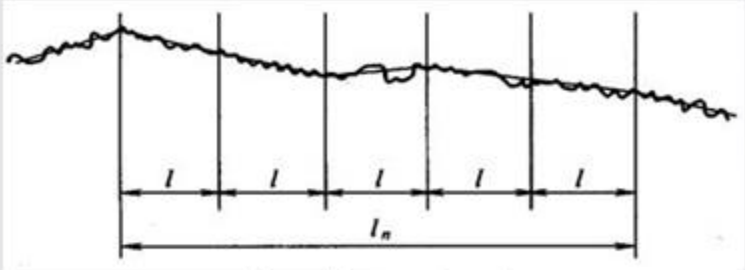

Graphic method

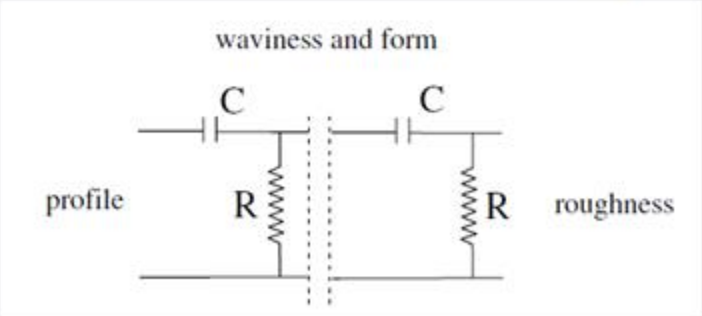

Reason: 2RC Electrical Circuit

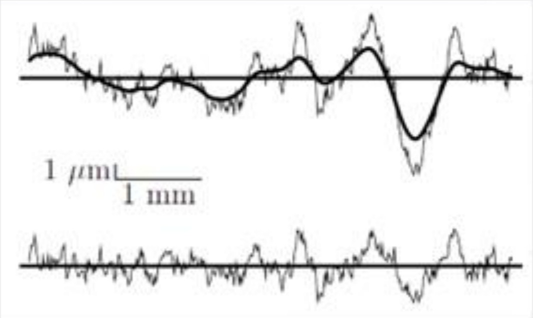

1960s Whitehouse & Reason: digital & phase corrected

- Envelope system (E-system)

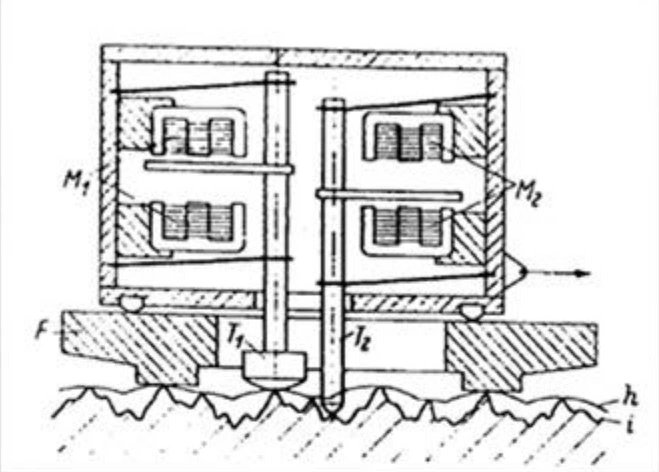

Von Weingraber: envelope method

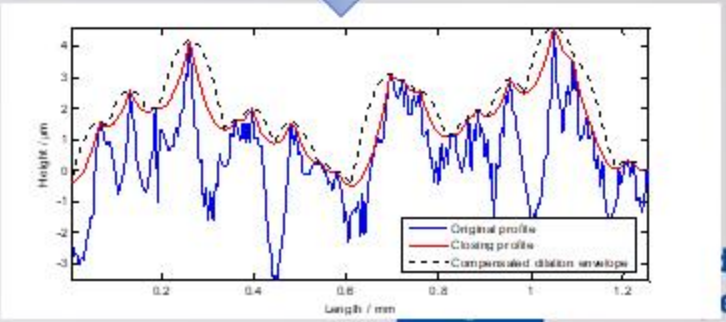

1974 Shumugan & Radhakrishnan: digital implementation of the E-filter

FLASH

Third period: 1990s - present

- The nature of surface: 3D, from profile to area

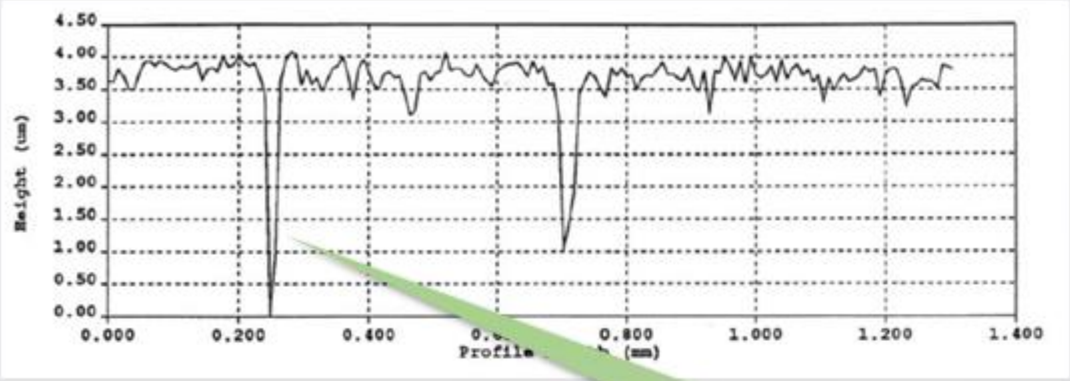

Pit or trough?

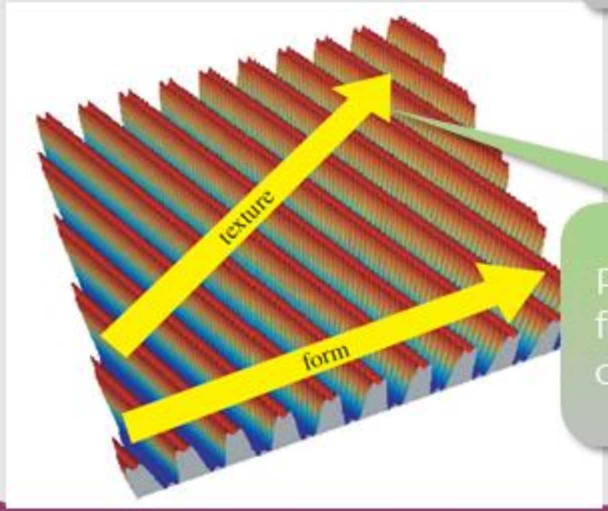

Profile texture and form had two different coordinate systems

- 1990s Europe framework 4-5: ISO 25178 series

  Part 1: Indication of surface texture

  Part 2: Terms, definitions and surface texture parameters

  Part 6xx: Metrological characteristics for areal-topography measuring methods

  Part 700: Calibration of surface texture measuring instruments

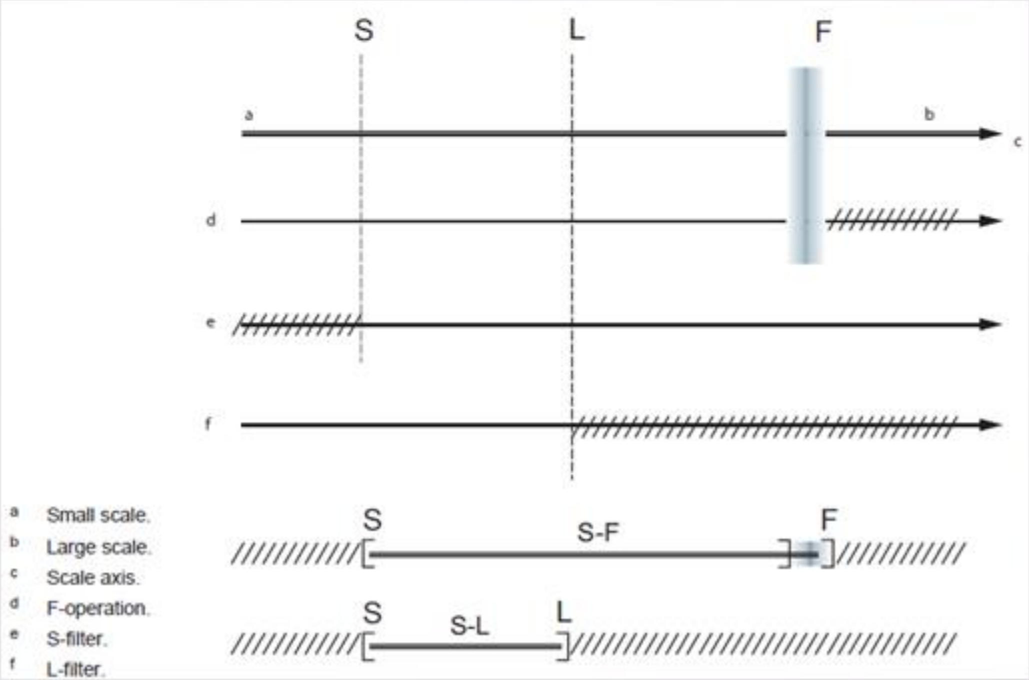

2. Modern Surface Metrology

- Surface measurement instruments
- Surface texture characterisation

Flexible Laser-Based Manufacturing

Co-funded by the European Union

2. Modern Surface Metrology

- Surface measurement instruments

Co-funded by the European Union

Popular instruments used in surface metrology

- **1990s~2000s Versatile technologies**

  Phase-shifting interferometry
  White-light interferometry
  Confocal microscopy
  Focus variation microscopy

  Scanning electron microscopy
  Atomic force microscopy

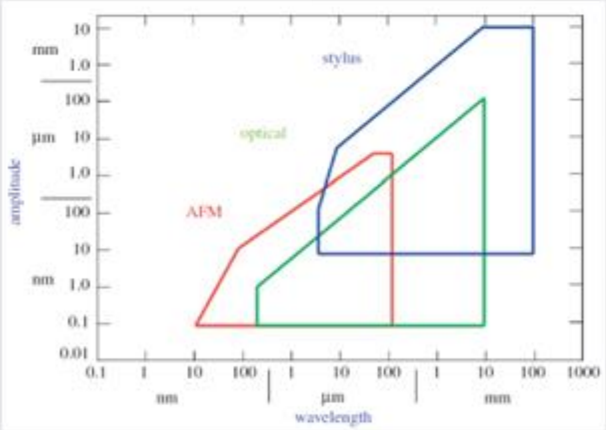

Tactile profilometry (Taylor Hobson GPI)

White light interferometry (Zygo NewView™)

Optical coherence tomography (OptoRes)

Focus Variation Microscope (Bruker Alicona)

Confocal microscope (Zeiss Smartproof)

FLASH

Surface measurement instruments

- **1996 Form Talysurf PGI: Phase grating interferometry**

  Vertical range: 24 mm

  Vertical resolution: 0.8 nm

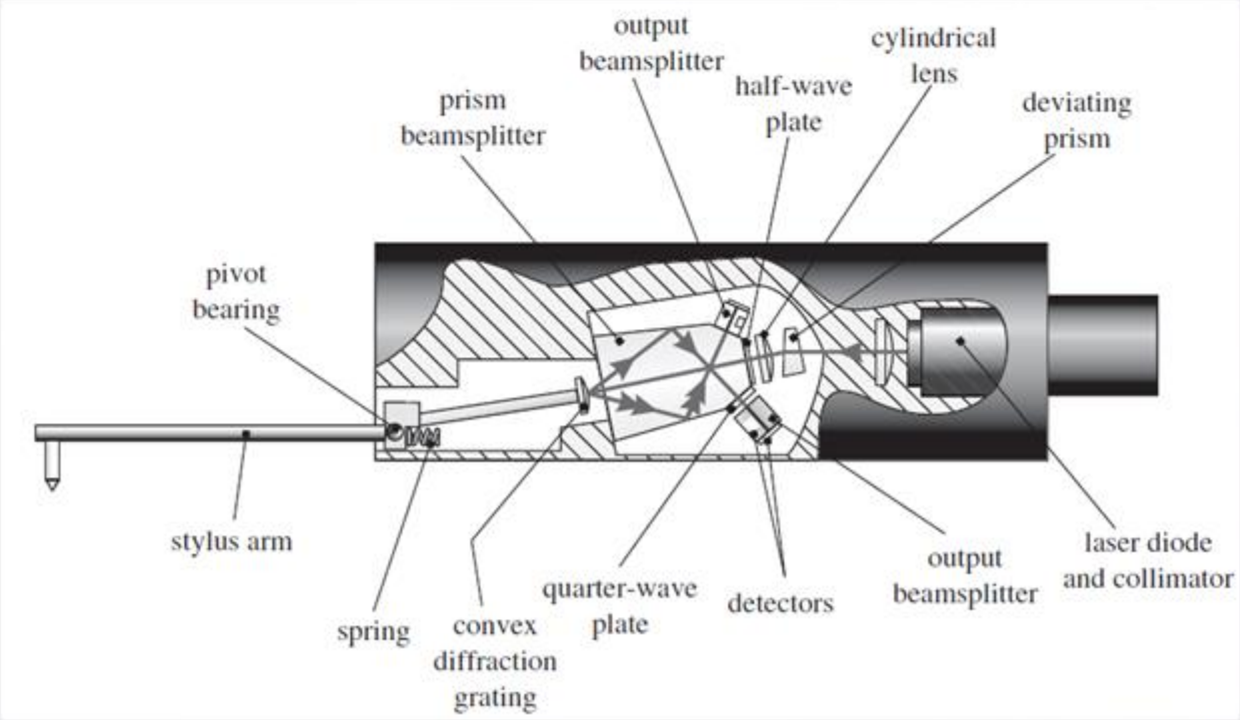

Co-funded by the European Union

Surface measurement instruments

- **Interferometry**

Interference pattern can be obtained by superposing two split waves

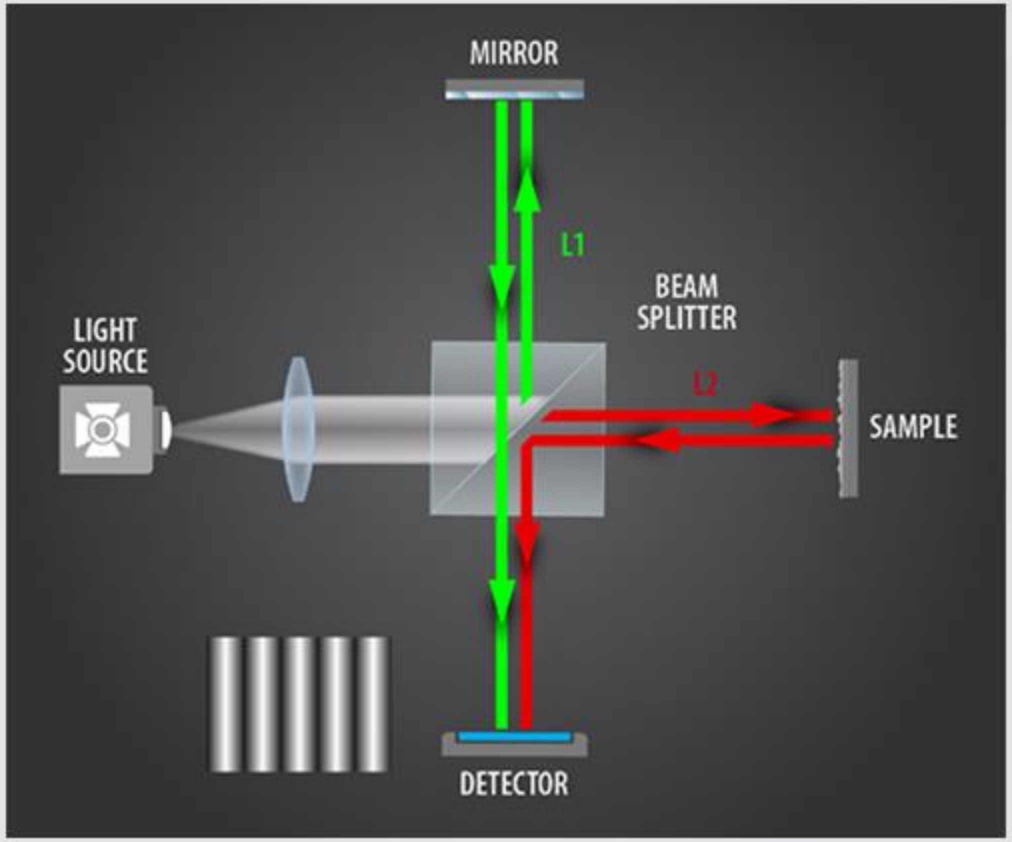

(src.: Sensofar)

$$I = (E_1 + E_2)^2$$

$$I = I_1 + I_2 + 2\sqrt{I_1 I_2}\cos(\Delta\phi)$$

I_1: Intensity of the first wave
I_2: Intensity of the second wave
$\Delta\phi$: Phase difference between the two waves

$$I = (E_1 + E_2)^2 \qquad I = {E_1}^2$$

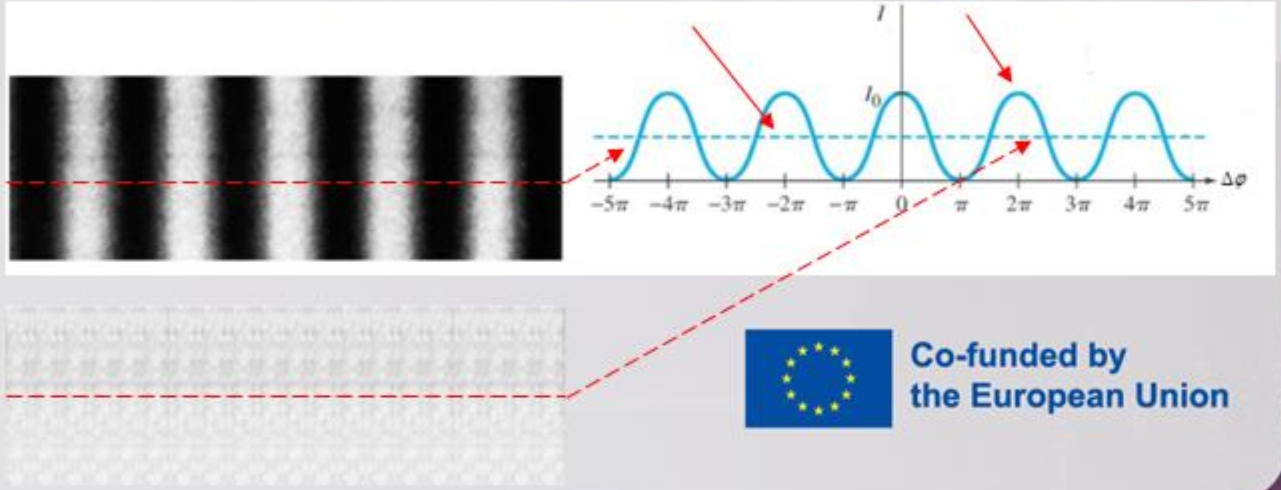

Co-funded by the European Union

Surface measurement instruments

- Confocal microscopy

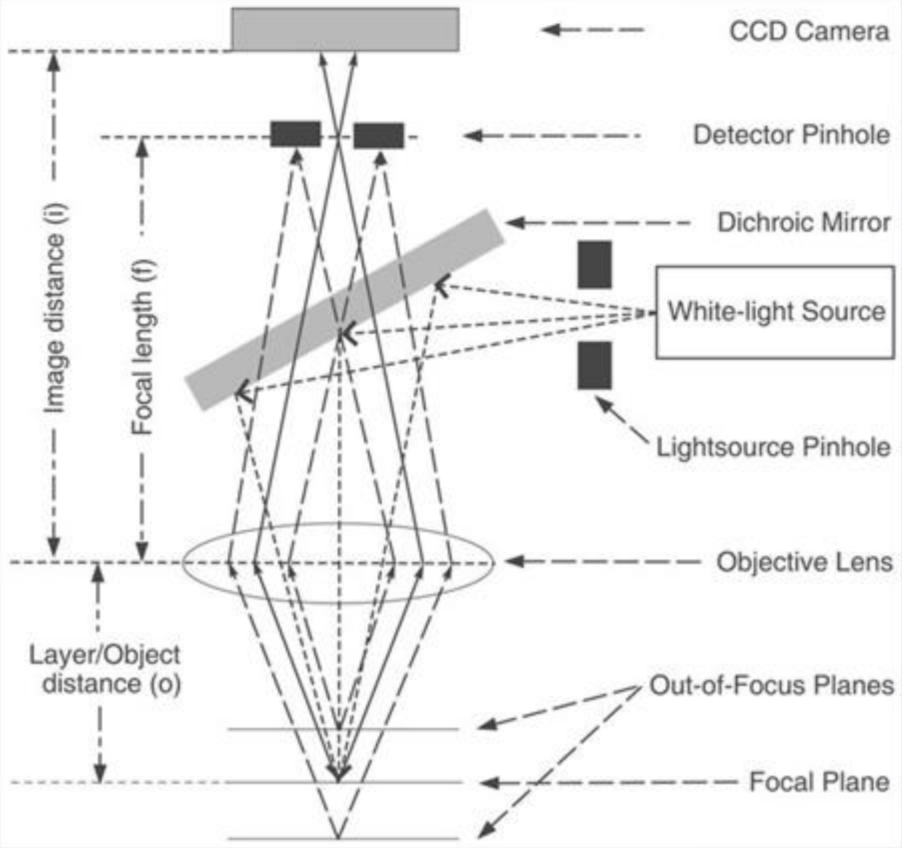

(Ref: Balasubramanian, et al.,2007. Journal of Electronic Imaging, 16.)

- Upgrade: chromatic, dual spinning disks

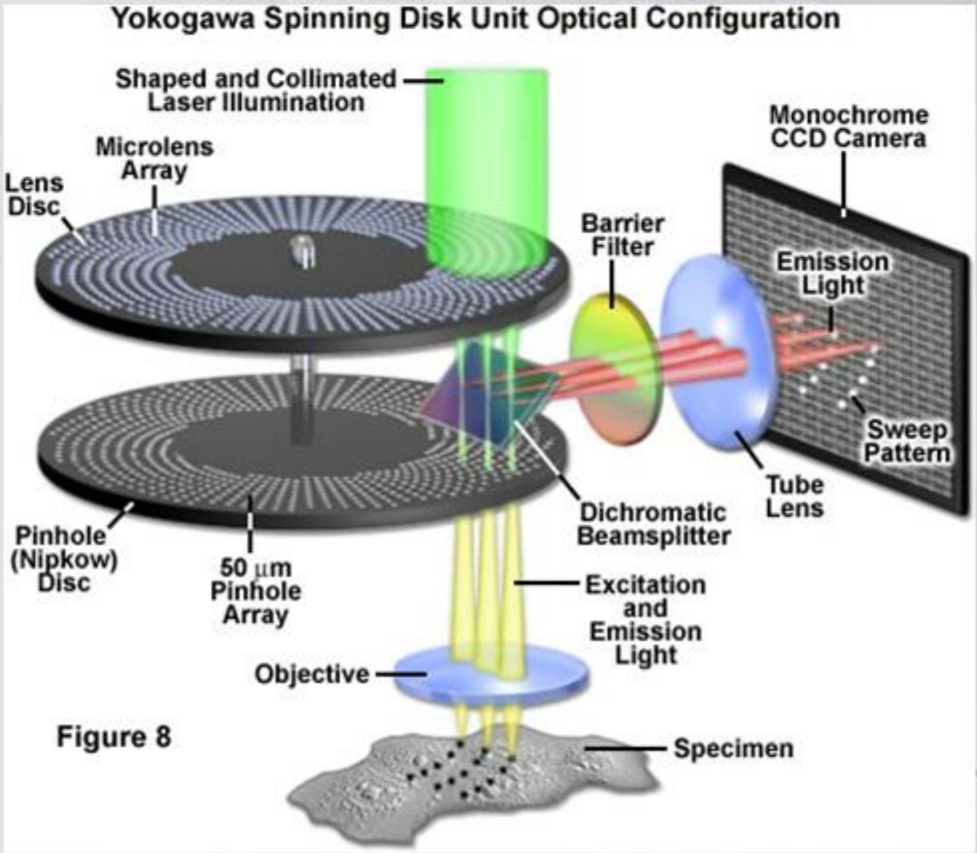

(Ref: zeiss-campus.magnet.fsu.edu)

Union

Surface measurement instruments

- Focus variation microscopy

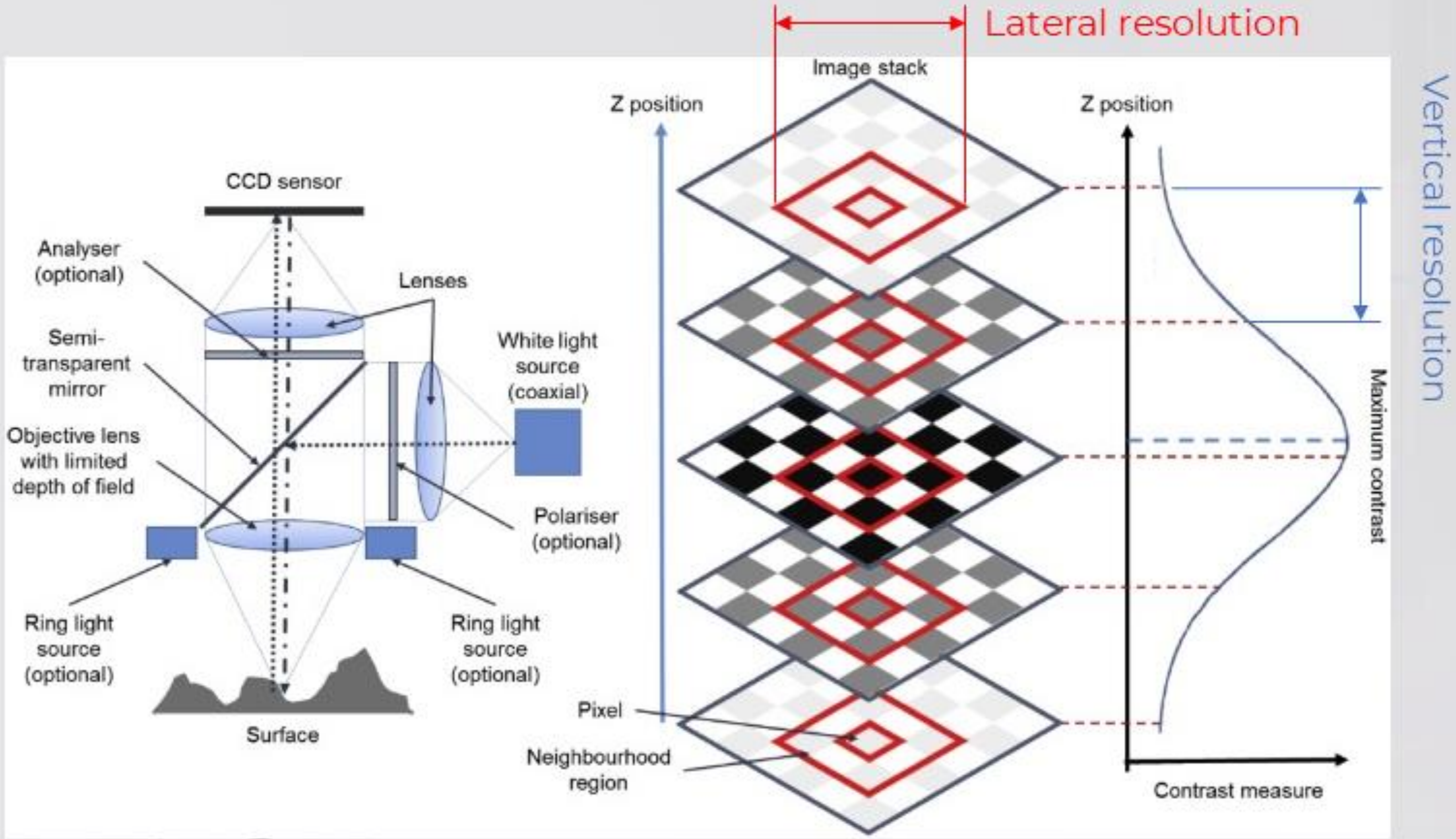

(Ref: Newton, L., et al. *Additive Manufacturing*, *25*)

- Compare to Confocal

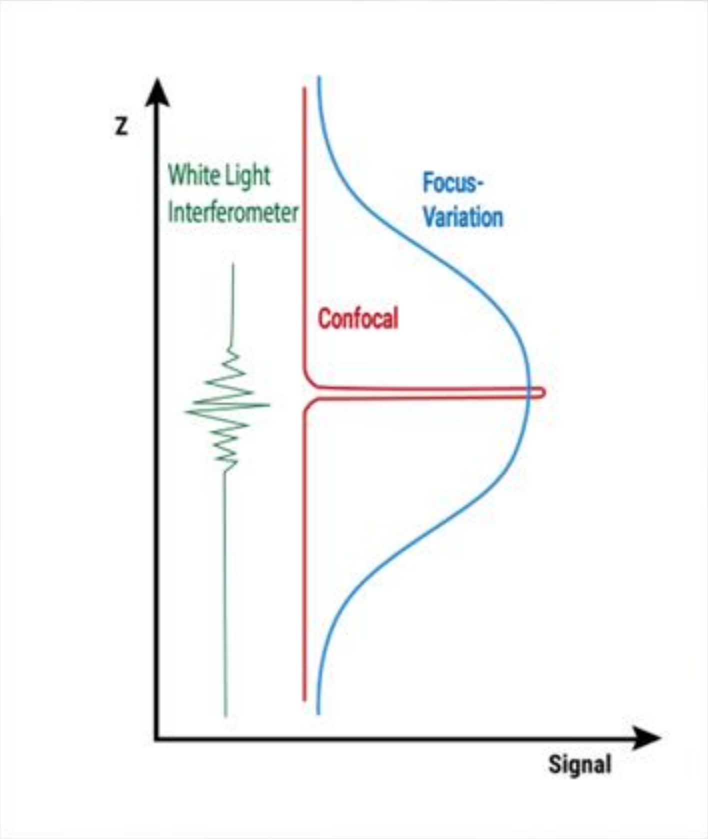

(Ref: Bruker Alicona.)

Surface measurement instruments

- Optical coherence tomography

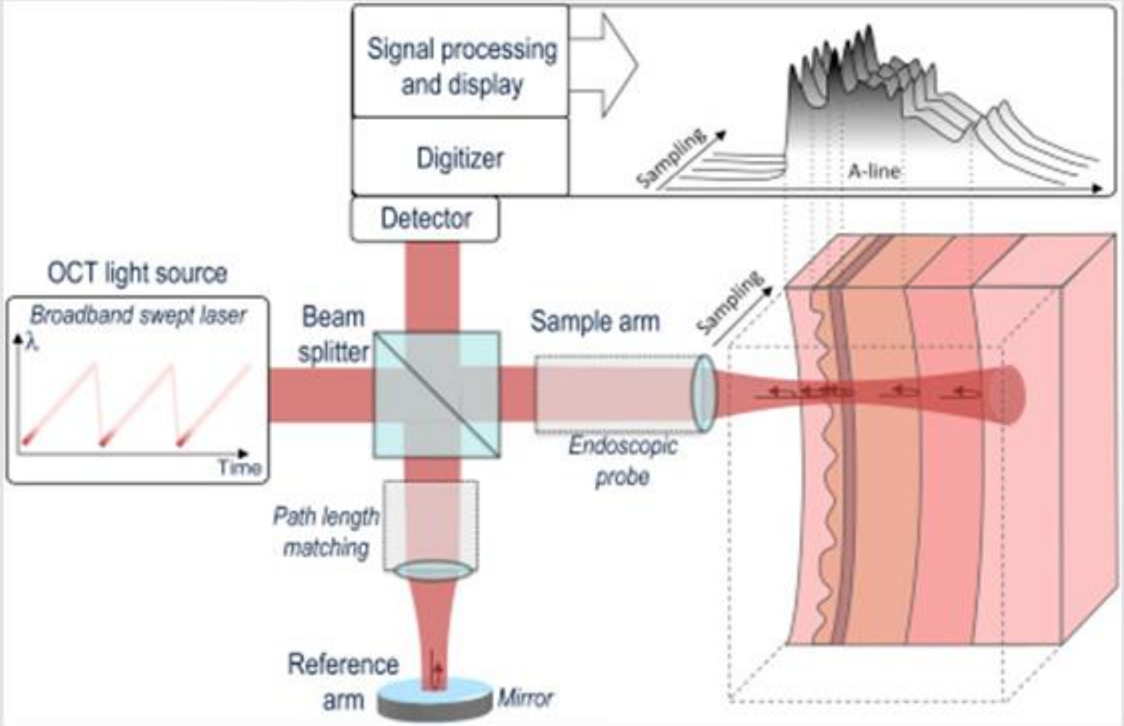

(Ref: Gora, M.J. and Tearney, G.J., 2016. Enhanced imaging of the esophagus: Optical coherence tomography.)

- Upgrade: Fourier-domain OCT

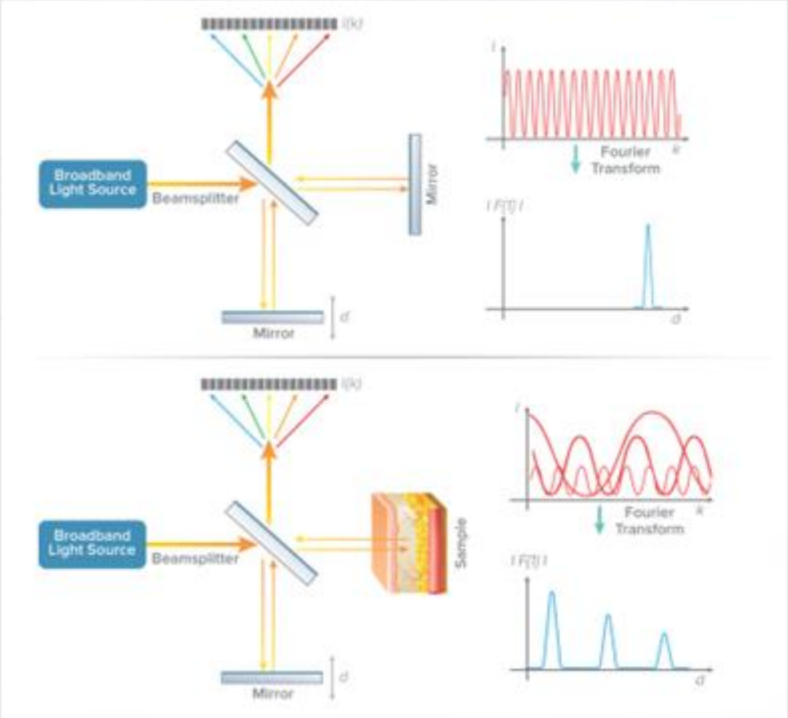

(Ref: Wasatch photonics)

Co-funded by the European Union

2. Modern Surface Metrology

- Surface texture characterisation

Co-funded by the European Union

Surface characterisation: filtration techniques

- TC 213 Workgroup: ISO 16610 Series

ISO 16610 Filtration Toolbox

- Linear filters
  - Gaussian filter
  - Spline filter
  - Spline wavelet filter
- Robust filters
  - Robust Gaussian regression filter
  - Robust spline filter
- Morphological filters
  - Closing filter
  - Opening filter
  - Alternating symmetrical filters
  - Scale space filter
- Segmentation filters

Gaussian filter

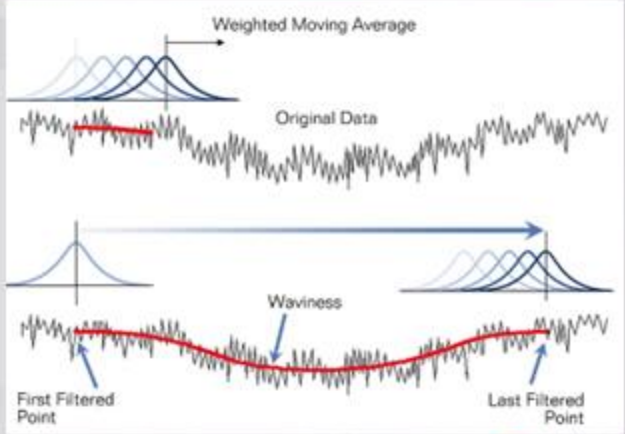

Spline filter

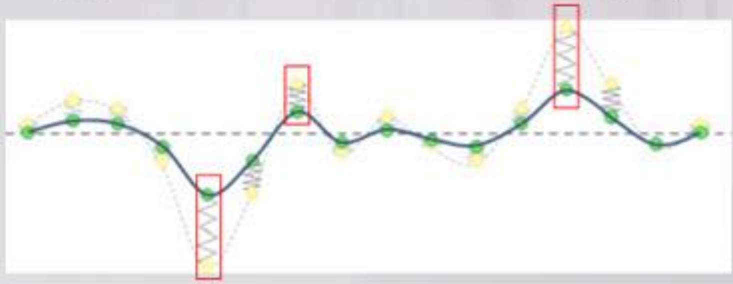

Morphological filters

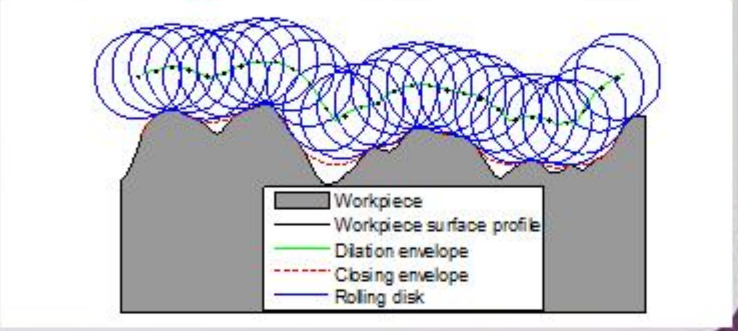

Surface characterisation: robustness & regression

- **Robustness**

  Insensitivity of the output data against specific phenomena (outliers, scratches and steps etc) in the input data.

Outlier

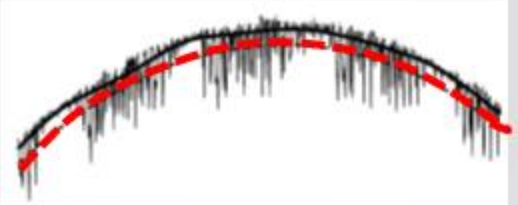

Deep valleys

- **Regression**

  Ability to follow the surface form.

Significant form

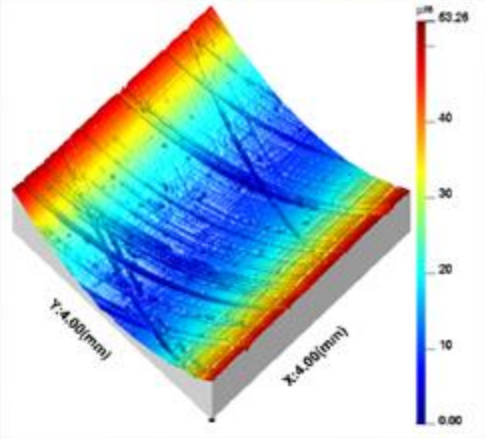

Measured cylinder liner surface

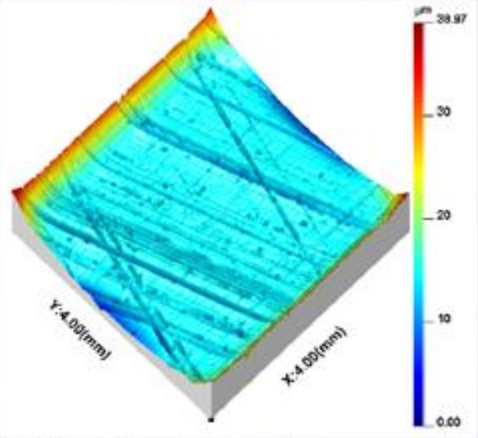

Roughness surface (linear Gaussian filter)

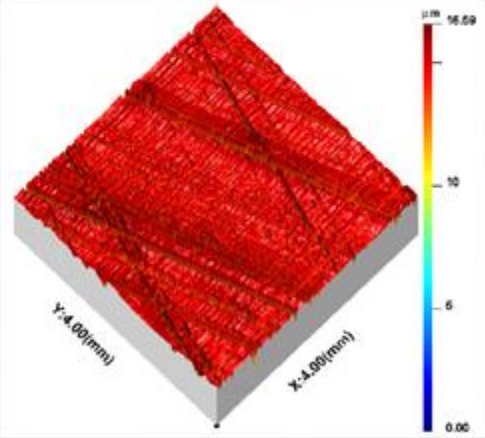

Roughness surface (2 order Gaussian filter)

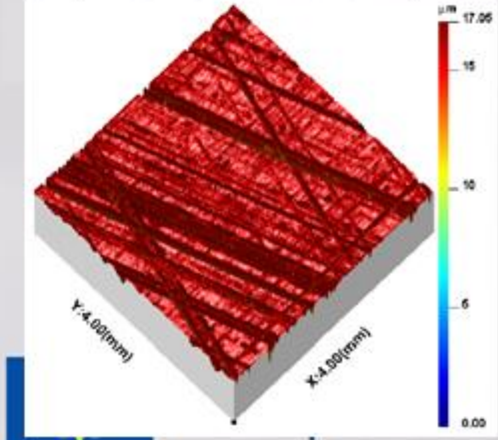

Roughness surface (Robust Gaussian filter)

FLASH

Surface characterisation: spline & morphological filters

- Spline filter

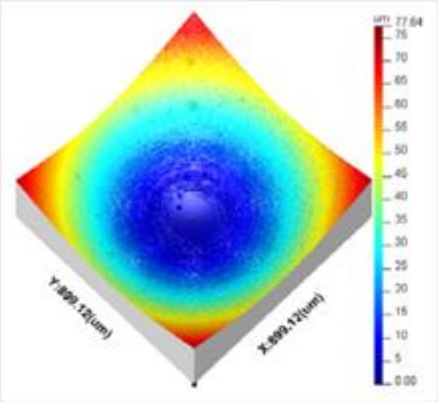

Measured Aspheric lens surface

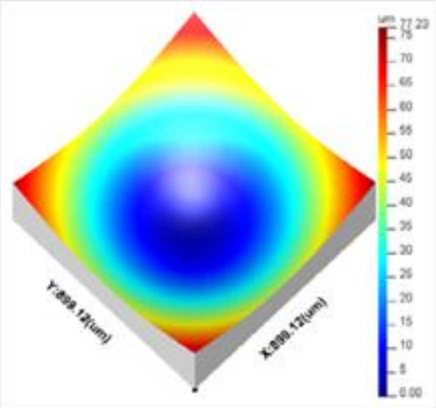

Filtered/reference surface

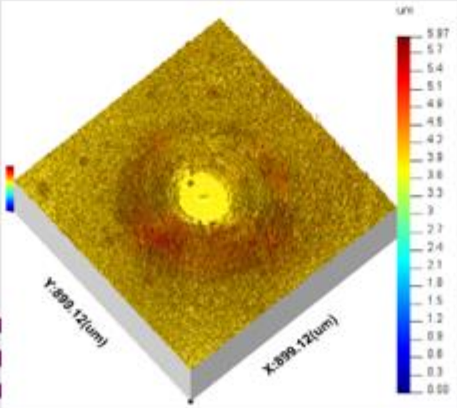

Residual surface

- Morphological filters

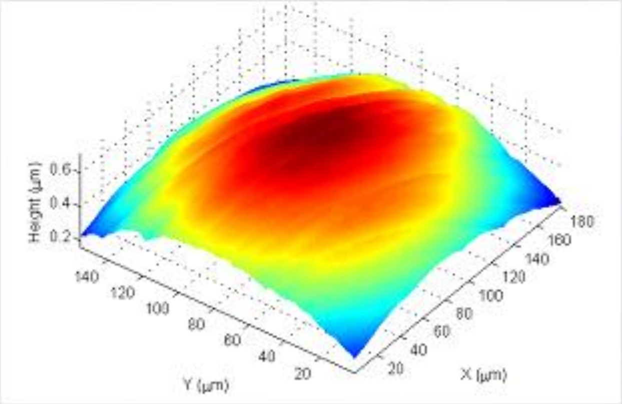

Worn artificial knee joint replacement surface

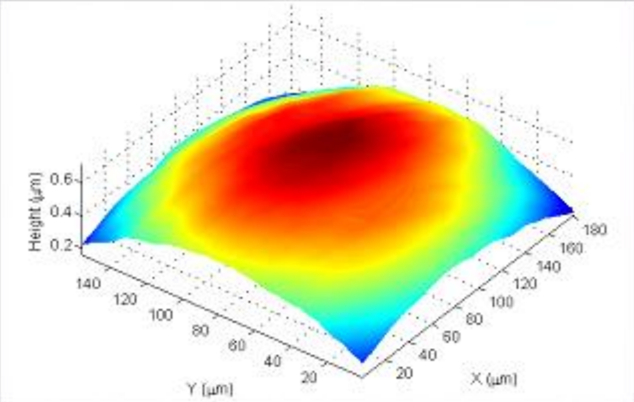

Morphological closing envelope with ball radius 5mm

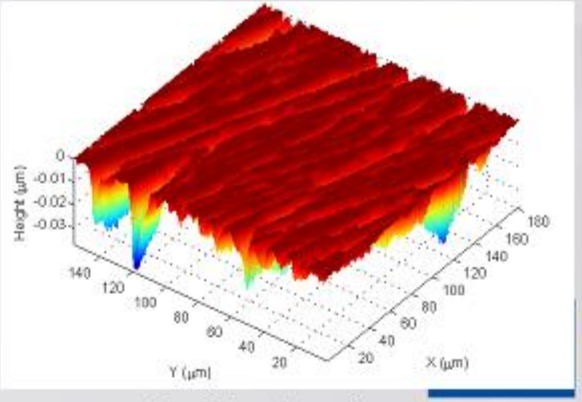

Residual surface

FLASH

Co-funded by the European Union

Surface characterisation: watershed segmentation

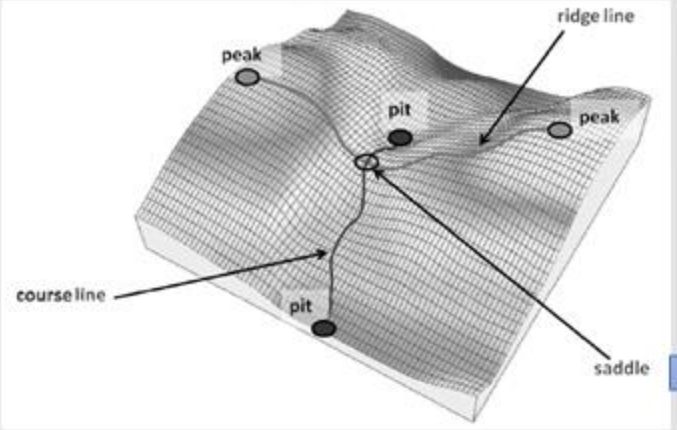

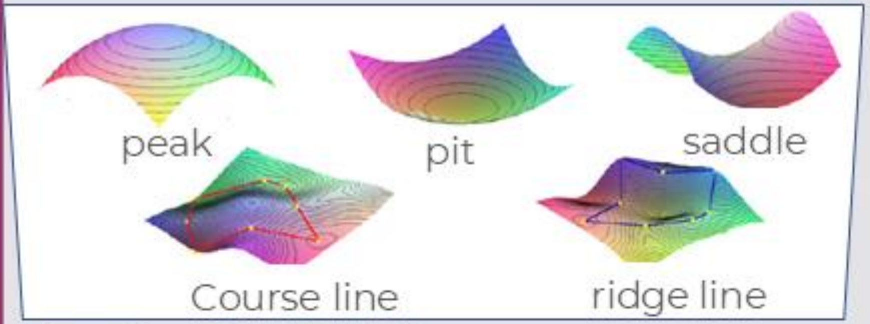

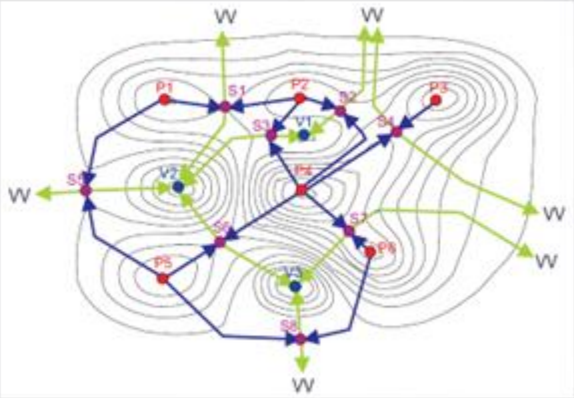

Phalfz graph

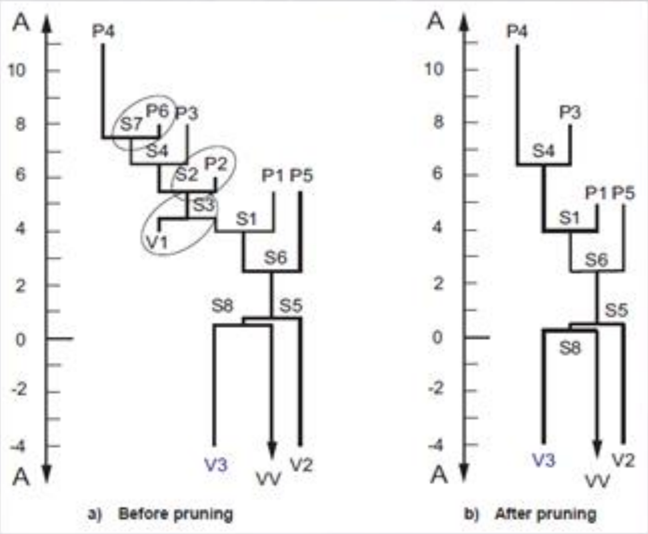

Wolf pruning

FLASH

Co-funded by the European Union

Surface characterisation: watershed segmentation

- Identify the active grains on a grinding wheel surface
- Identify the features on structured surfaces

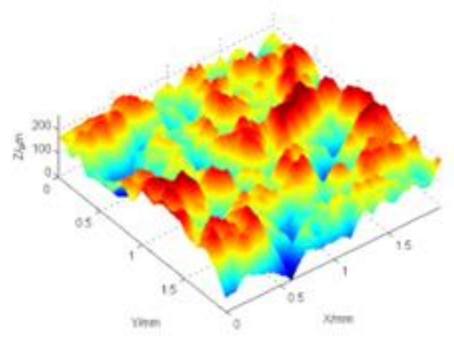

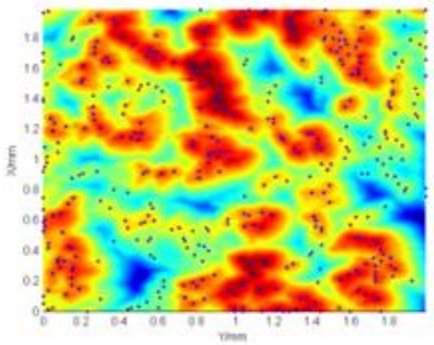

Peak count: 409

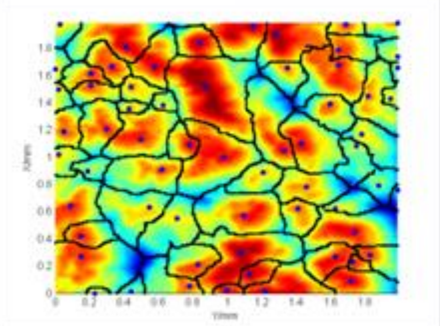

Peak count: 64 with Wolf-pruning 5%

Spd	15.678 Pts/mm²
Ssc	28.273 1/mm
S10z	188.500 µm
Sha	0.0149 mm²
Shv	0.000335 mm³

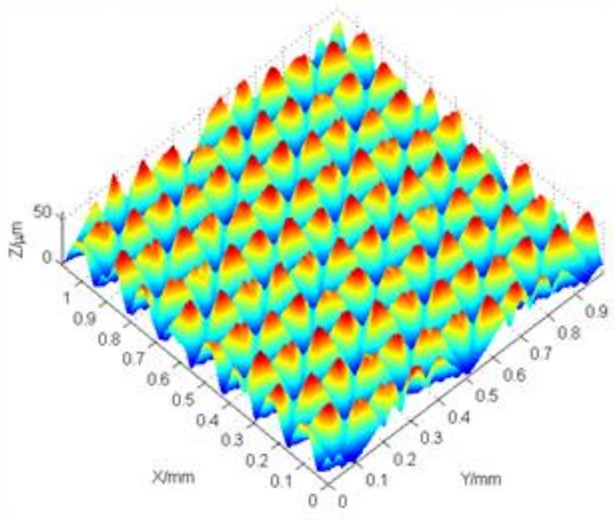

3M Trizact abrasive surface with pyramid structure

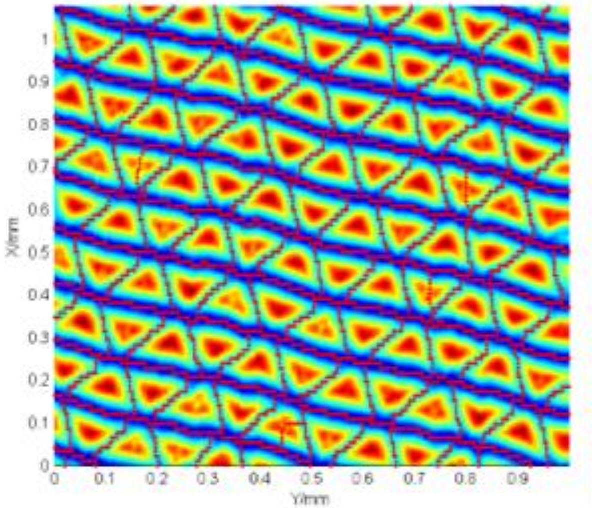

Segmented structured surface with wolf pruning 10%

Co-funded by the European Union

Surface characterisation: parameterisation

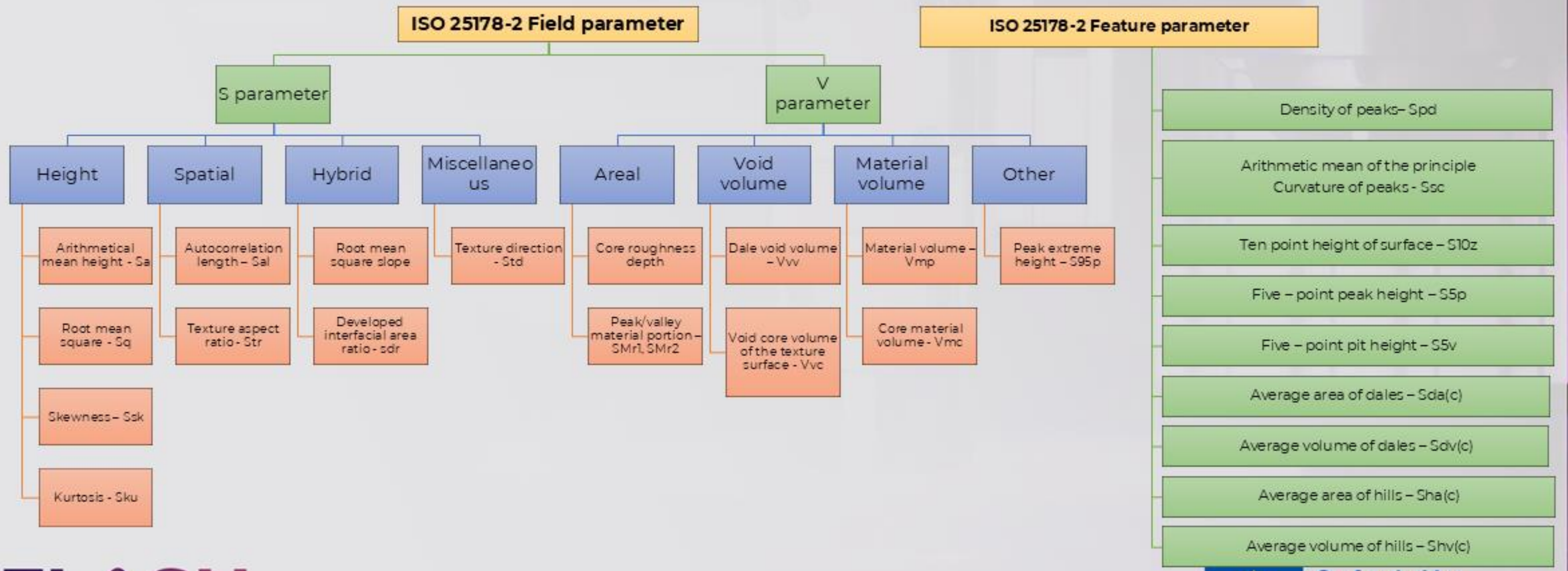

Co-funded by the European Union

Surface characterisation: parameterisation

- Parameter's performances to discriminate the wear degrades

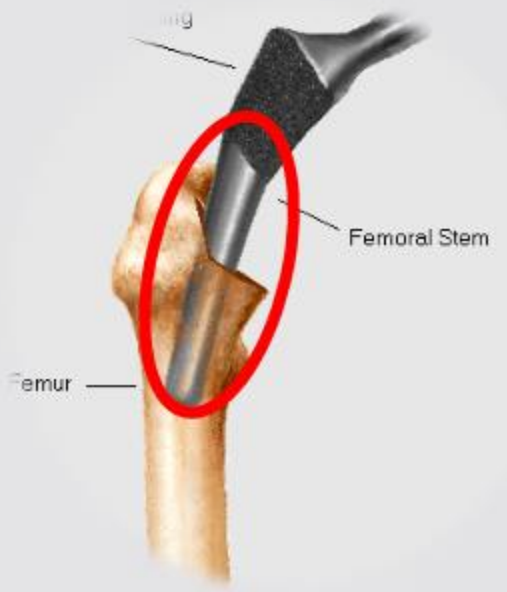

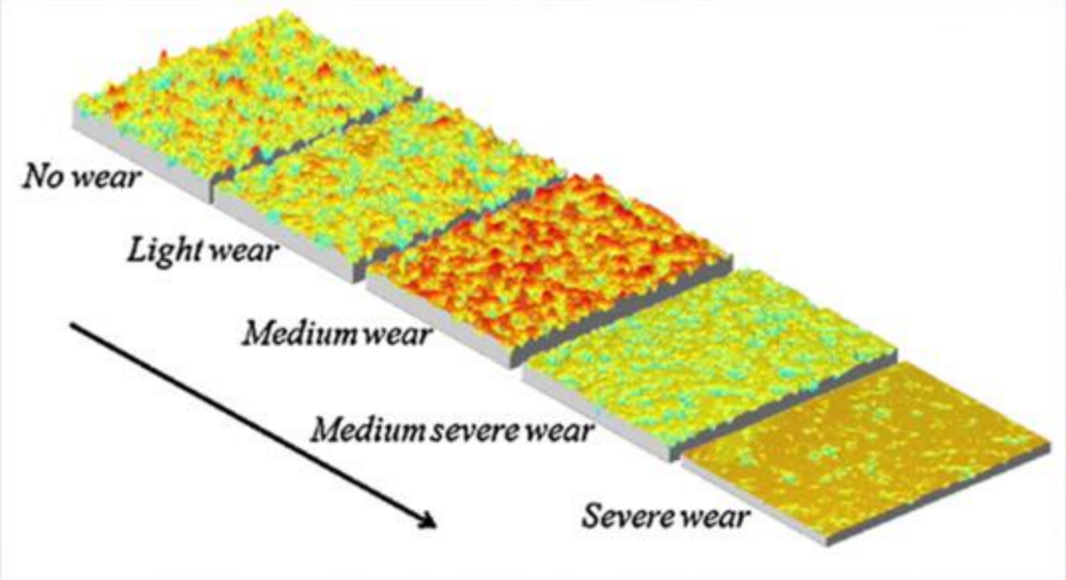

Amplitude				Spatial			Hybrid			Volume		
Sq	Sz	Ssk	Sku	Str	Sal	Std	Sdq	Ssc	Sdr	Vmp	Vvc	Vv
●	●	●	Δ	○	Δ	○	●	Δ	●	●	●	●

● Significant discrimination; Δ Some discrimination; ○ Little or no discrimination

Surface evolution: shape and texture independent

- Surface shape and texture are playing determinant roles

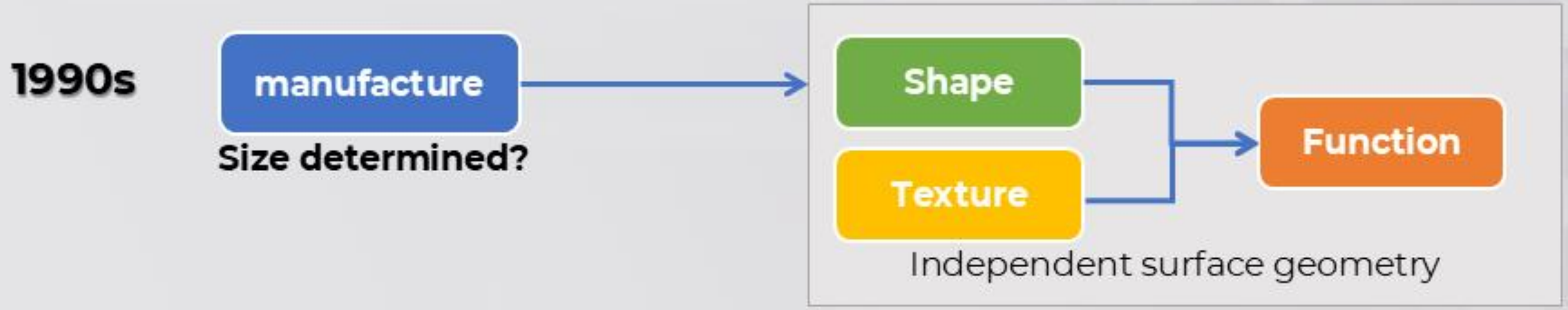

- Freeform surfaces
  continuous surfaces having no translational and rotational symmetry

- Structured surfaces
  Surfaces with a dominant deterministic feature pattern and usually with high aspect ratio

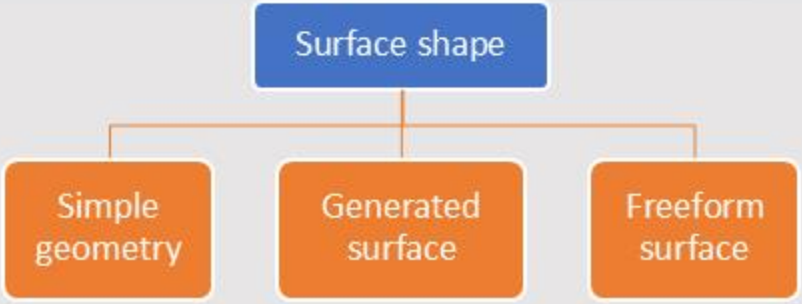

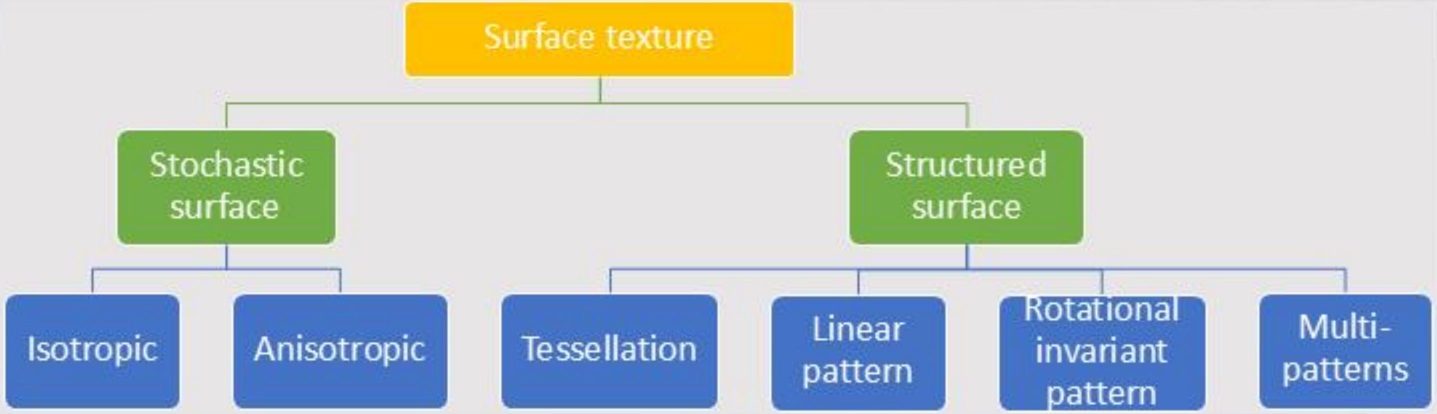

Surface evolution: complex structured surfaces

- Complex structured surfaces

  Single surface having both types of geometry (freeform and structured) for multiple/optimised function.

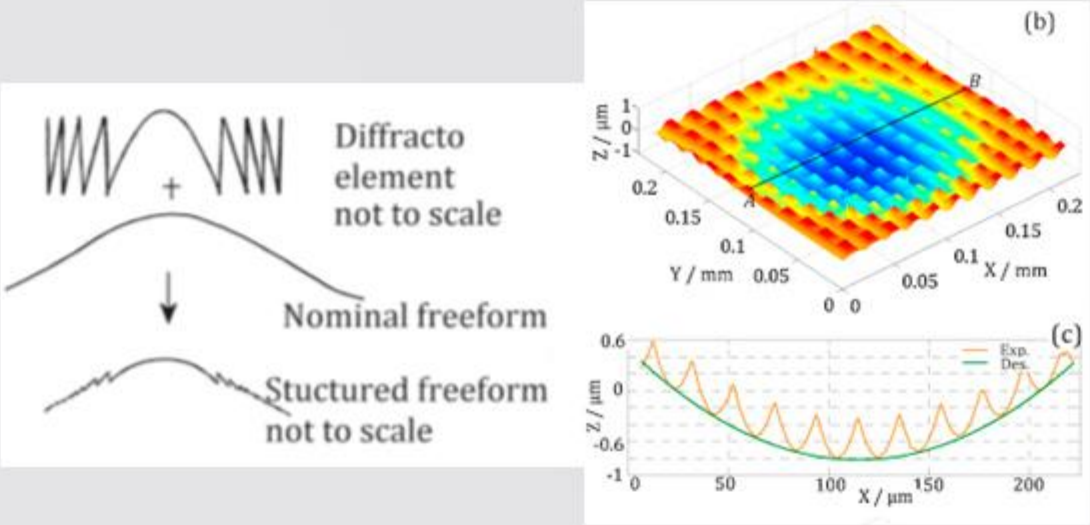

Advanced optical components

(ref: Suet To et al., 2015 CIRP Annal.)

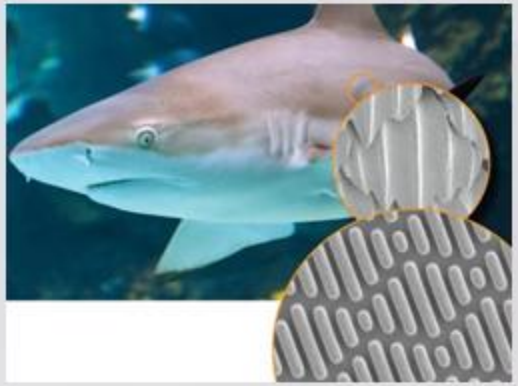

Bioengineering surfaces

(src: www.sharkwatchsa.com)

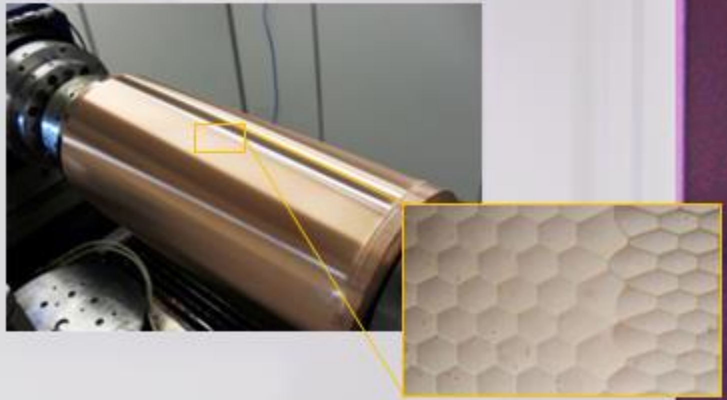

Roll-to-roll drum surface

(src: USP2 website)

Co-funded by
the European Union

Characterisation techniques for structured surfaces

- Nonlinear adaptive diffusion filter

$$\frac{\partial f(x,y,t)}{\partial t} = \nabla c \cdot \nabla f(x,y,t) + c(x,y,t) \cdot \Delta f(x,y,t)$$

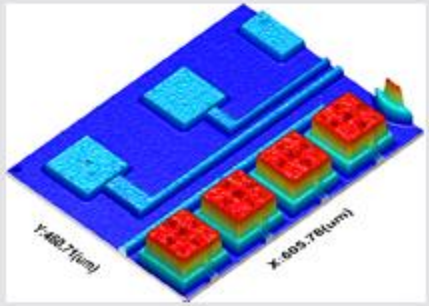

(a) Measured MEMS surface

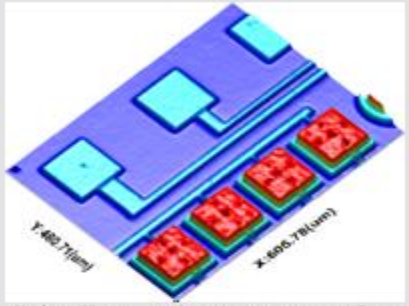

(b) Filtered MEMS surface

- Clustering filter

$$z = \frac{\sum_i z_i \omega_i e^{-\beta(z_i - z)^2}}{\sum_i \omega_i e^{-\beta(z_i - z)^2}}$$

$$\omega_i = e^{-\alpha \|x_i - x\|^2}$$

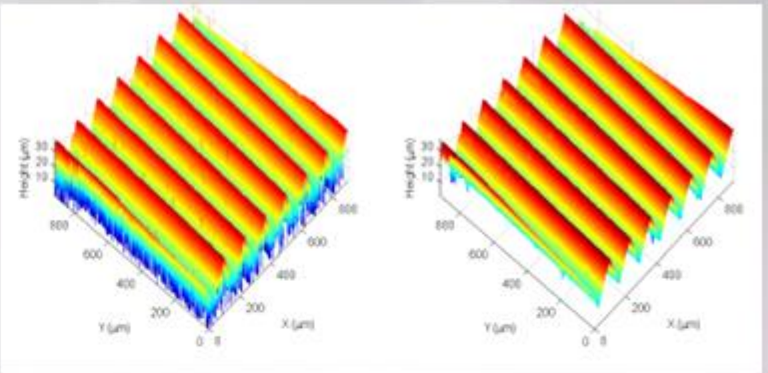

- Watershed segmentation

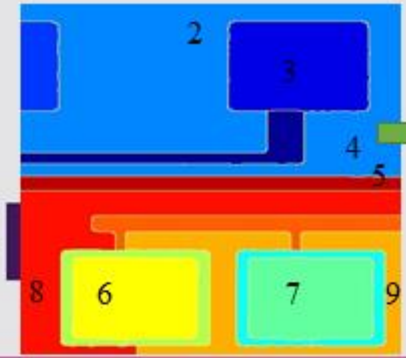

Step plane	Mean height (um)
1	0.920
2	0.920
3	0.733
4	0.745
5	0.746
6	1.693
7	1.673
8	4.269
9	4.270

FI

- AACF for tessellated surfaces

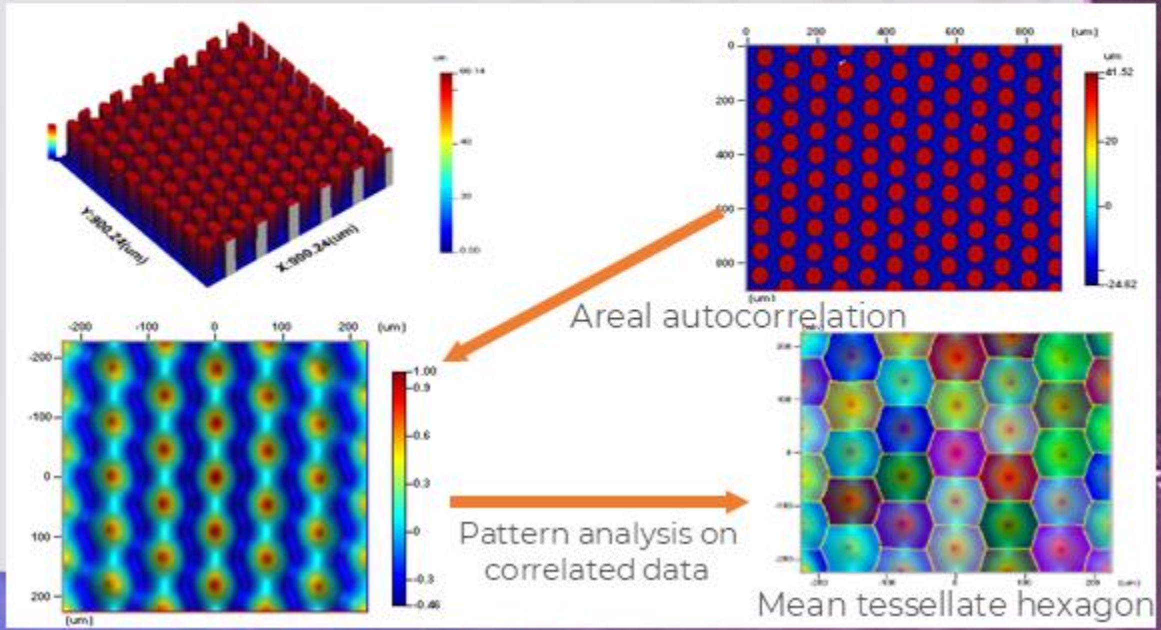

3. CPT Recent Development

- Embedded sensors and instruments
- Machine-learning based surface characterisation for structured surfaces
- Triangular-mesh based surface characterisation utilising XCT data

Co-funded by the European Union

3. CPT Recent Development

- Embedded sensors and instruments

Co-funded by
the European Union

Embedded sensor

Interferometry

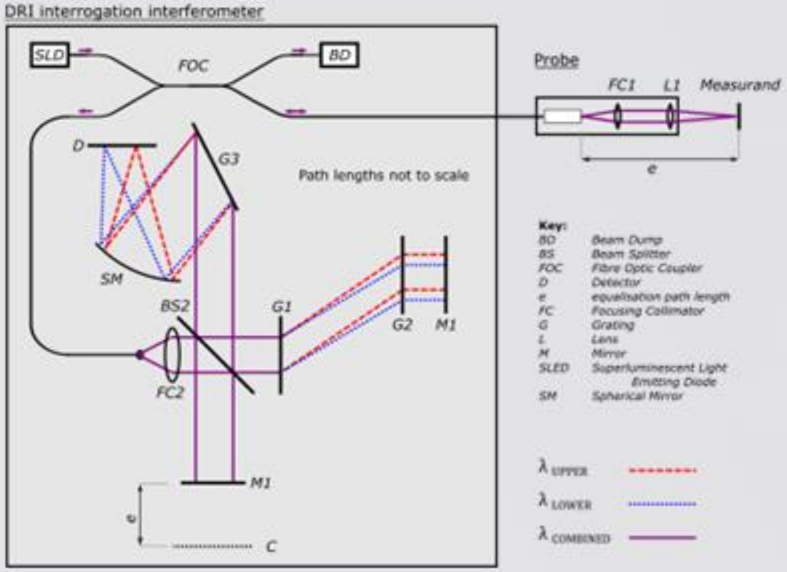

Deflectometry

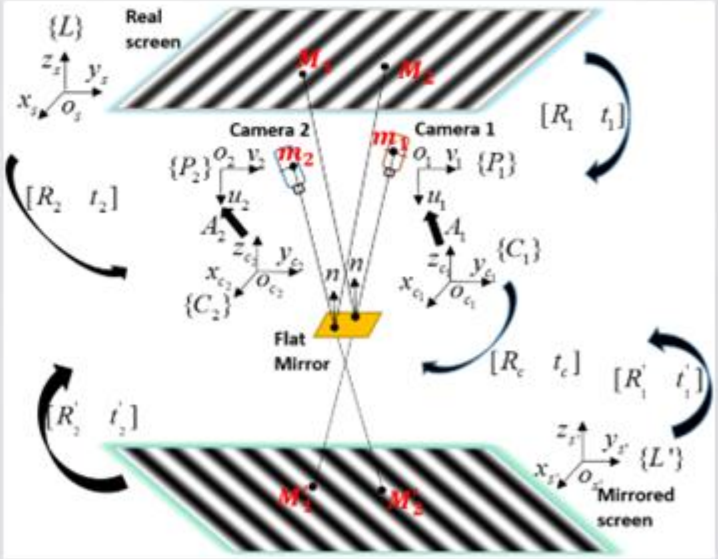

Fringe Projection

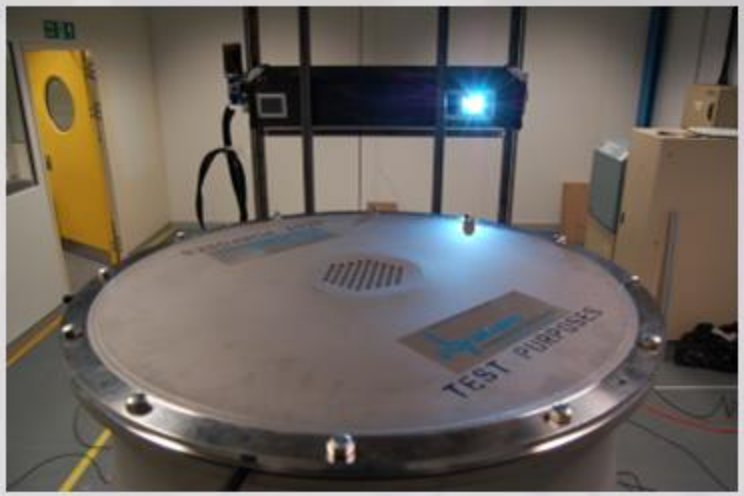

Embedded sensors in machine systems and science experimental systems

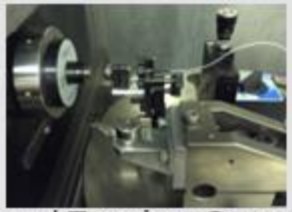

Diamond Turning Centre

Multi-Machining Centre

Roll-to-Roll Manufacturing

Wavelength scanning interferometer (WSI)

- Operation principles

Acousto-Optic Tuneable Filter tunes the wavelength from (680-580)nm without moving parts.

During the wavelength scanning, images are captured with a high-speed CCD camera. (e.g. 128 or 256 frames)

Captured Frames

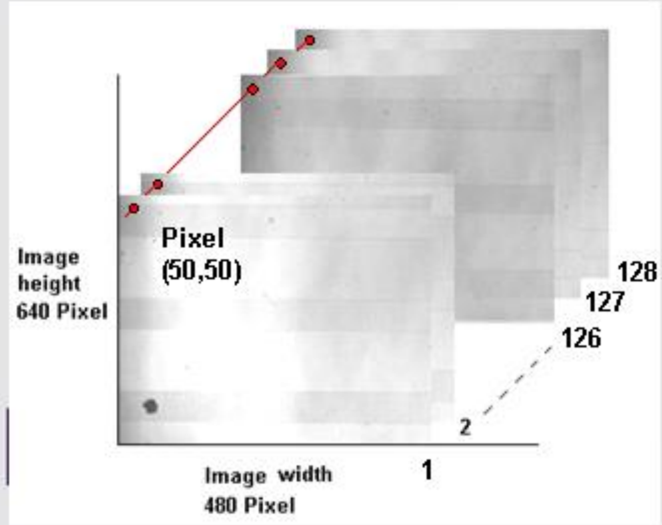

Single Pixel Result

Frequency determines height

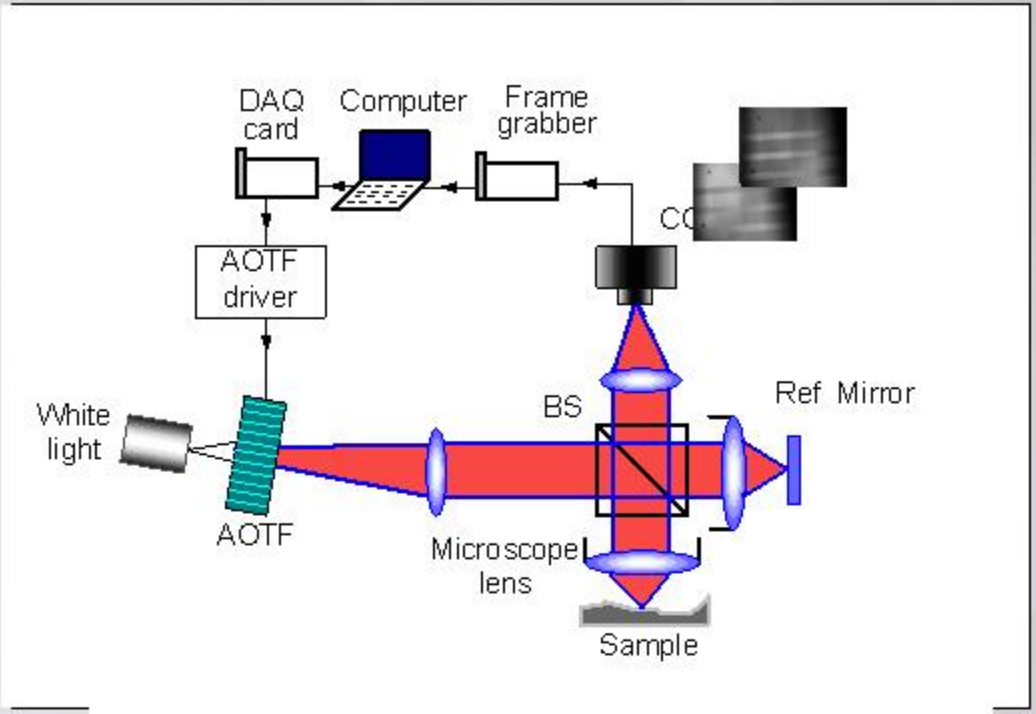

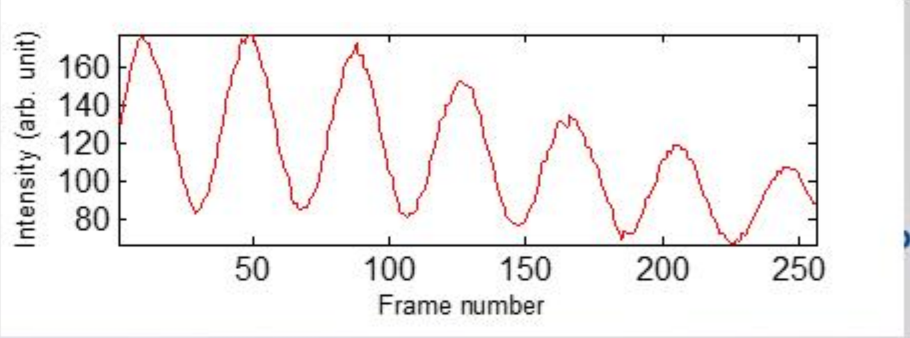

Performance comparison

Feature	PSI	CSI	WSI	Focus variation	Confocal
Axial range : limited by	λ/4 (sub-micron)	Translation stage (sub millimetre)	Depth of focus (tens of micron)	Translation stage (millimetre-scale)	Translation stage (millimetre-scale)
Axial resolution	Independent of objective NA (less than 1 nm)	Independent of objective NA (less than 1 nm)	Independent of objective NA (10 to < 1 nm)	Dependent of objective NA (10 - 100 nm)	Dependent of objective NA (few - 10 nm) (1.5 um for thin films)
Lateral range	Field-of-View of the objective lens (e.g. 0.9x0.9 mm for 20x)	Field-of-View of the objective lens (e.g. 0.9x0.9 mm for 20x)	Field-of-View of the objective lens (e.g. 0.9x0.9 mm for 20x)	Field-of-View of the objective lens (e.g. 0.9x0.9 mm for 20x)	Scanning of the beam or aperture
Lateral resolution	Dependent of objective NA Note: complex optical alignment for high NA	Dependent of objective NA Note: complex optical alignment for high NA	Dependent of objective NA Note: complex optical alignment for high NA	Dependent of objective NA Note: Simpler optical alignment for high NA	Dependent of objective NA Note: Simpler optical alignment for high NA)
Stabilisation	YES (for single-shot techniques)	NO	YES	NO (less susceptible to vibration than confocal)	NO

Dispersive reference interferometer (DRI)

- A single-point surface topography and distance interferometer
- Small on-machine fibre-linked probe connected to a remote interrogation interferometer
- Unbalanced interferometer brings reference and measurement beams into coherent interference
- Determine balance point wavenumber to measure surface height/standoff

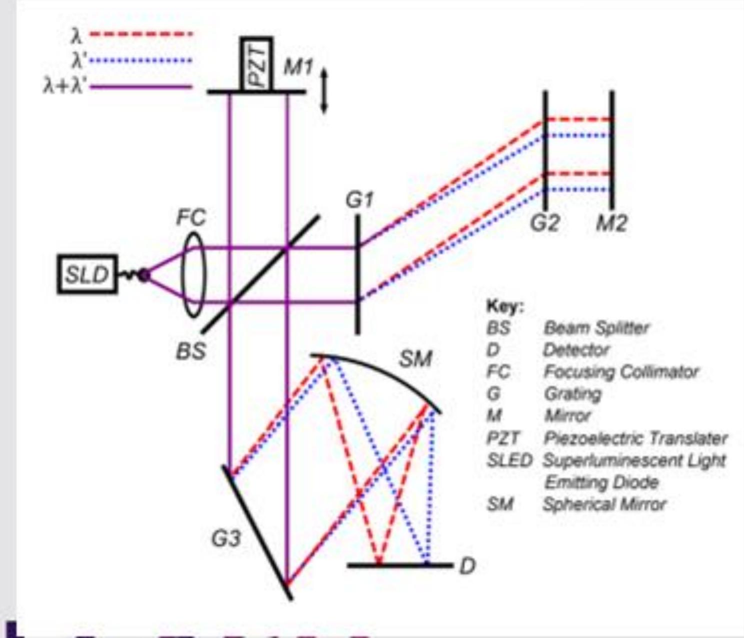

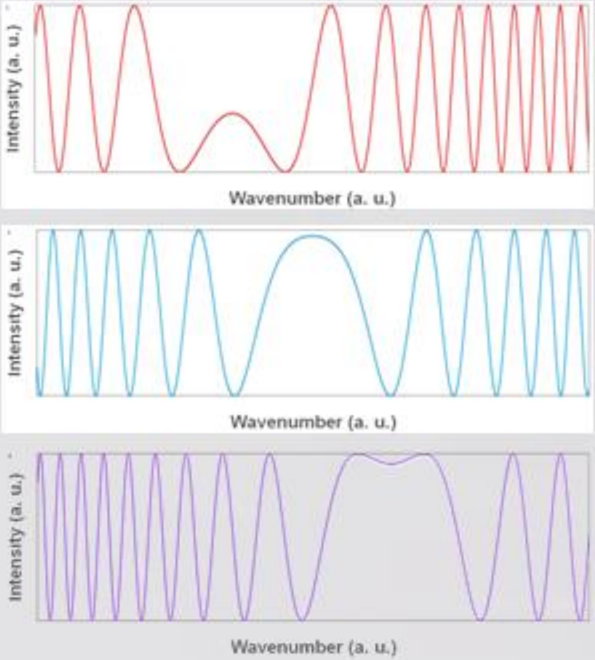

Absolute Range	1 mm
Resolution	<5 nm
Dynamic Range	200,000
Measurement Rate	5k Hz

Optics express 24.9 (2016): 10103-10114.

Co-funded by the European Union

Single-shot dispersive profile interferometer (SDPI)

- Instantaneous line profile measurement for surface topography
- combining technologies: low coherence interferometry, hyperspectral imaging and parallel signal processing.
- Provides high-speed measurement over a millimetre range while achieving nanoscale resolution.

Technology

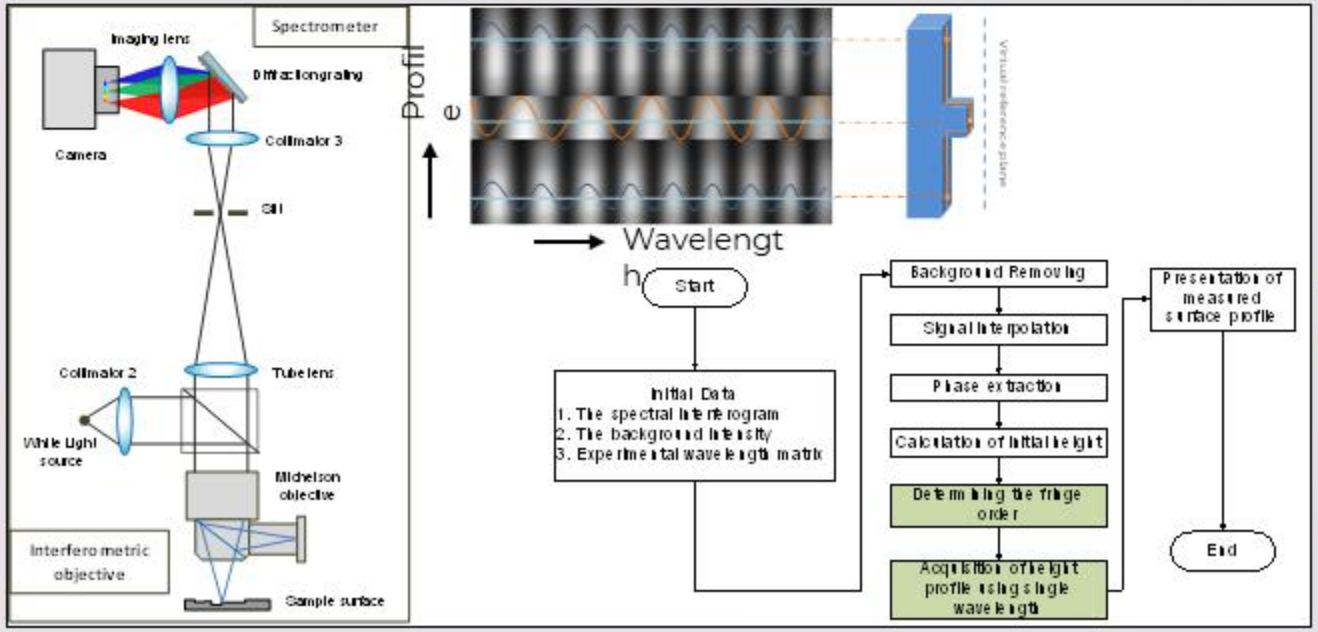

Prototype

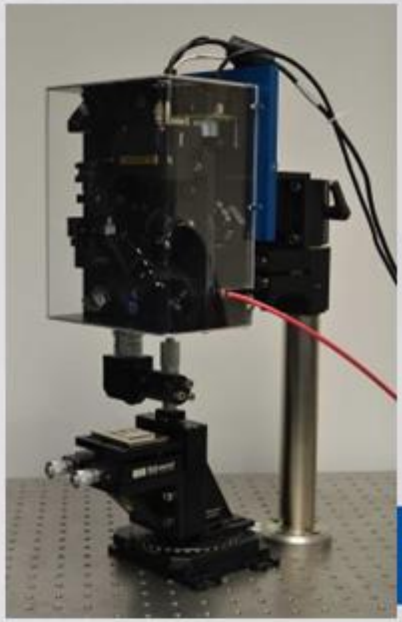

Measurement

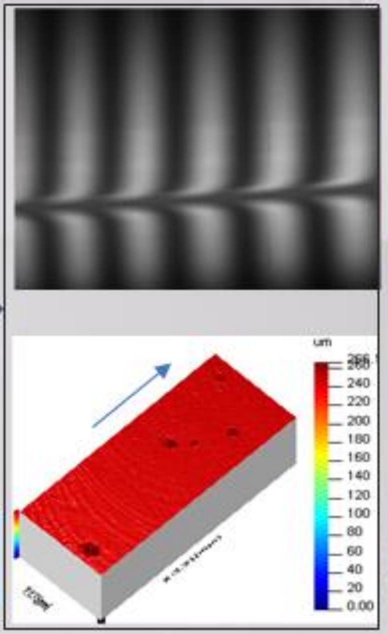

Meta-surfaces: minimisation of measurement sensors

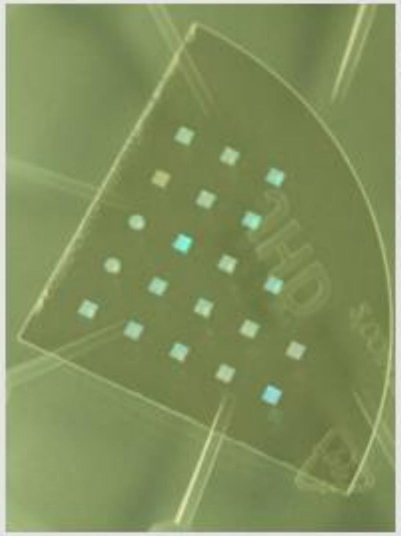

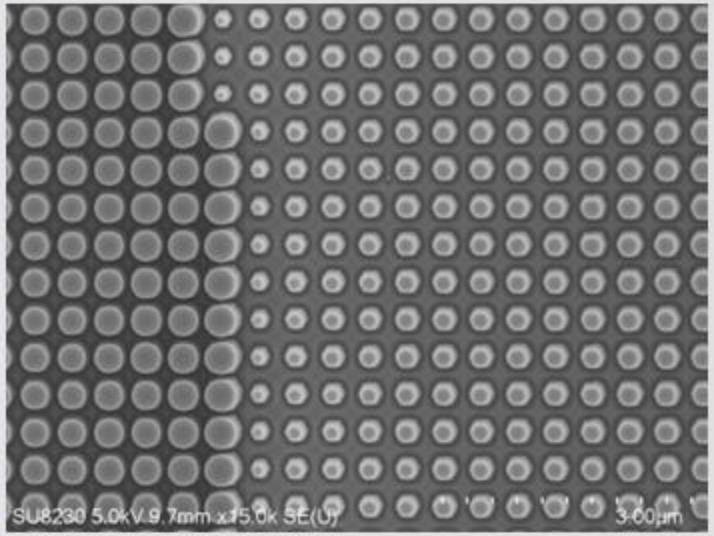

Meta-surfaces made by Kelvin Nanotechnology Ltd
The pillars are 750 nm high GaN pillars etched from a layer of GaN on Al_2O_3

- Confocal microscopy

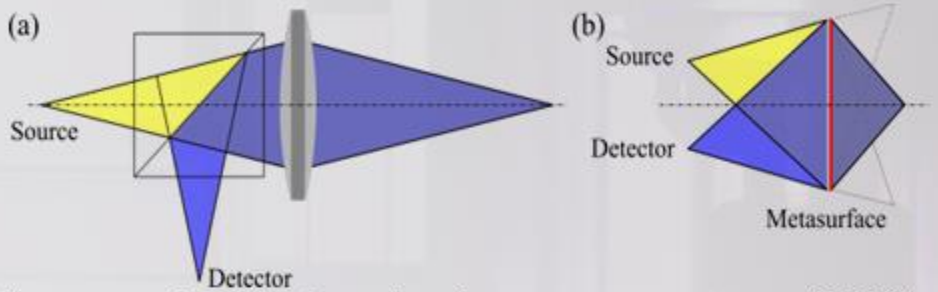

- Chromatic confocal microscopy

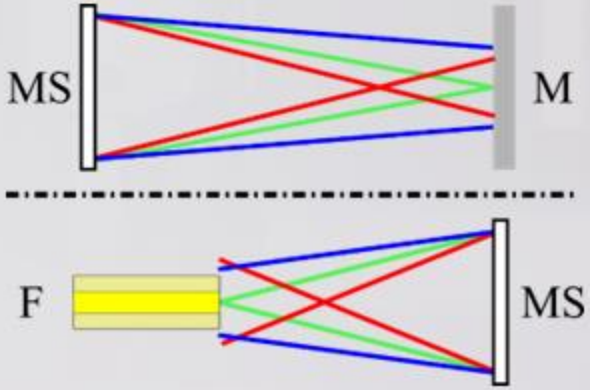

- SDPI

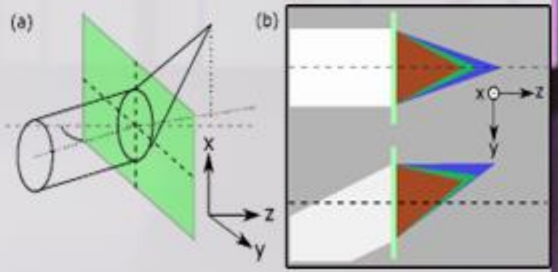

FLASH

Co-funded by the European Union

3. CPT Recent Development

- Machine Learning based surface characterisation techniques for structured surfaces

Co-funded by the European Union

Rule-based approach VS learning-based approach

	Rule-based approach	Learning-based approach
Pros	• Simplicity: well-established, straightforward, and relatively easy to implement. • Consistency: mathematical basis, easier to interpret and validate, producing consistent results under defined conditions. • Efficiency: computationally efficient, requires less power.	• Adaptability and generalisation: learn complex patterns and features, adapt to a wide range of image types, and handle complex surfaces. • Autonomous and high efficiency: can automatically process arbitrary inputs without user intervention, compatible with large datasets.
Cons	• Limited adaptability: lack of flexibility to adapt to various surface patterns. • Manual intervention: model selection, parameter adjustments, time-consuming, and prone to human error. • Sensitivity to parameter tuning: highly sensitive to parameter settings, which must be carefully tuned for each specific application.	• Need training data: require a large amount of labelled training data, time-consuming and labour-intensive • Computational requirements: computationally intensive and requires powerful hardware • Complexity: Implementation and optimisation, involving intricate architectures and hyperparameter tuning.

ML-based surface characterisation for structured surfaces

- General structure
  an intelligent surface characterisation system to enable automatic analyse of structured surfaces, accurate extraction of surface patterns, and quantification of key parameters for enhanced surface assessment and quality control.

Surface data acquisition
- Optical measurement

Form removal
- F-operator
- Lage-scale

Denoising
- Filtration
- Small-scale

Feature extraction
- Segmentation
- Feature-specific

Parameterisation
- Feature attributes

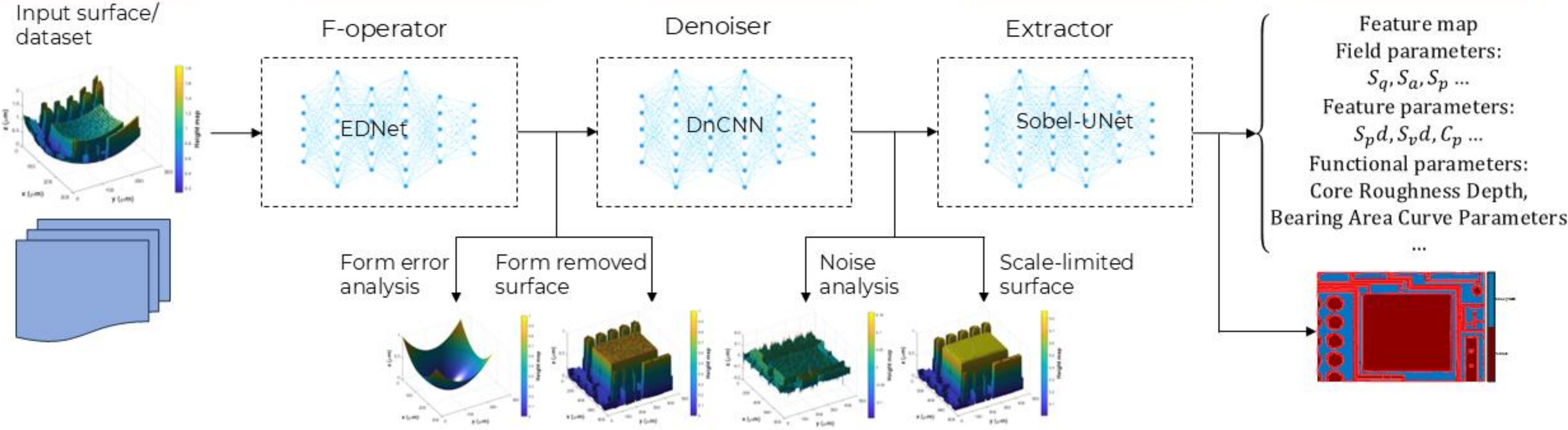

Form removal: ResBlur-EDNet

Encoder-decoder based architecture, incorporating residual learning, skip connection, and Gaussian blurring kernel

- Encoder decoder: maintain the input and output dimensions; retain the structural information
- Residual learning: capture fine details; correct errors; improve convergence speed and accuracy
- Skip connection: mitigate vanishing gradient problems; preserve low-level features while integrating higher-level abstractions
- Robust loss: inspired by M-estimator, using weight function penalty large error caused by features

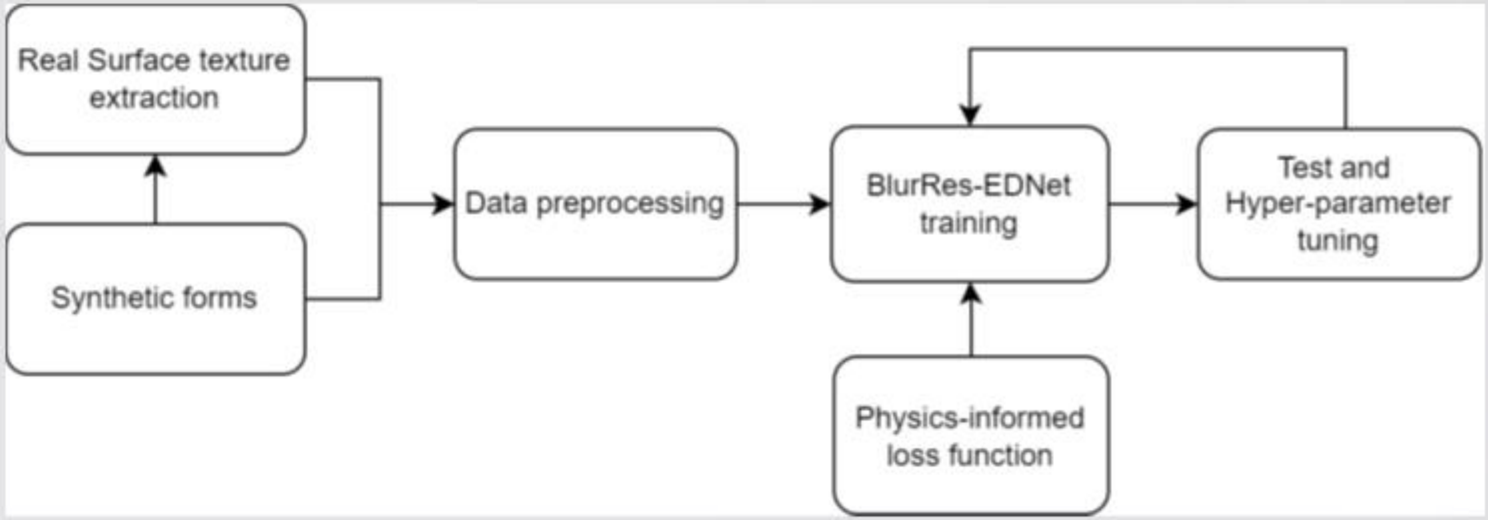

Workflow of building learning-based F-operator

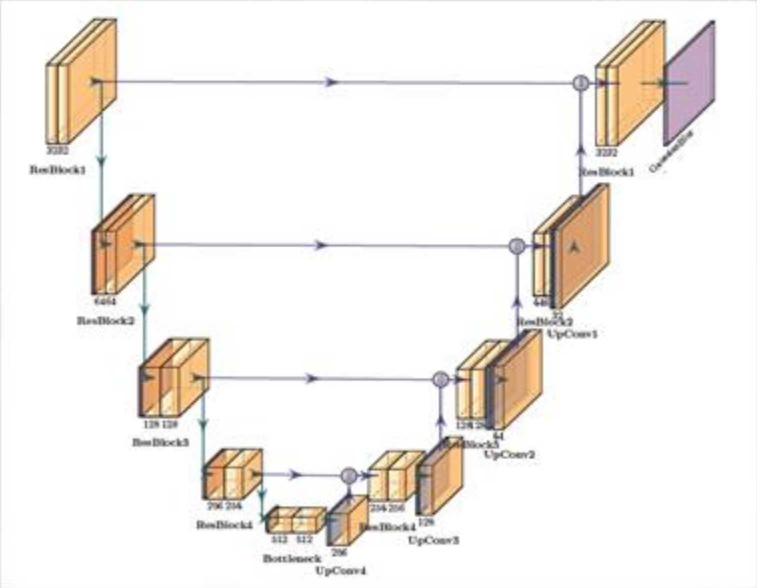
BlurRes-EDNet model architecture

Form removal: ResBlur-EDNet performance

- The lowest values across all metrics, demonstrating superior performance compared to traditional methods.
- Can recognise different order polynomial forms from complex structured surfaces with high accuracy and efficiency; Once the model is well trained, it can automatically process arbitrary input surfaces without any user operation.
- Processing time of 486 test surfaces with 3.6s on the GPU (T4 GPU), significantly outperforming the CPU processing time of 108.9s on the CPU.

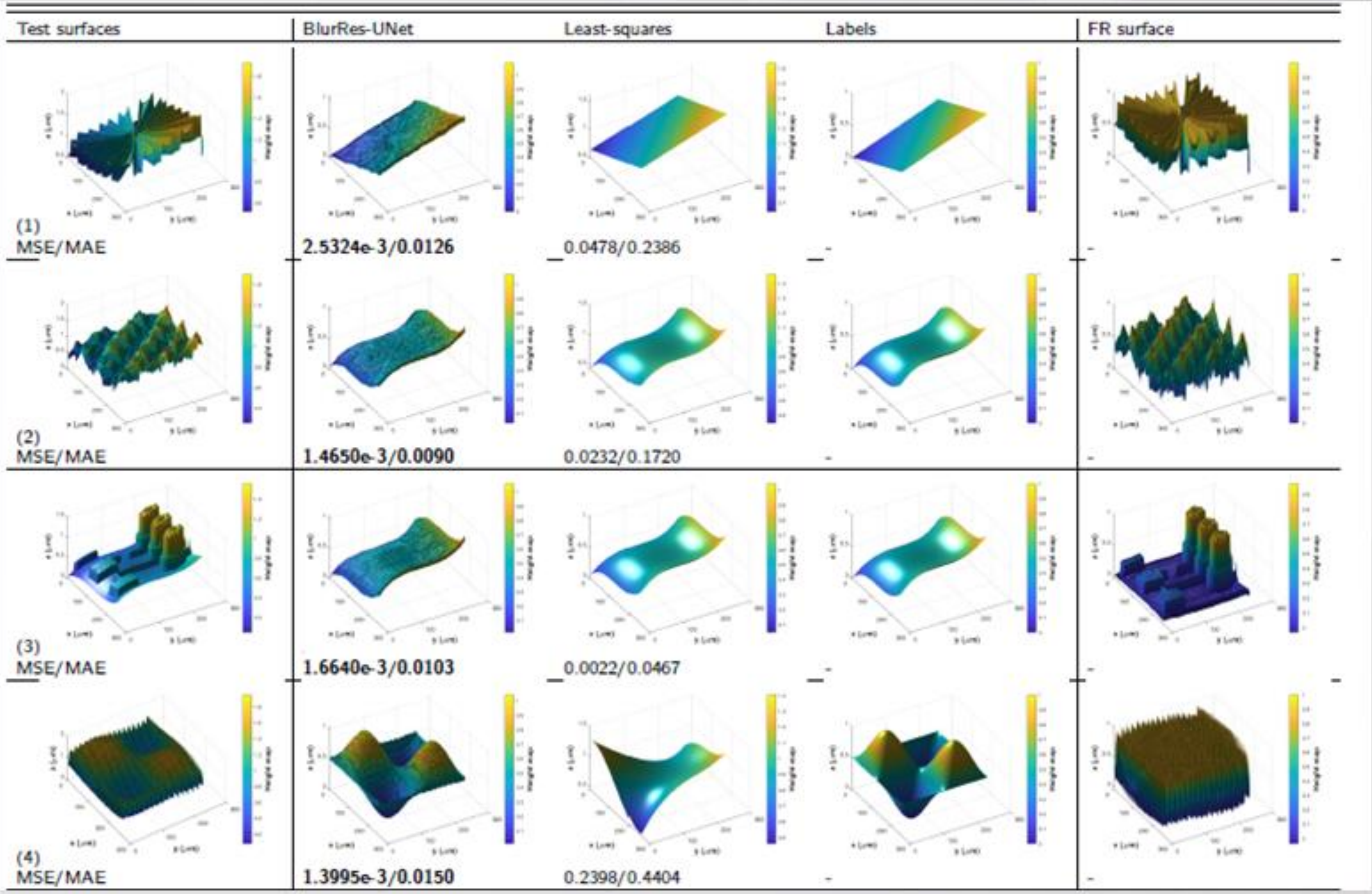

Noise removal: PI-DnCNN

PI-DnCNN is proposed as an intelligent denoiser, integrating physics-informed loss and hybrid data augmentation techniques with deep denoising neural networks.

- DnCNN can handle mix-level Gaussian noise which matches surface noise distribution.
- Hybrid data augmentation: going beyond conventional approaches by further generating customized noise maps to enhance recognition of complex components.
- Physics-inform loss: incorporating filtering techniques (total variation and Laplacian operator) with neural network training, tapping into data characteristics for enhanced model performance.

$$\mathcal{L}_{tv} = \frac{1}{m}\sum_{j=1}^{m}\left(\frac{1}{2}\hat{N}^2 + \lambda * (|\hat{U}_x| + |\hat{U}_y|)\right) \quad \mathcal{L}_{new} = \mathcal{L}_{mse} + w_1 * \mathcal{L}_{tv} + w_2 * \mathcal{L}_{lap}$$

$$\min_{\hat{s}}\left(\frac{1}{2}\sum(s-\hat{s})^2 + \lambda * \sum(|\hat{s}_x| + |\hat{s}_y|)\right) \quad \mathcal{L}_{lap} = \frac{1}{m}\sum_{j=1}^{m}\left(R_{xx}^2 + R_{yy}^2\right)$$

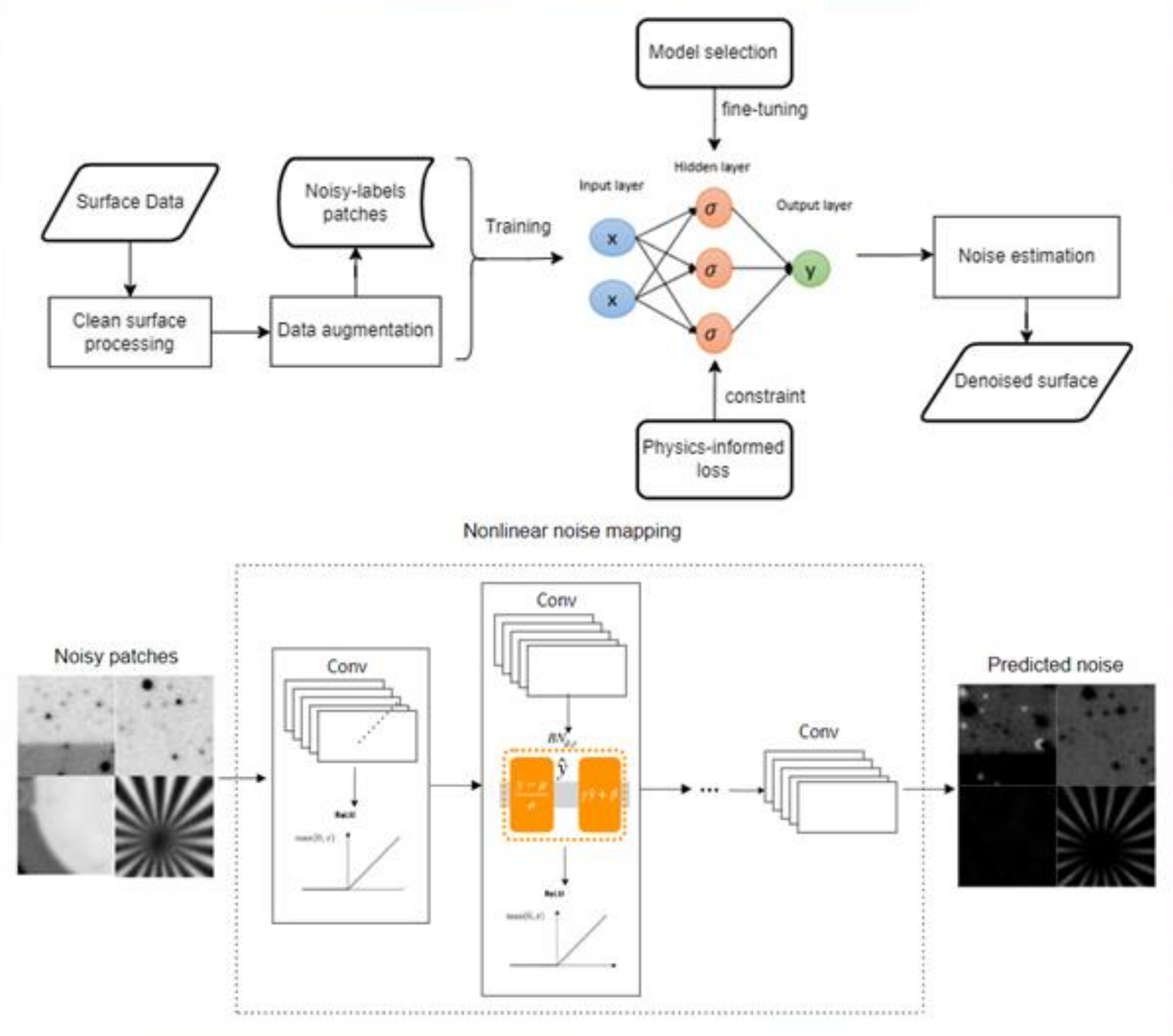

Noise removal: PI-DnCNN performance

- PI-DnCNN attains the lowest MSE value of 1.82e−04, the highest PSNR of 42.4028, and the highest SSIM of 0.9882, achieving the best average score compared to traditional filters.
- Superior average performance, as it has learned the properties of all filters including smoothing and structure-preserving.
- Average processing time of the test surface of approximately 0.8s on CPU, which was reduced to a mere 0.07s on GPU, in MATLAB(2023a) platform.

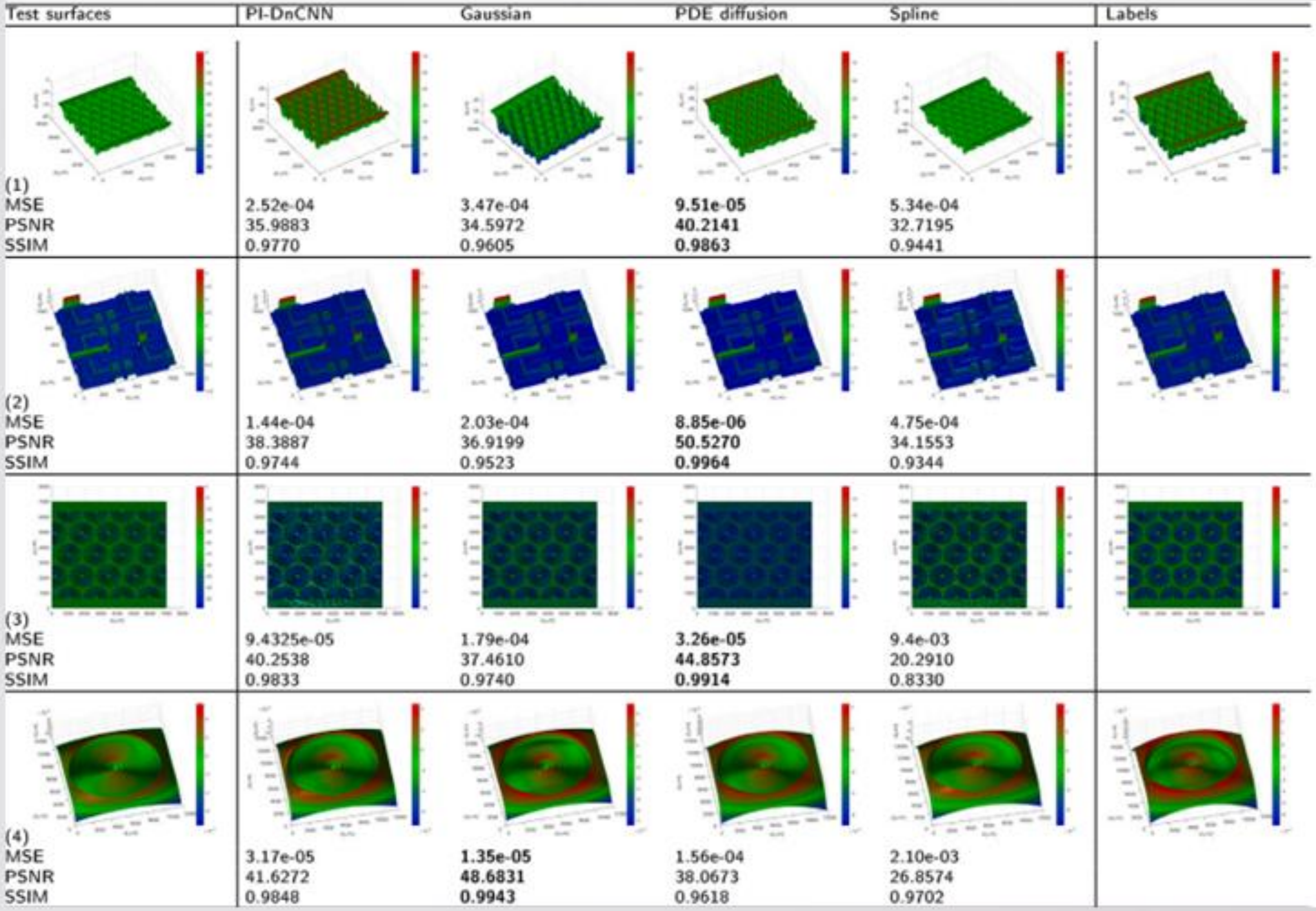

Test surfaces	PI-DnCNN	Gaussian	PDE diffusion	Spline	Labels
(1) MSE	2.52e-04	3.47e-04	**9.51e-05**	5.34e-04	
PSNR	35.9883	34.5972	**40.2141**	32.7195	
SSIM	0.9770	0.9605	**0.9863**	0.9441	
(2) MSE	1.44e-04	2.03e-04	**8.85e-06**	4.75e-04	
PSNR	38.3887	36.9199	**50.5270**	34.1553	
SSIM	0.9744	0.9523	**0.9964**	0.9344	
(3) MSE	9.4325e-05	1.79e-04	**3.26e-05**	9.4e-03	
PSNR	40.2538	37.4610	**44.8573**	20.2910	
SSIM	0.9833	0.9740	**0.9914**	0.8330	
(4) MSE	3.17e-05	**1.35e-05**	1.56e-04	2.10e-03	
PSNR	41.6272	**48.6831**	38.0673	26.8574	
SSIM	0.9848	**0.9943**	0.9618	0.9702	

Small sample learning

A general strategy: incorporating domain-specific insights with neural networks to improve learning performance

- Data preprocessing: extract features
- Loss function
- Enhancement layer

Table 7
Average scores produced by approaches trained in various sizes of training dataset

	Exps	MSE				PSNR				SSIM			
		15	30	45	60	15	30	45	60	15	30	45	60
(1)	DA1+$\mathcal{L}$[illegible]	6.58e-04	5.22e-04	4.15e-04	3.53e-04	34.0160	35.7825	36.3553	37.0596	0.9346	0.9532	0.9675	0.9706
(2)	DA2+$\mathcal{L}$[illegible]	5.11e-04	4.09e-04	3.27e-04	2.92e-04	35.9458	36.7689	37.3525	38.7153	0.9505	0.9668	0.9736	0.9745
(3)	DA1+$\mathcal{L}$[illegible]	3.81e-04	2.89e-04	2.56e-04	2.06e-04	37.1495	38.8175	39.4175	40.7226	0.9675	0.9762	0.9793	0.9820
(4)	DA2+$\mathcal{L}$[illegible]	2.97e-04	2.48e-04	2.05e-04	1.82e-04	37.7448	39.2996	40.3217	42.4082	0.9690	0.9786	0.9814	0.9882

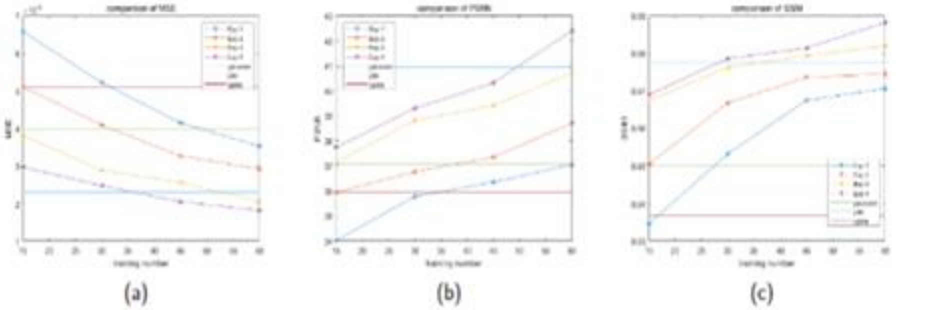

Figure 15: performance curves of MSE, PSNR and SSIM vs data amounts on different experimental settings (a) Performance curves of MSE. (b) Performance curves of PSNR. (c) Performance curves of SSIM

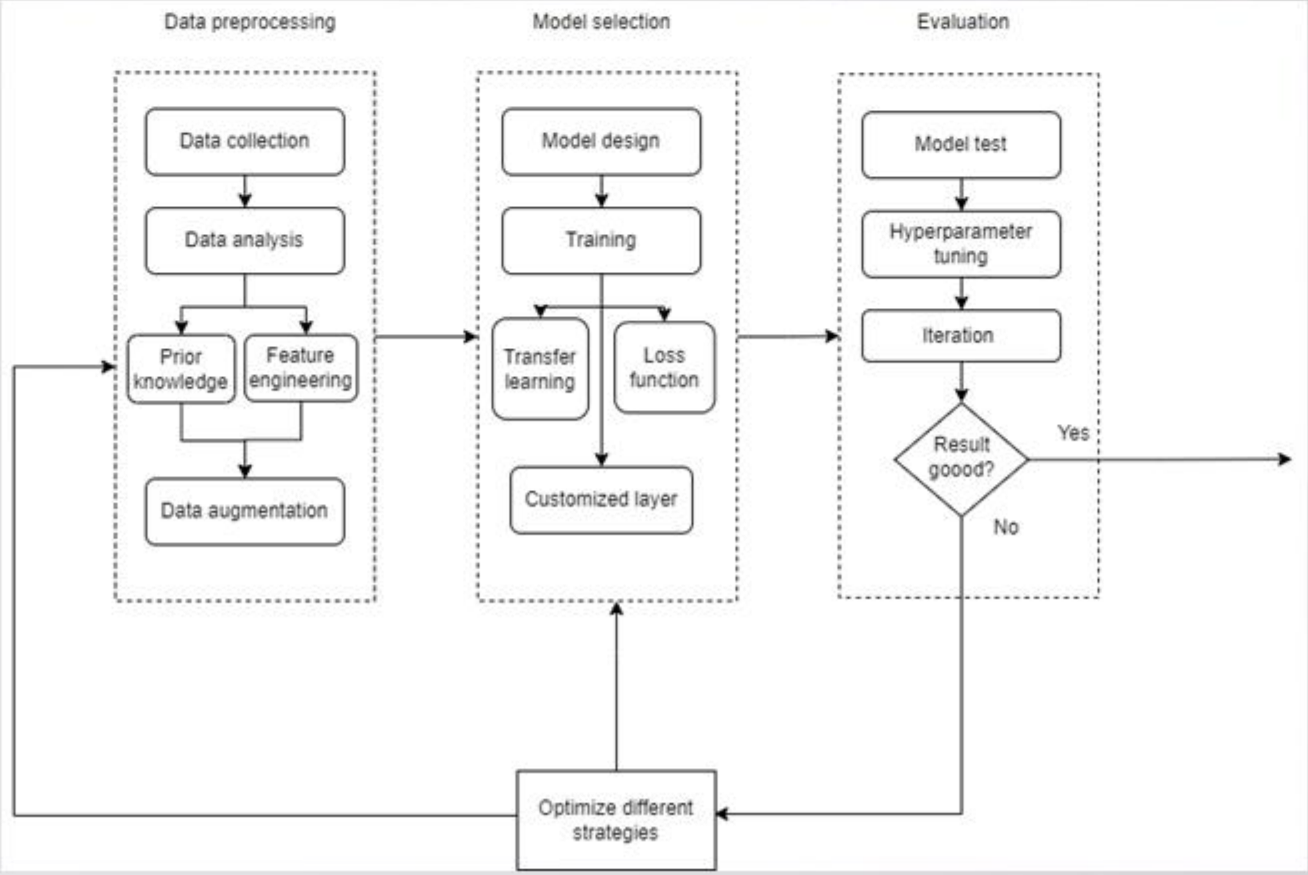

3. CPT Recent Development

- Triangular-mesh based surface characterisation techniques utilising XCT data

Co-funded by
the European Union

Mesh-based surface texture characterisation

- General framework

$\boldsymbol{r}(u, v)$

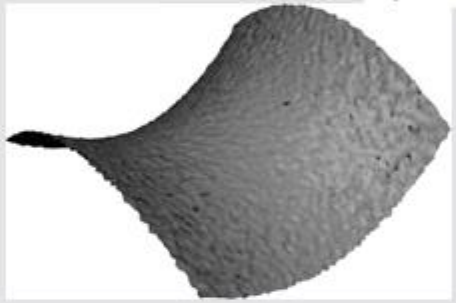

$\boldsymbol{r}_{form}(u, v)$

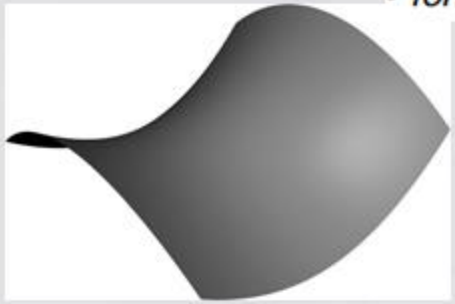

$\boldsymbol{r}_{sl}(u, v)$

Stage 1: Measured Surface(sampling and representation) → Stage 2: Surface Decomposition and Reconstruction → Stage 3: Surface analytics and parameterisation

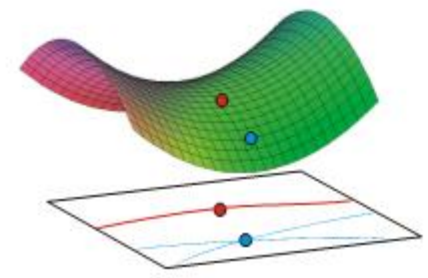

A non-Euclidean geometry

Association

Nominal form is known
- Best fit surface based on the nominal form
- Orthogonal distance
- Usually one that works in two stages: a coarse approximation fit, followed by a more refined optimised fit

Filtration

Nominal form is unknown
- filtration operator that does not require a reference surface can be used to determine the reference surface
- Morphological;
- Laplacian;
- MCF;
- etc..

Co-funded by the European Union

Mesh-based 3D surface texture characterisation

- Decomposition - association

$$\boldsymbol{r}(u,v) = \boldsymbol{r}_{form}(u,v) + \boldsymbol{r}_{sl}(u,v)\sim$$

$$\boldsymbol{r}(u,v) = \boldsymbol{r}_{form}(u,v) + r_{sl}(u,v) \cdot \boldsymbol{n}_f(u,v)$$

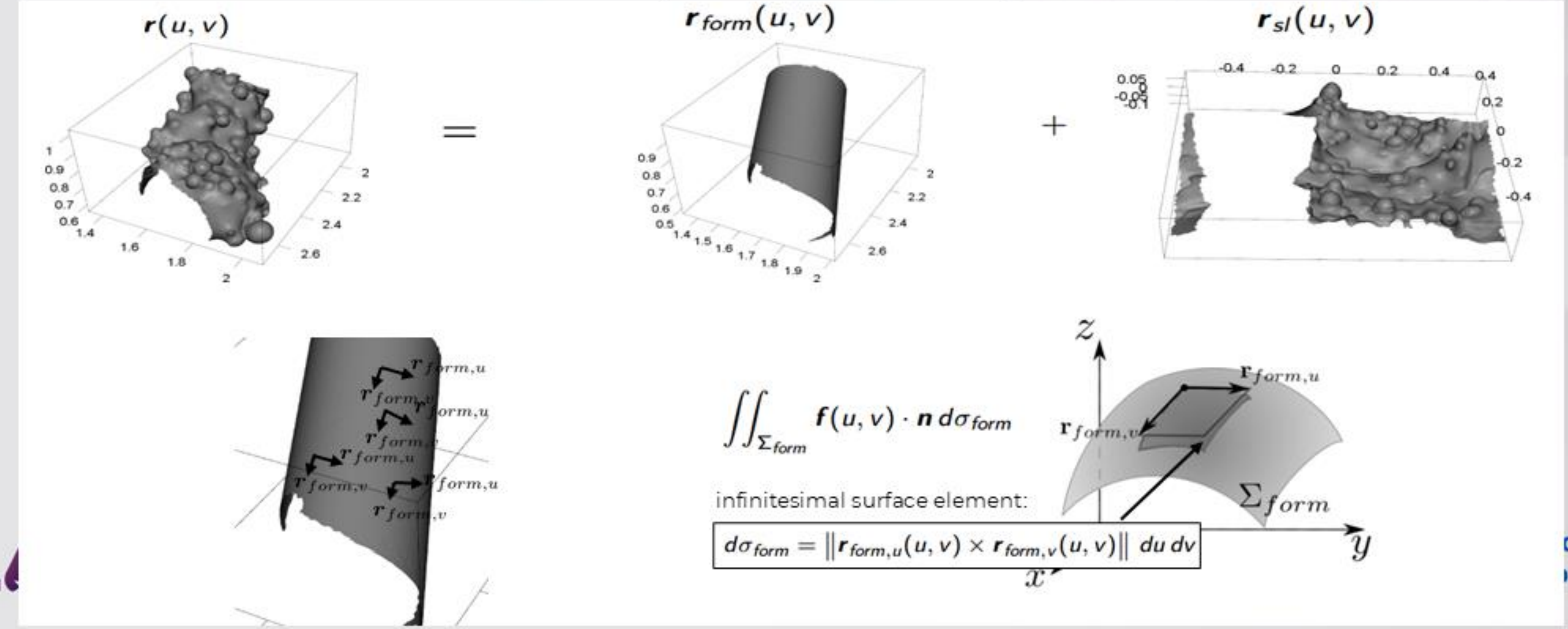

Mesh-based 3D surface texture characterisation

- Association

$$\hat{\boldsymbol{\beta}} = arg\ min_{\boldsymbol{\beta}} \sum_{i=1}^{n} \left(\boldsymbol{x}_i - \boldsymbol{f}(\boldsymbol{\beta}, \boldsymbol{x}_i)\right)^2$$

Total Least square

$$\hat{\boldsymbol{\beta}} = arg\ min_{\boldsymbol{\beta}} \sum_{i=1}^{n} w_i \cdot \left(\boldsymbol{x}_i - \boldsymbol{f}(\boldsymbol{\beta}, \boldsymbol{x}_i)\right)^2$$

$$w_i = \frac{1}{k} \sum_{j \in N_i} A_j$$

Weighted Total least square

$$\hat{\boldsymbol{\beta}} = arg\ min_{\boldsymbol{\beta}} \sum_{i=1}^{n} \rho_i \left(w_i \cdot \left(\boldsymbol{x}_i - \boldsymbol{f}(\boldsymbol{\beta}, \boldsymbol{x}_i)\right)^2\right)$$

Robust Total least square

cylinder

$$\min_{r, \boldsymbol{x}_0, \boldsymbol{a}} \sum_{i=1}^{n} w_i \cdot [r - \|\boldsymbol{x}_i - \boldsymbol{x}_0 + (\boldsymbol{x}_i - \boldsymbol{x}_0) \cdot \boldsymbol{a}\|]^2.$$

sphere

$$\min_{r, \boldsymbol{x}_0} \sum_{i=1}^{n} w_i \cdot (r - \|\boldsymbol{x} - \boldsymbol{x}_0\|)^2.$$

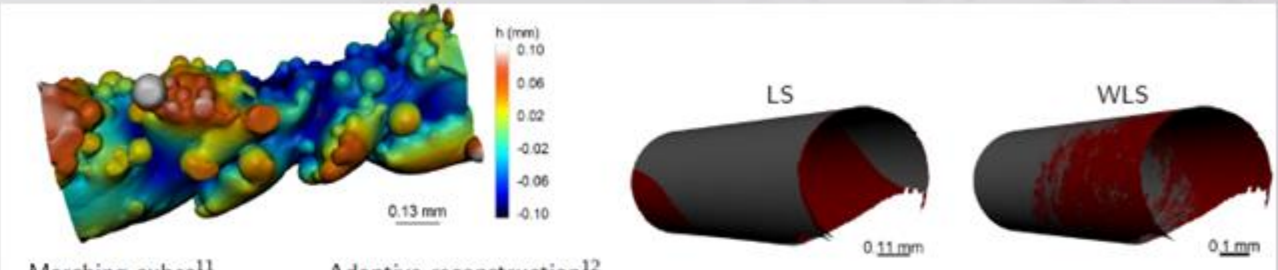

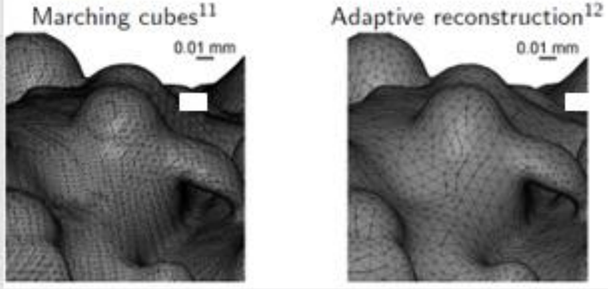

Fitting method	LS		WLS	
Reconstruction method	MC	AR	MC	AR
Radius (µm)	209.35	205.08	209.24	209.28
Diff (%)	-	2.08	-	0.02

FLASH

Mesh-based 3D surface texture characterisation

- Surface decomposition - Laplacian filtration

$$\frac{\partial f(p,t)}{\partial t} - \Delta f(p,t) = 0$$

$$t \approx 0.0176\lambda_c^2$$

Diffusion time: 0.1126s
Gaussian cutoff wavelength: 0.8 mm

$$\mathbf{p}_i := \begin{cases} \frac{1}{|adj(i)|}\sum_{j\in adj(i)} \mathbf{q}_j, & i \in V_{var}, \\ \mathbf{q}_i, & i \in V_{fix}. \end{cases}$$

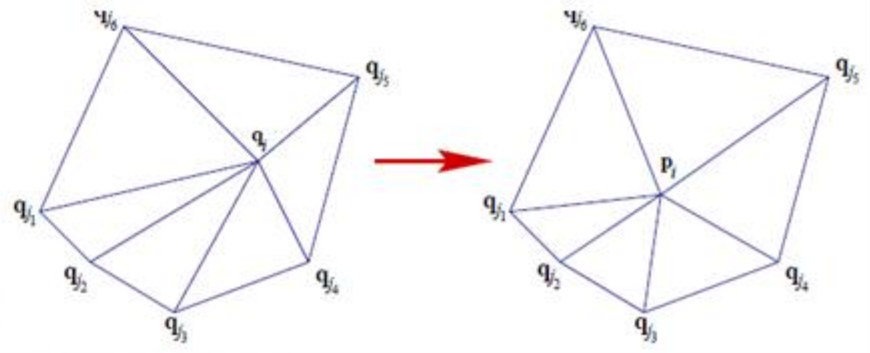

F

Improved LBO using weighted average of the neighborhood vertex, such as Gaussian weighting depends on the triangle area or the edge length.

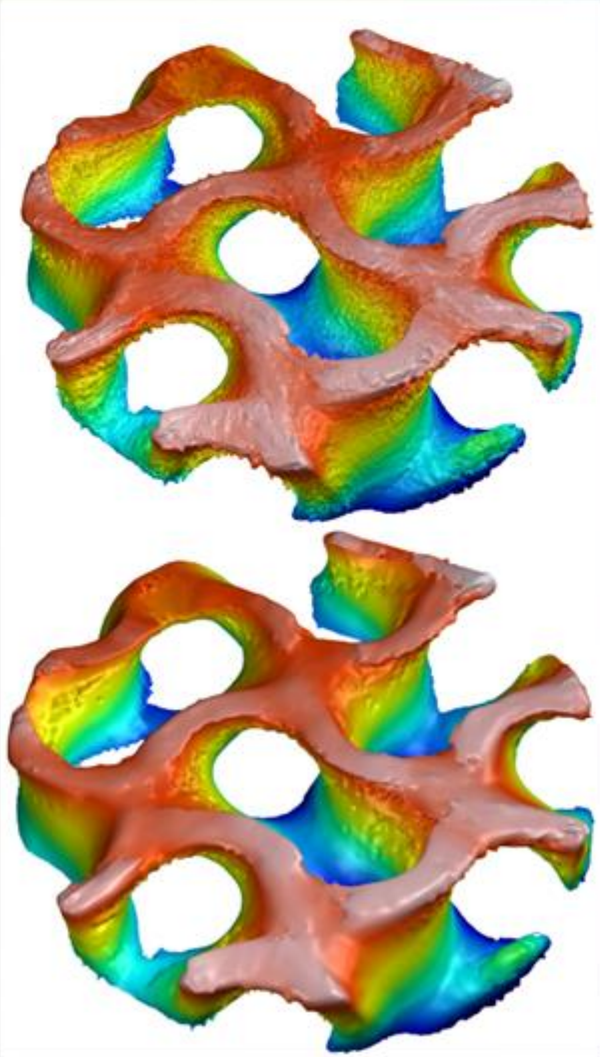

Advantages:

- Easy to implement;
- Fast;
- Direct link between the LBO and the Gaussian filter

Disadvantages:

- Shrinkage problems;
- Boundary problem;

Improved LBO diffusion

- No shrinkage;
- No boundary problem;
- Meet the requirement for metrology

Co-funded by the European Union

Mesh-based 3D surface texture characterisation

- Surface decomposition – 3D watershed segmentation

A portion of the measured AM lattice structure

Reference form computed by morphological operations

Residuals displayed as the signed distance colourmap

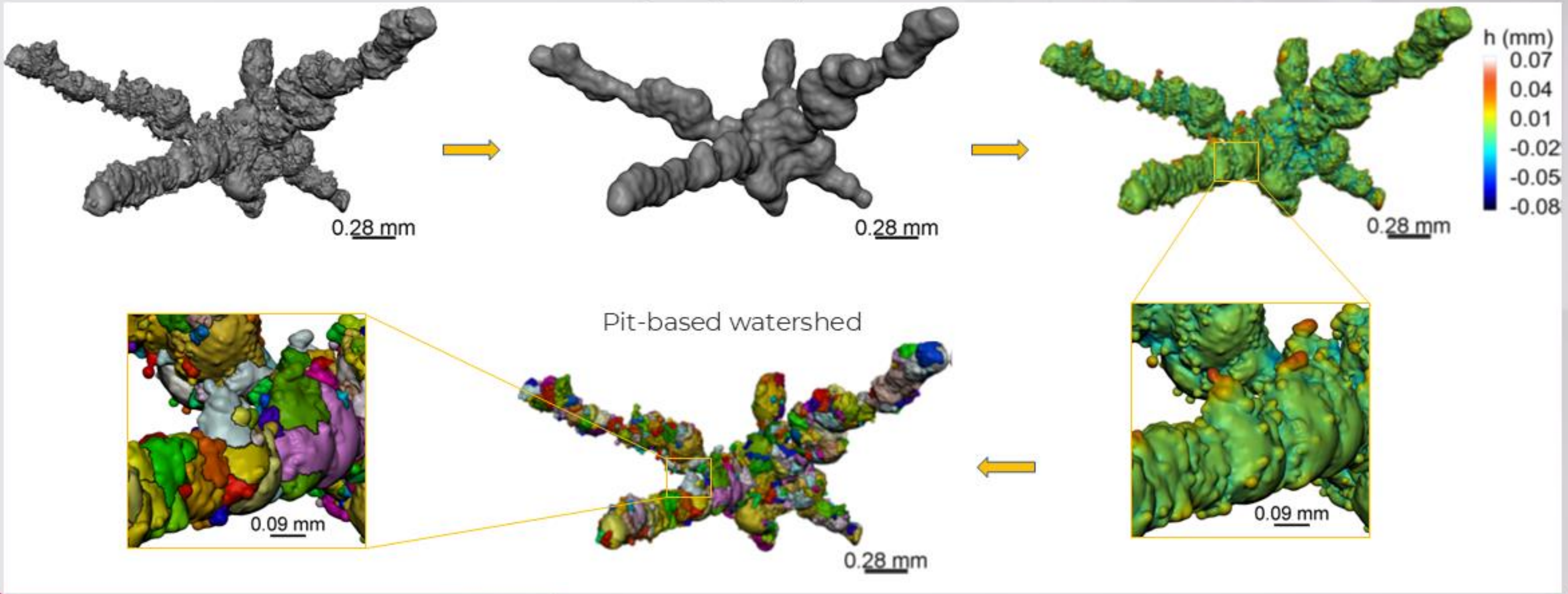

Mesh-based 3D surface texture characterisation

- Surface parameterisation - Height parameters

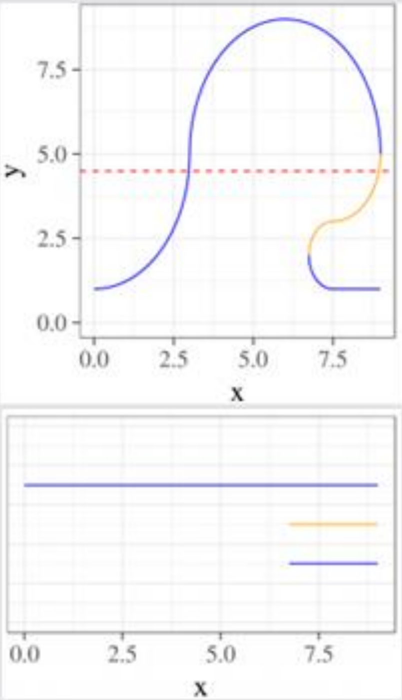

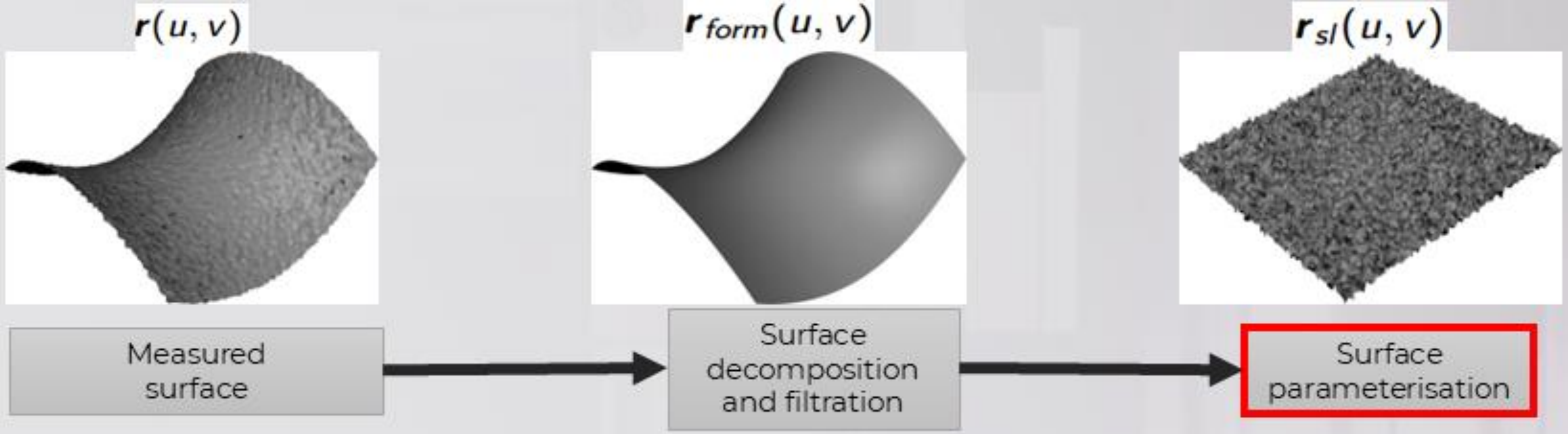

	ISO 25178-2		Proposed
A	$(x_1 - x_0) \cdot (y_1 - y_0)$	$\rightarrow$	$\iint_{\Sigma_{form}} d\sigma_{form}$
Sa	$\frac{1}{A}\int_{x_0}^{x_1}\int_{y_0}^{y_1} \lvert z(x,y)\rvert \, dx\, dy$	$\rightarrow$	$\frac{1}{A}\iint_{\Sigma_{form}} \lvert \boldsymbol{r}_{sl}(u,v)\cdot \boldsymbol{n}_{form}(u,v)\rvert \, d\sigma_{form}$
Sq	$\sqrt{\frac{1}{A}\int_{x_0}^{x_1}\int_{y_0}^{y_1} z^2(x,y)\, dx\, dy}$	$\rightarrow$	$\sqrt{\frac{1}{A}\iint_{\Sigma_{form}} (\boldsymbol{r}_{sl}(u,v)\cdot \boldsymbol{n}_{form}(u,v))^2 \, d\sigma_{form}}$
Ssk	$\frac{1}{A\, Sq^3}\int_{x_0}^{x_1}\int_{y_0}^{y_1} z^3(x,y)\, dx\, dy$	$\rightarrow$	$\frac{1}{A\, Sq^3}\iint_{\Sigma_{form}} (\boldsymbol{r}_{sl}(u,v)\cdot \boldsymbol{n}_{form}(u,v))^3 \, d\sigma_{form}$
Sku	$\frac{1}{A\, Sq^4}\int_{x_0}^{x_1}\int_{y_0}^{y_1} z^4(x,y)\, dx\, dy$	$\rightarrow$	$\frac{1}{A\, Sq^4}\iint_{\Sigma_{form}} (\boldsymbol{r}_{sl}(u,v)\cdot \boldsymbol{n}_{form}(u,v))^4 \, d\sigma_{form}$
Sp	$\lvert \max_{x,y} z(x,y)\rvert$	$\rightarrow$	$\lvert \max_{u,v} \boldsymbol{r}_{sl}(u,v)\cdot \boldsymbol{n}_{form}(u,v)\rvert$
Sv	$\lvert \min_{x,y} z(x,y)\rvert$	$\rightarrow$	$\lvert \min_{u,v} \boldsymbol{r}_{sl}(u,v)\cdot \boldsymbol{n}_{form}(u,v)\rvert$
Sz	$\max_{x,y} z(x,y) - \min_{x,y} z(x,y)$	$\rightarrow$	$\max_{u,v} \boldsymbol{r}_{sl}(u,v)\cdot \boldsymbol{n}_{form}(u,v) - \min_{u,v} \boldsymbol{r}_{sl}(u,v)\cdot \boldsymbol{n}_{form}(u,v)$

Mesh-based 3D surface texture characterisation

- Surface parameterisation - Hybrid parameters

$$Sdq = \sqrt{\frac{1}{A}\int_{x_0}^{x_1}\int_{y_0}^{y_1}\left(z_x^2 + z_y^2\right)\,dx\,dy} \rightarrow Sdq = \sqrt{\frac{1}{A}\iint_{\Sigma_{form}}\left\|\boldsymbol{J}_{form}\left(\boldsymbol{G}_{form}^{-1}\right)^T\boldsymbol{\nabla}_{\boldsymbol{u}} r_{sl}(u,v)\right\|^2 d\sigma_{form}}$$

$$Sdr = \frac{1}{A}\int_{x_0}^{x_1}\int_{y_0}^{y_1}\left(\sqrt{1 + z_x^2 + z_y^2} - 1\right)dx\,dy \rightarrow Sdr = \frac{1}{A}\left(\iint_U \|\boldsymbol{r}_u(u,v)\times\boldsymbol{r}_v(u,v)\|\,du\,dv - A\right)$$

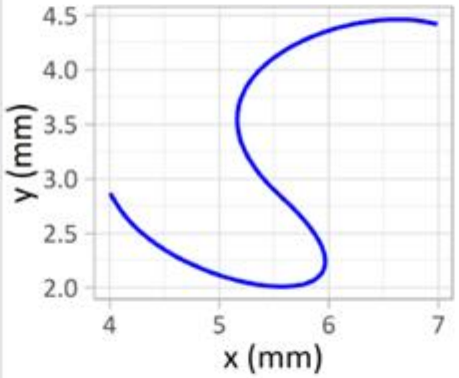

$\Rightarrow$

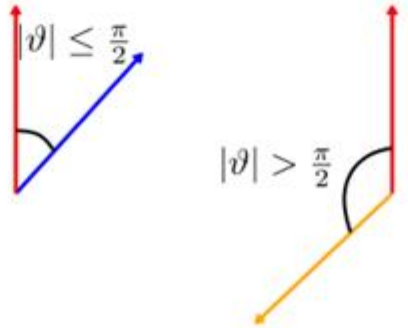

$\Rightarrow$

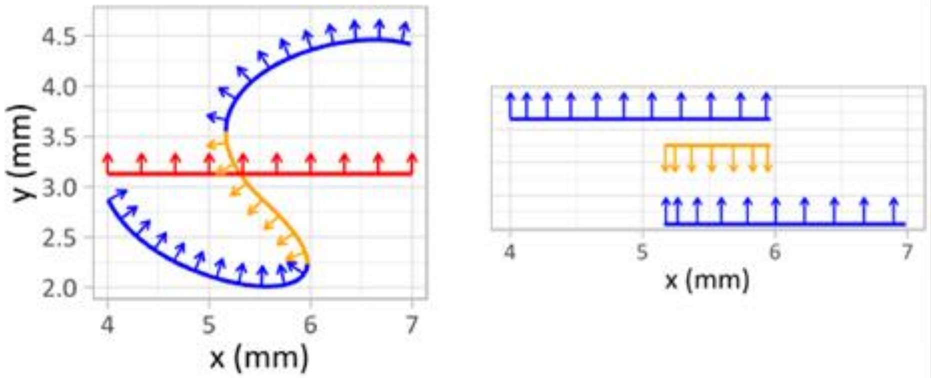

$$A_{shadow} = \iint_{\Sigma_{form}} k(u,v)\,d\sigma_{form} \quad Sdr' = \frac{A - A_{shadow}}{A_{shadow}} \quad Srf = \frac{A - A_{shadow}}{2\,A_{shadow}}$$

Mesh-based 3D surface texture characterisation

- Surface parameterisation - Functional parameters

$$V = \iint_{\Sigma'_{form}} k(u,v) \cdot h(u,v) \quad d\sigma'_{form}$$

$V = V_1 + V_2$

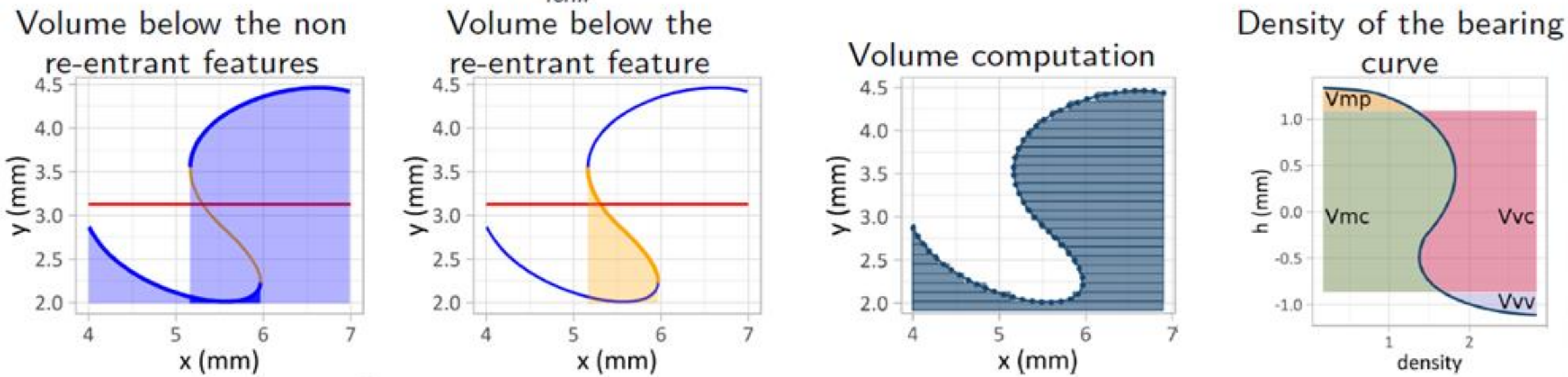

$$Vm(p) = \frac{h_{max} - h_{min}}{A_{max}} \int_p^1 f_V(h^*)\, dh^*, \qquad Vv(p) = \frac{h_{max} - h_{min}}{A_{max}} \int_0^p f_{V,max}(h^*) - f_V(h^*)\, dh^*$$

where A_{max} is the maximum section area

Co-funded by the European Union

3. Case Studies

- Impact of surface orientation on multi-scale geometries of LPBF components
- Utilisation of XCT for surface measurement of metal additive manufacturing components

Co-funded by the European Union

Case Study 1

- Impact of building orientation on multi-scale geometries of LPBF components

Co-funded by the European Union

Artefact design and surface measurement

- Truncheon artefact

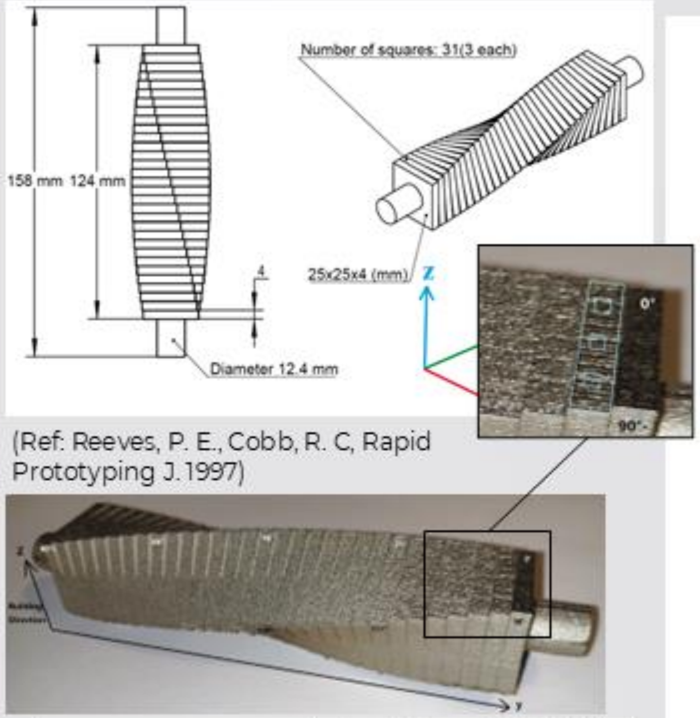

(Ref: Reeves, P. E., Cobb, R. C, Rapid Prototyping J. 1997)

Process	Renishaw 400 SLM
Laser power	110 w
Scan speed	5000 mm/s
Hatch spacing	110 µm
Layer thickness	50 µm
Powder	SS 316L

Up-skin (0°-45°) Up-skin (45°-90°) Down-skin (90°-132°)

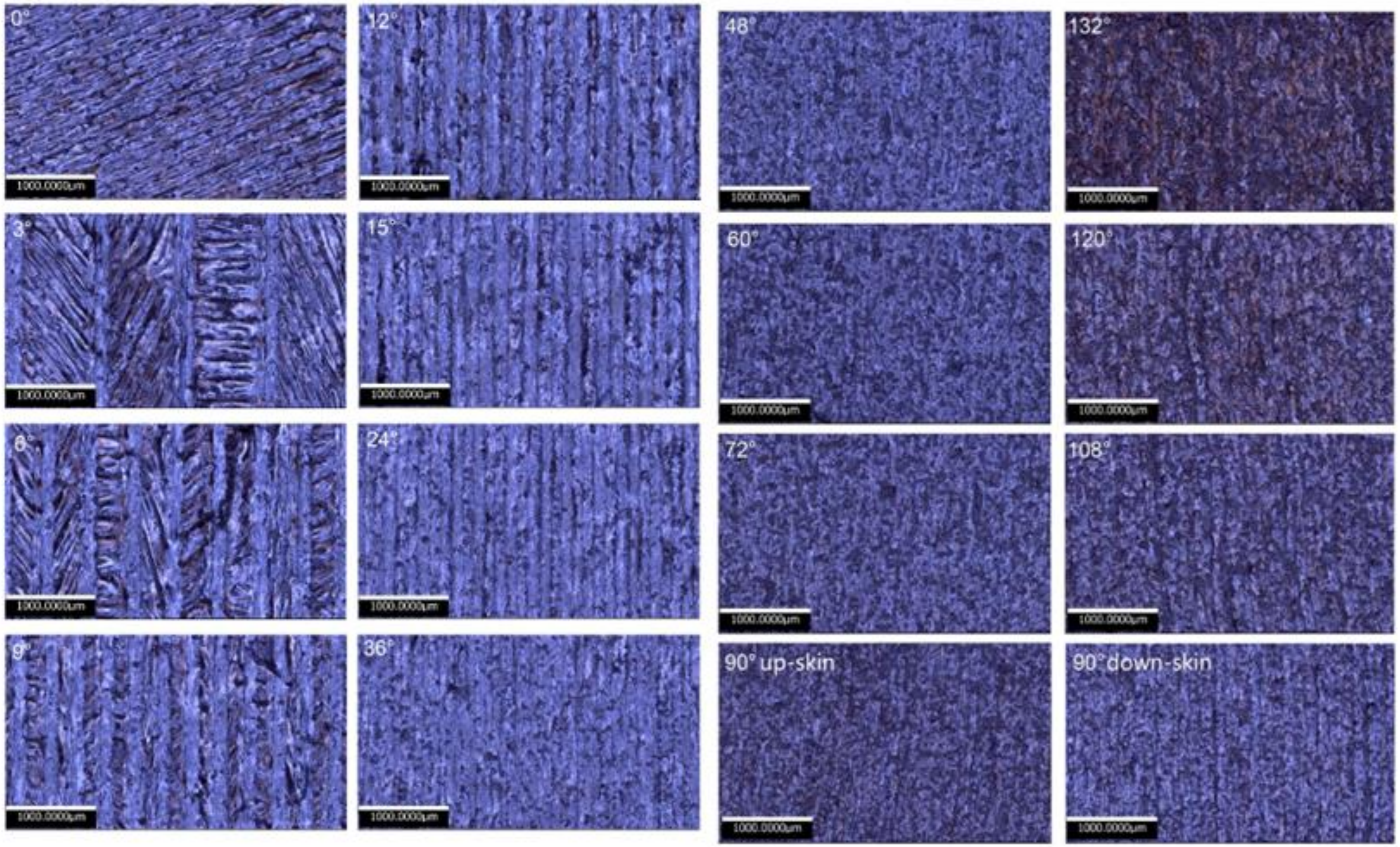

Staircase modelling & surface characterisation protocol

- Staircase effect & its prediction model based on trigonometry

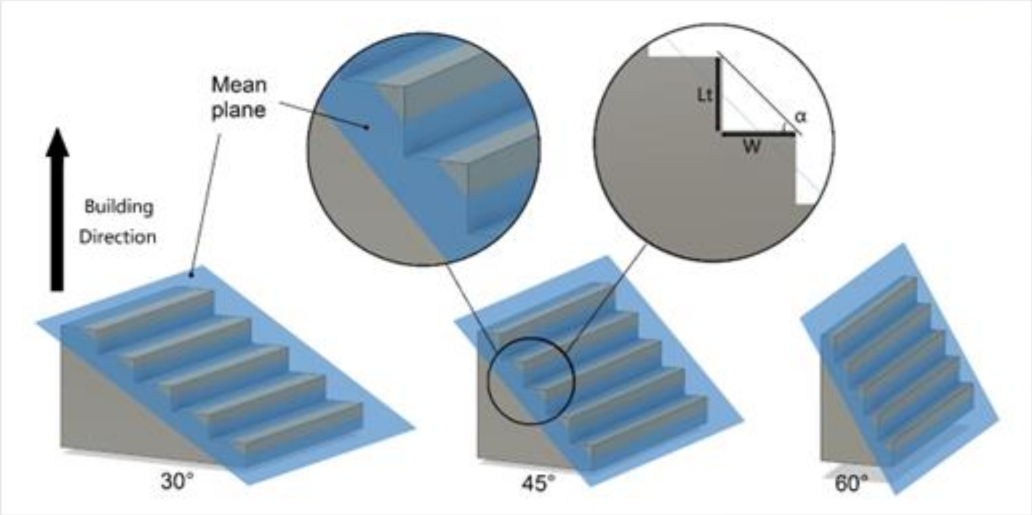

$$\mathrm{Ra} = \frac{1}{4} L_t \cos(\alpha)$$

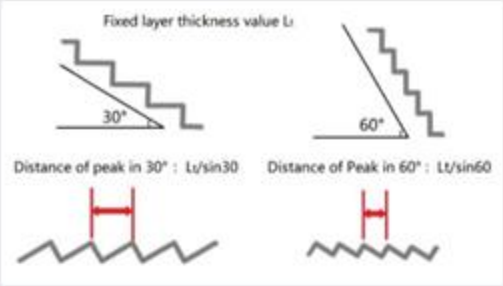

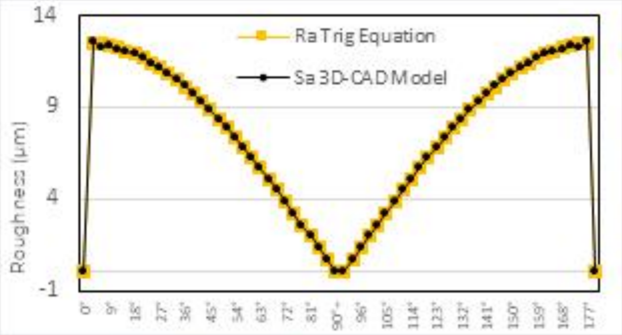

- Separation of staircase and particles

Robust Gaussian filter (λc 80 µm)

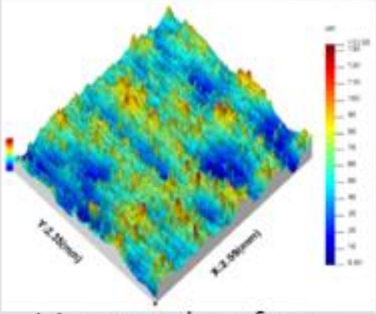

Measured surface

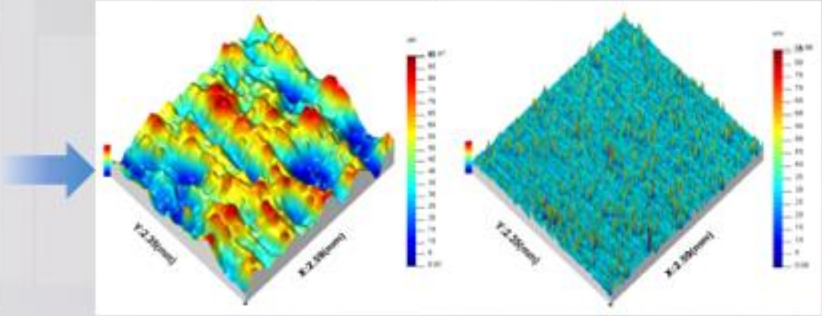

Staircase surface Particle surface

- Areal surface texture parameters

Categories	Surface texture parameters
Height Parameters	**Sa** (µm) -Arithmetical mean height of the scale-limited surface
	Sq (µm) -Root mean square height of the scale-limited surface
	Ssk -Skewness of the scale-limited surface
	Sku- Kurtosis of the scale-limited surface
Hybrid Parameters	**Sdq** -Root mean square gradient of the scale-limited surface
	Sdr (%) -Developed interfacial area ratio of the scale-limited surface
Functional parameters	**Smr1** (%) -Material ratio 1
	Vmp (mm^3/mm^2) -Peak material volume of the scale-limited surface
Spatial Parameters	**Sal** (µm) -Autocorrelation length (fastest decay to 0.2)
	Str -Texture aspect ratio
Feature parameters	**Spd** ($1/mm^2$) (Density of peaks) number of peaks per unit area
Particle analysis	Particle number/density/coverage

Surface parameterisation

- Height parameters

Sa

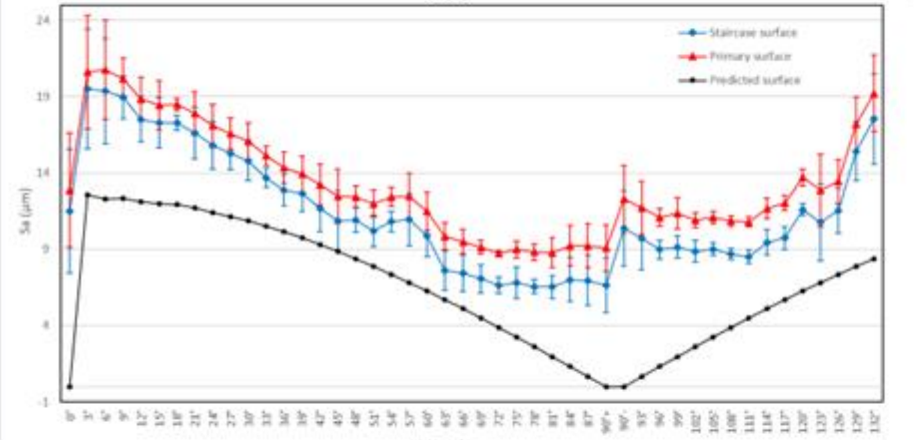

Sq

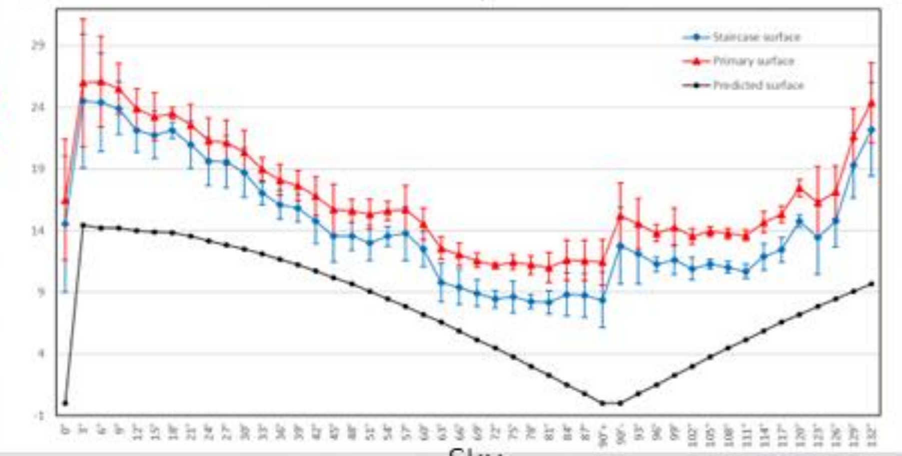

Ssk

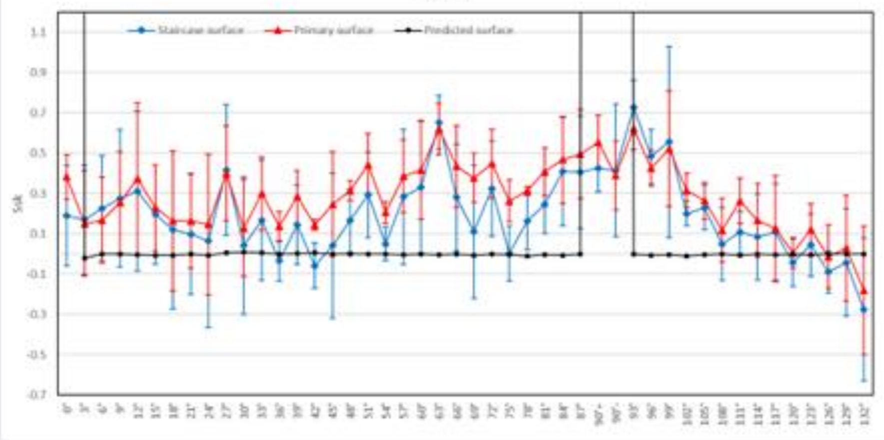

Sku

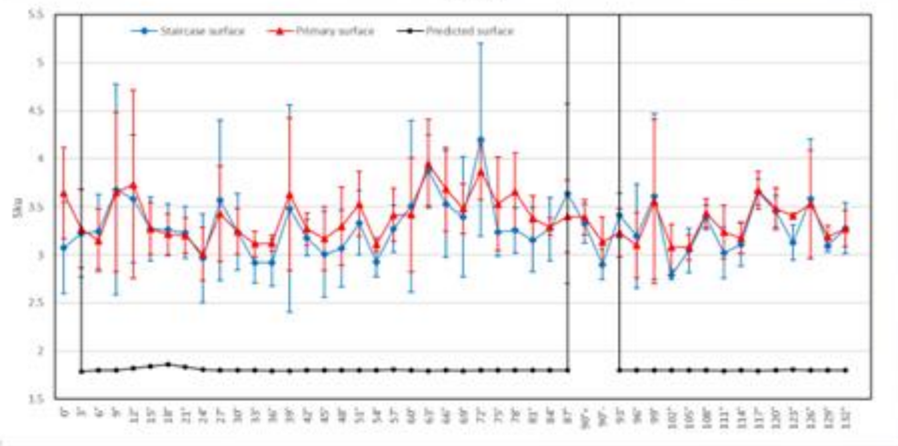

1) Changing trend aligns with the prediction model
2) Sa, Sq: staircase effect is the major contributor;
3) Sa, Sq: down-skin surface roughness is higher than the up-skin surface, due to the elevated temperature, e.g. down-skin 90° about 140% higher than up-skin 90°
4) Ssk: positive (<114°); surface is dominated by peak features
5) Sku: stable, slightly above 3; height distribution is basically normal distribution

Co-funded by the European Union

Surface parameterisation

- Spatial parameters

Sal

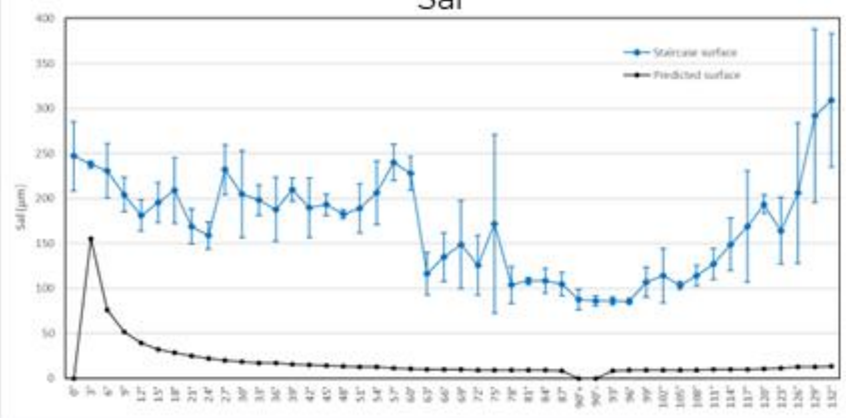

Str

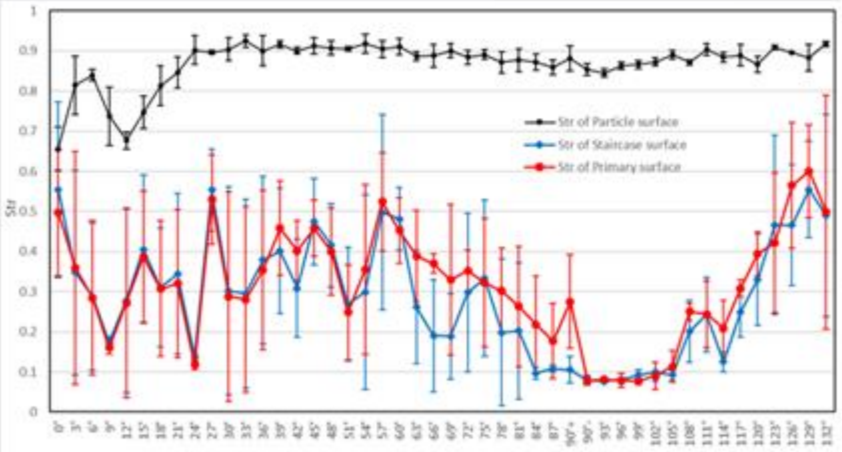

- Hybrid parameters

Sdr

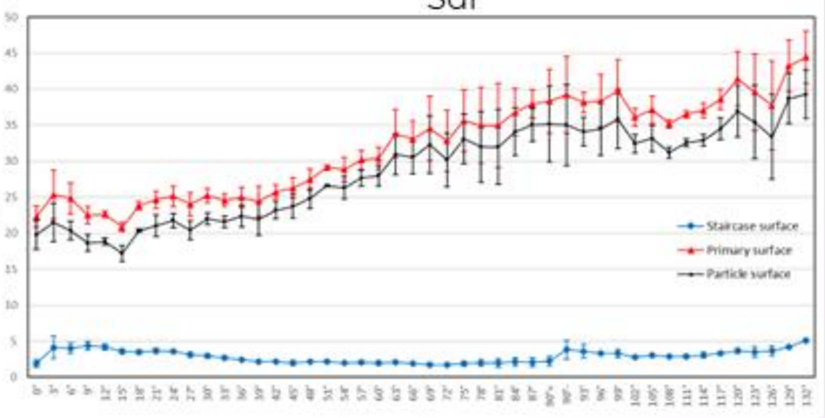

Sd
q

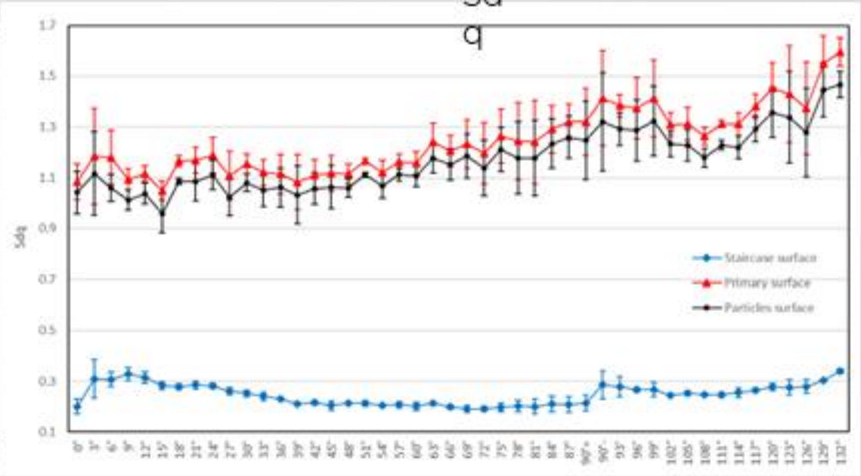

1) Sal: in general, decrease for the up-skin surfaces and increase for the down-skin surfaces; staircase is the major contributor
2) Str: a measure of uniformity of the surface texture; staircase is the major contributor
3) Sdr: general measure of surface area; increasing
4) Sdq: general measure of surface slope; increasing
5) Str, Sdq: particle features are the major contributor

Co-funded by the European Union

Surface characterisation: feature parameters

- Feature parameters

  Watershed segmentation, 5% Wolf pruning
  - Spd

- Particle analysis

  Threshold segmentation height threshold Smr1
  - Particle density ($1/mm^2$)
  - Number of particles
  - Particle coverage (%)

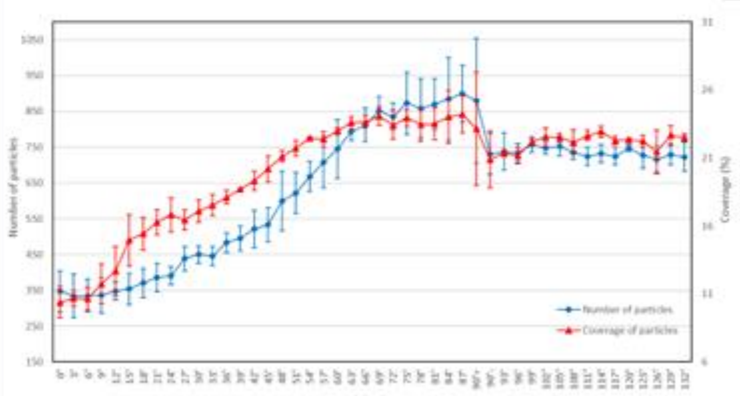

1) Spd: particle density increasing on the up-skin surface; slower decreasing with more variation on the down-skin surface
2) Higher Spd of 0° is attributed to the spatters on the horizontal surface
3) Down-skin surface: Spd decreases, Vmp increases -> number of big particles increases
4) Particle analysis descriptors consistent with Spd

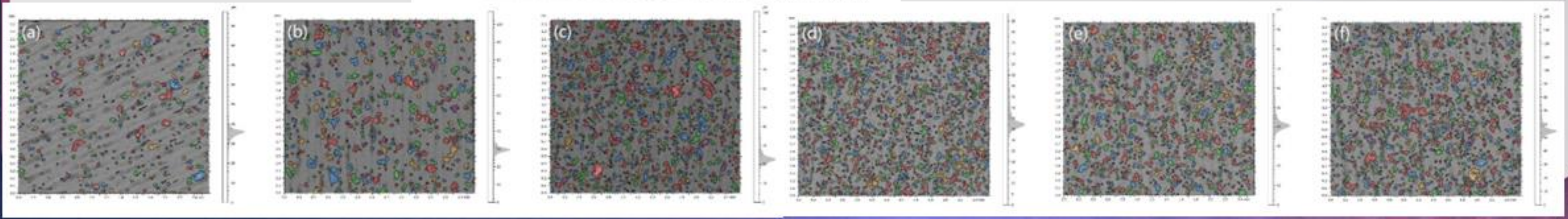

Follow-on: Impact of building orientation on surface roughness, sub-surface porosity, and dimensional accuracy of internal channels

- Artefact design

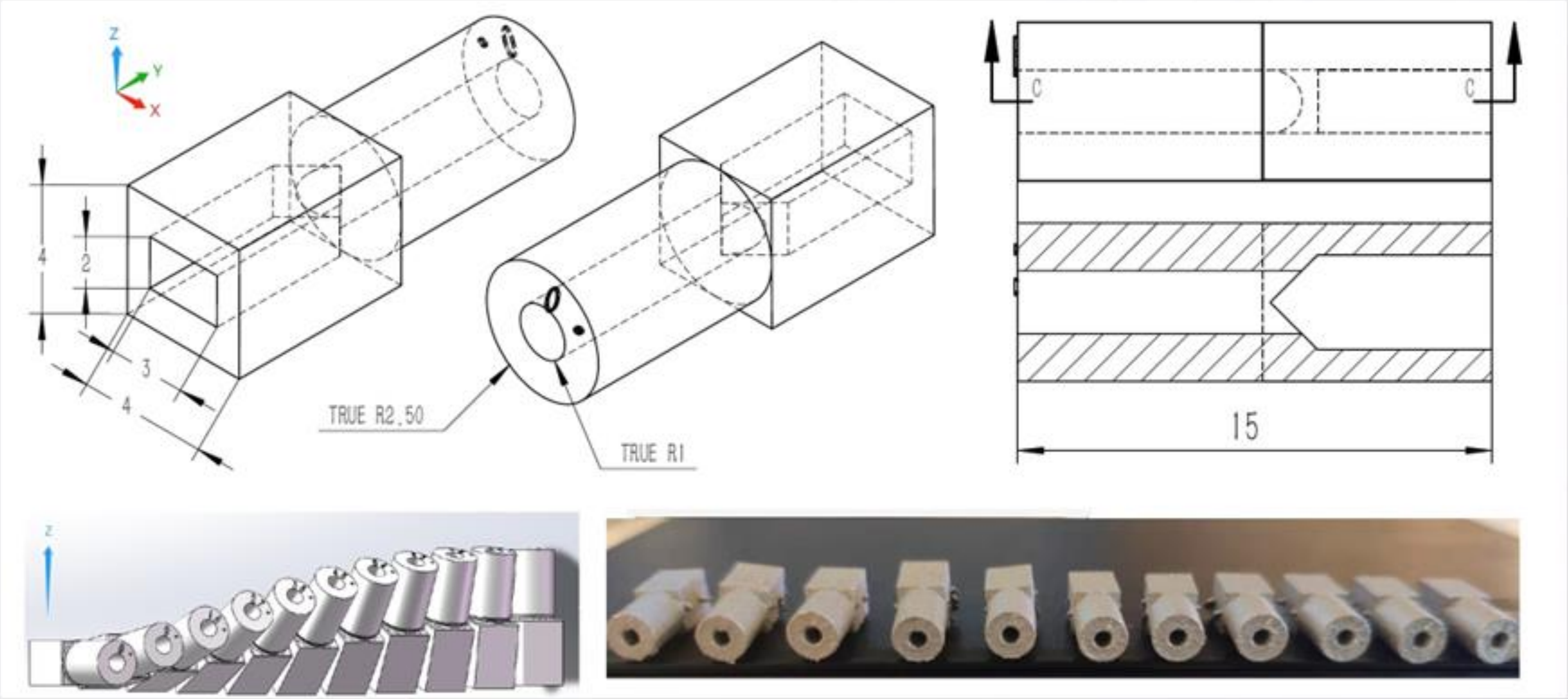

Co-funded by
the European Union

Sample design, fabrication and measurement

- XCT measurement configuration

  Measured by: Nikon XCT XTH 225

  Voltage: 163 kV

  Power: 13.2 W

  Voxel size: 20 µm

  Pre-filter: 0.5 mm Copper

  Reconstructed by: Nikon CT Pro SP2

  Surface determination: ISO 50 with Local iterative

- Surface texture characterisation

  Levelling applied to remove the form

  XCT low pass filter

  Parameterisation: *Sa, Spd, Sdr*

- Porosity (sub-surface)

  A depth 0.75 mm to the inner surface

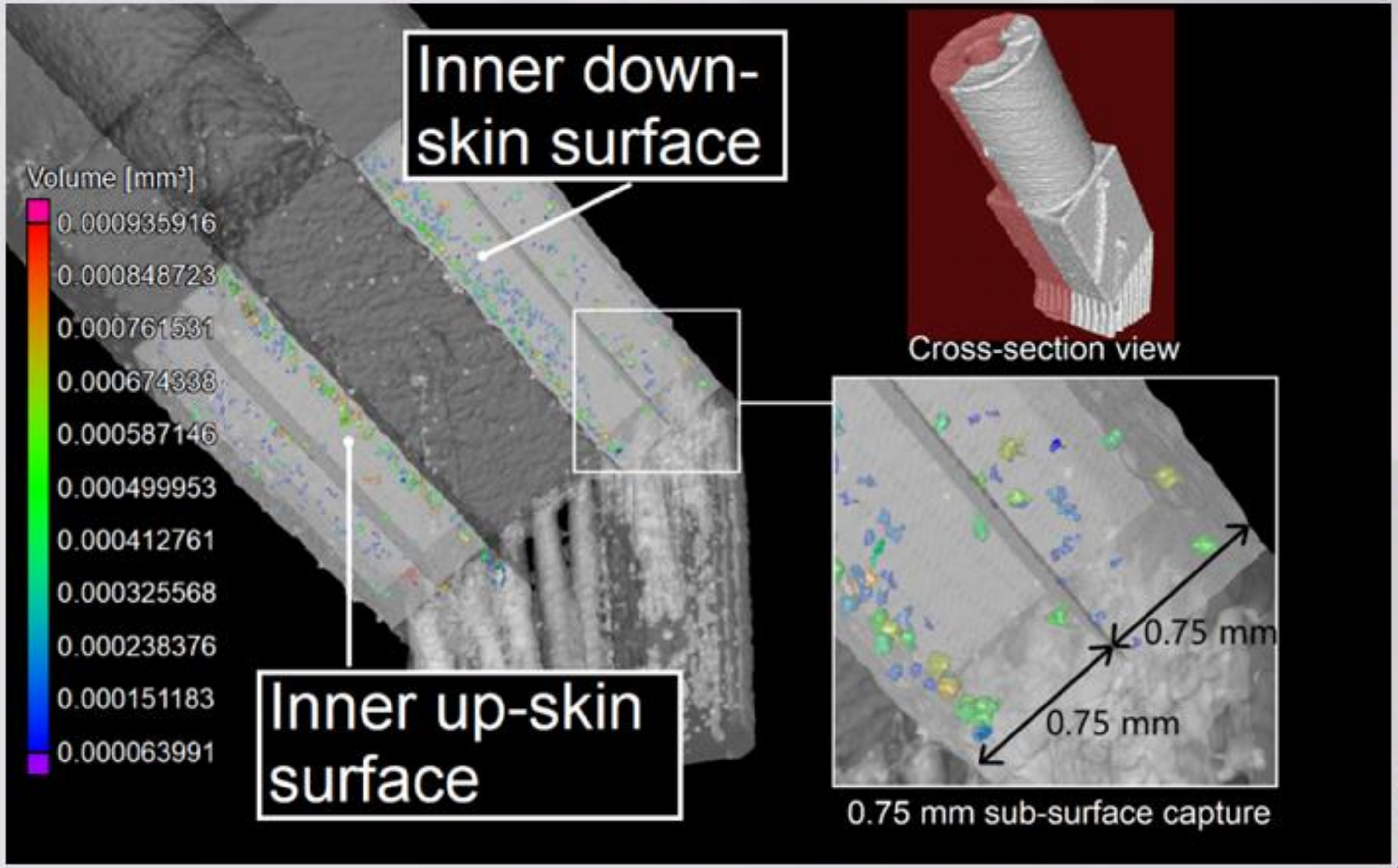

FLASH

Result and discussion: surface roughness

- Surface roughness – Sa

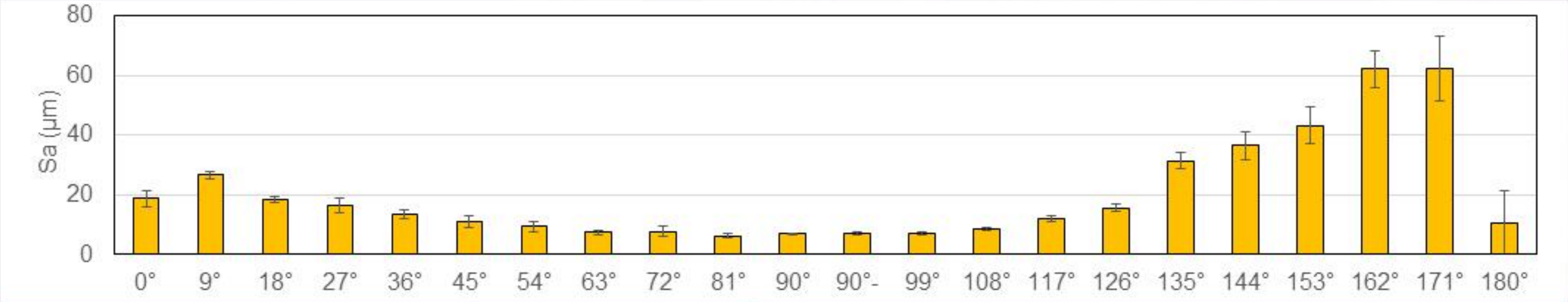

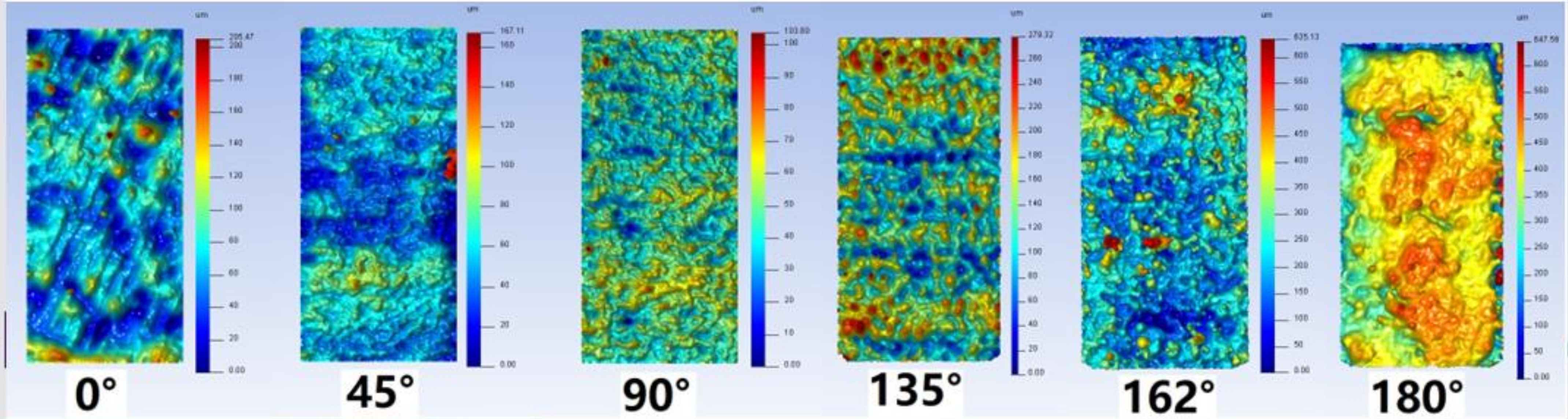

F... nion

Result and discussion: surface roughness

- Surface roughness – Spd (number of peaks per unit)

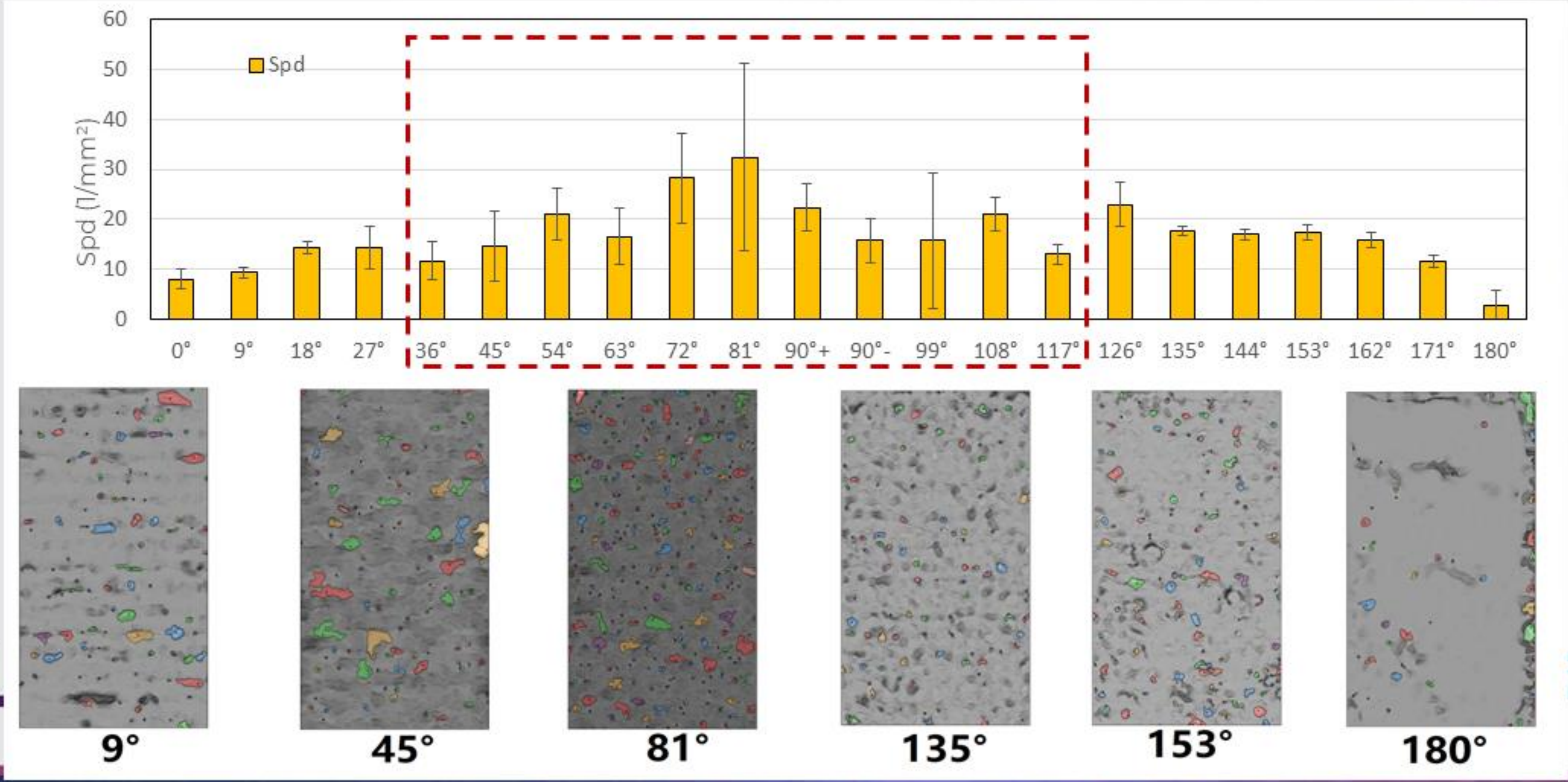

FL

y
n Union

Result and discussion: sub-surface porosity

- Sub-surface porosity

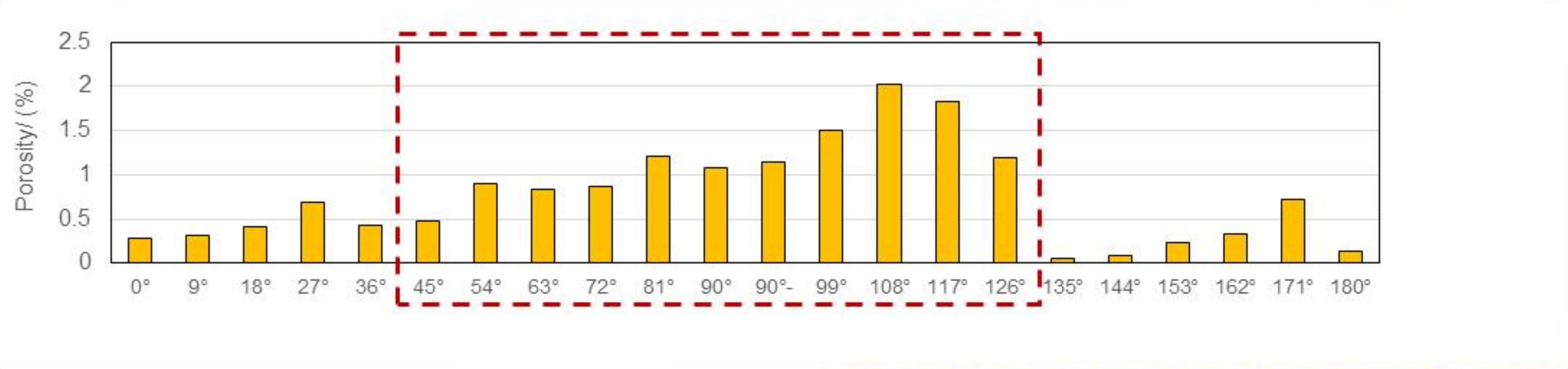

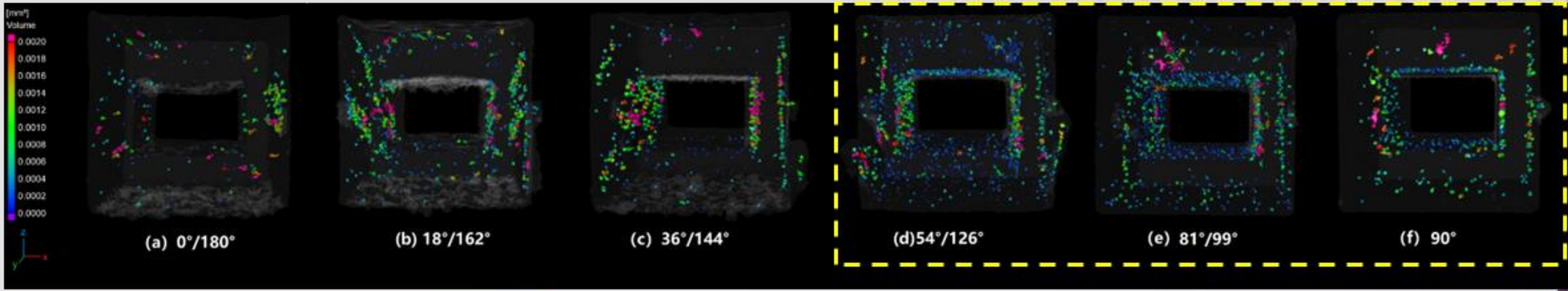

Result and discussion: correlation

- Correlation: roughness Sa/Spd/Sdr & porosity

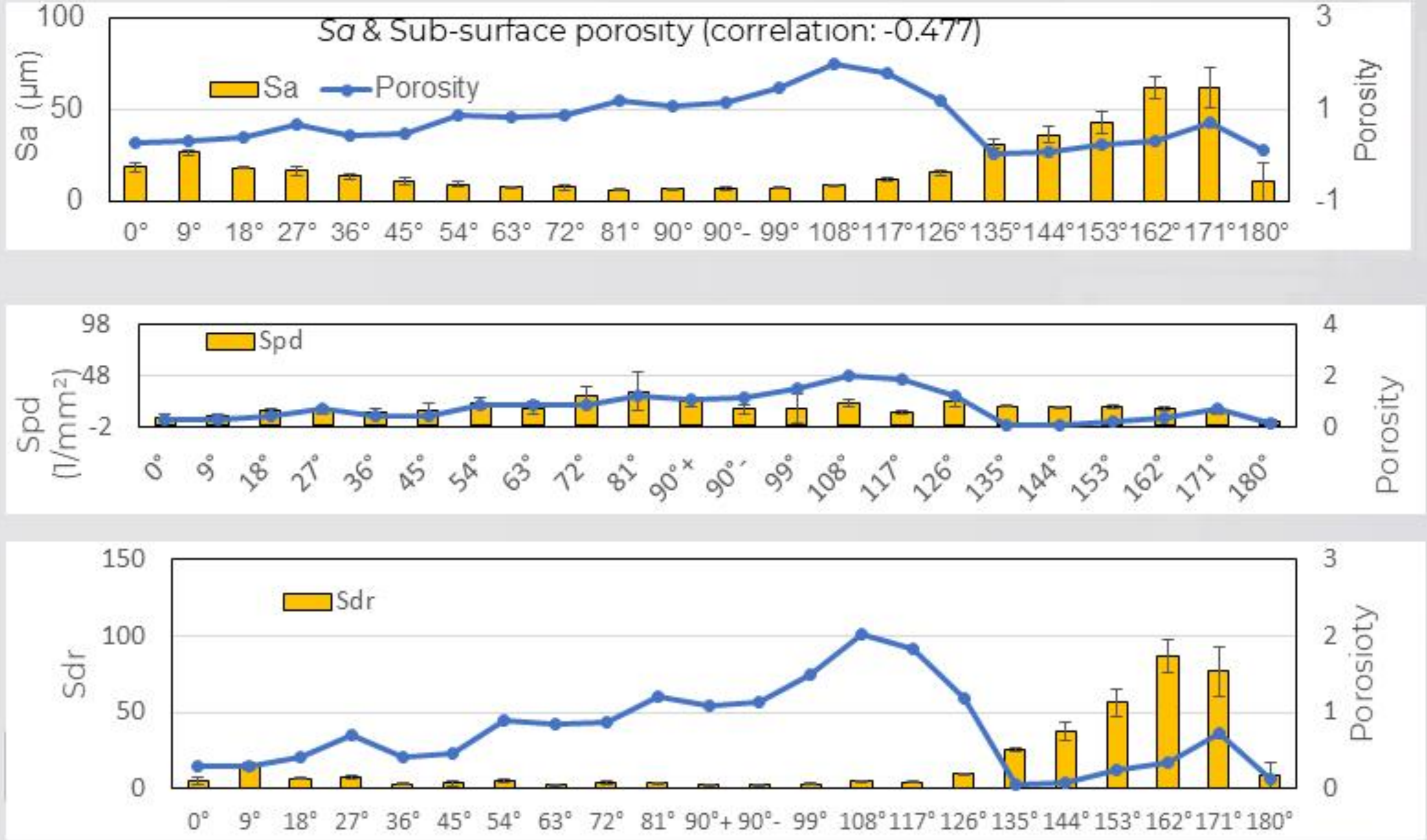

Correlation efficients	Porosity
Sa	-0.48
Sa (up-skin)	**-0.83**
Sa (down-skin)	-0.58
Spd	0.43
Spd (up-skin)	**0.90**
Spd (down-skin)	0.32
Sdr	-0.42
Sdr (up-skin)	-0.52
Sdr (down-skin)	-0.55

Co-funded by the European Union

Circular internal channels

- Data processing

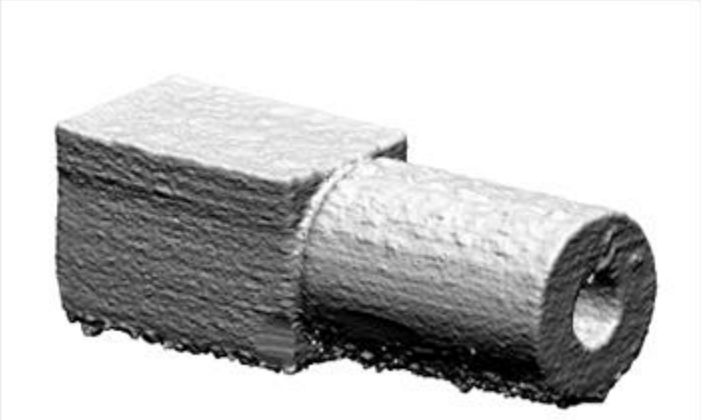

Measurement and reconstruction

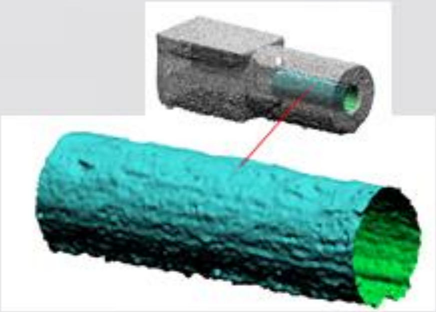

Extract internal channel

Extract profile for dimensional & shape deformation

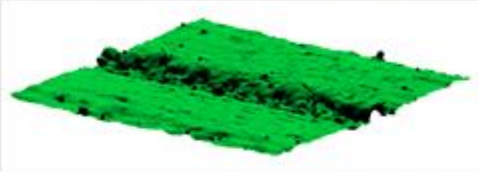

Unfold channel for surface roughness

Extract sub-surface volume

Sub-surface porosity analyses

Co-funded by the European Union

Circular internal channels

- Deviation against CAD

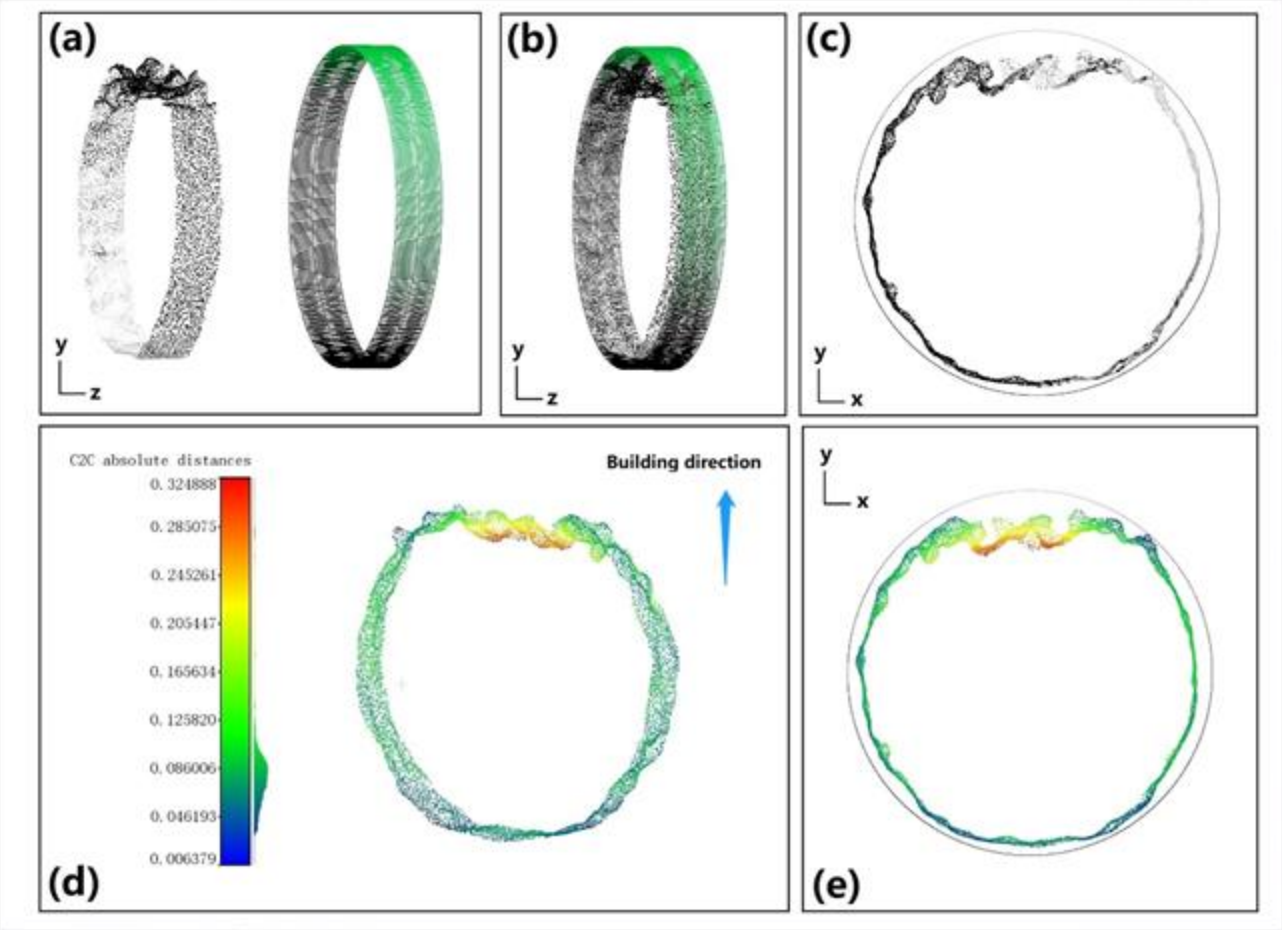

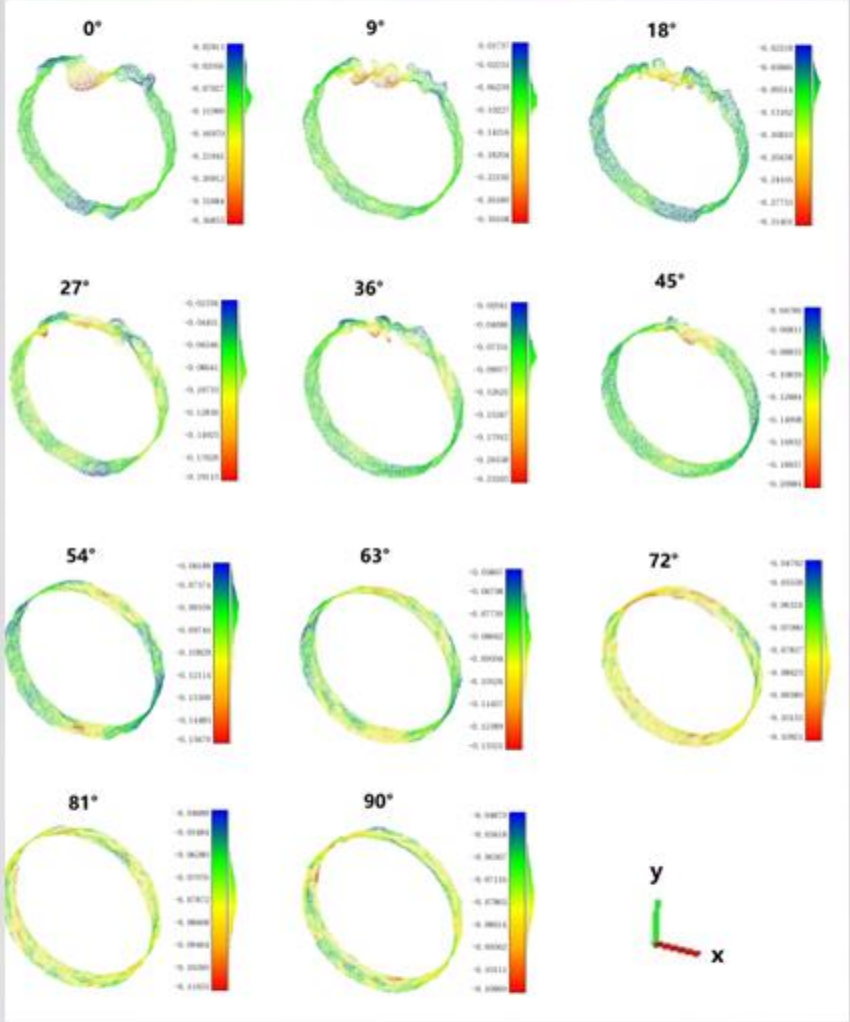

Result and discussion: dimensional accuracy, surface roughness, and sub-surface porosity

- Dimensional deviation

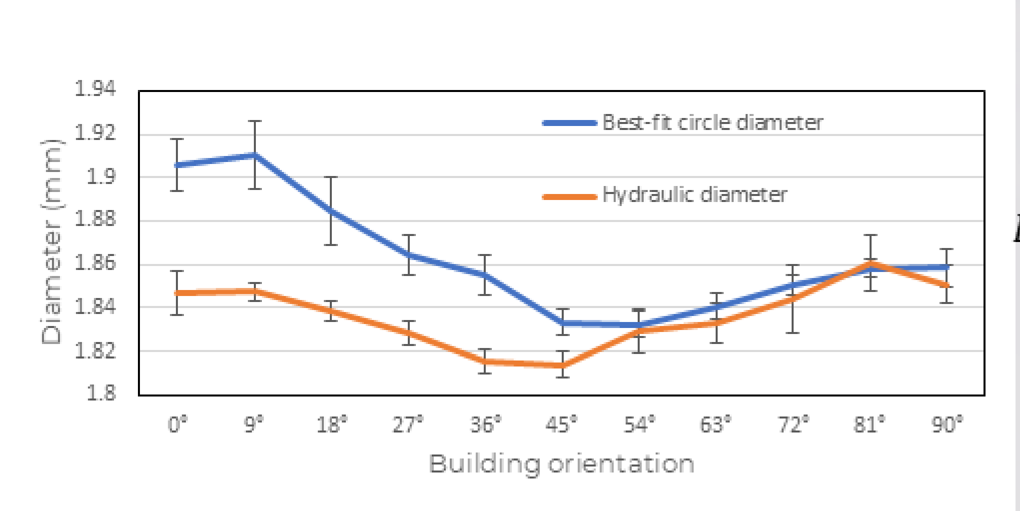

$$D_p = \frac{4A}{P}$$

- Surface roughness

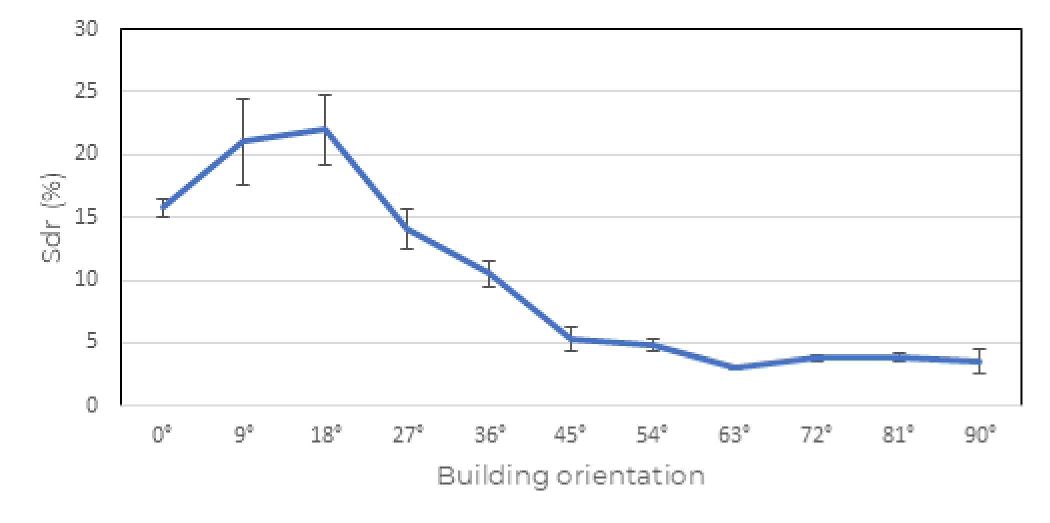

- Shape deformation (Ellipse minor/major)

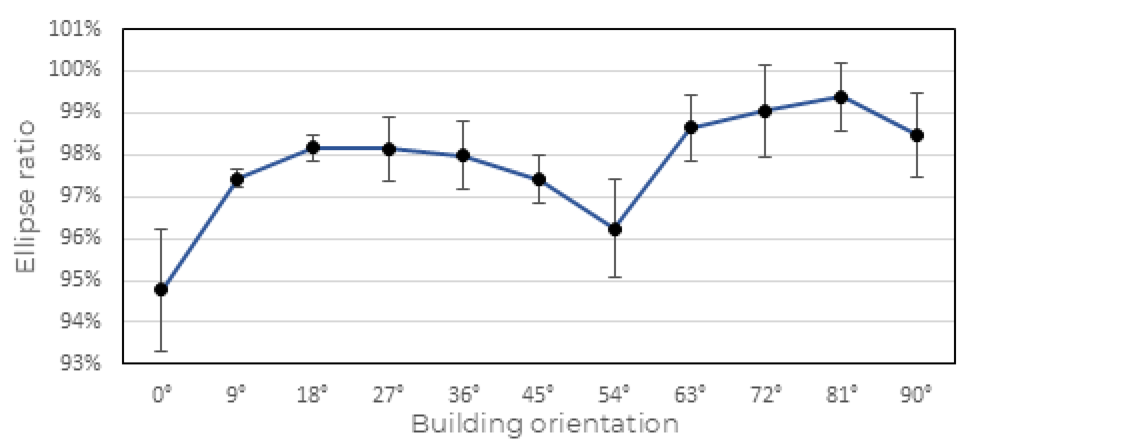

- Sub-surface porosity

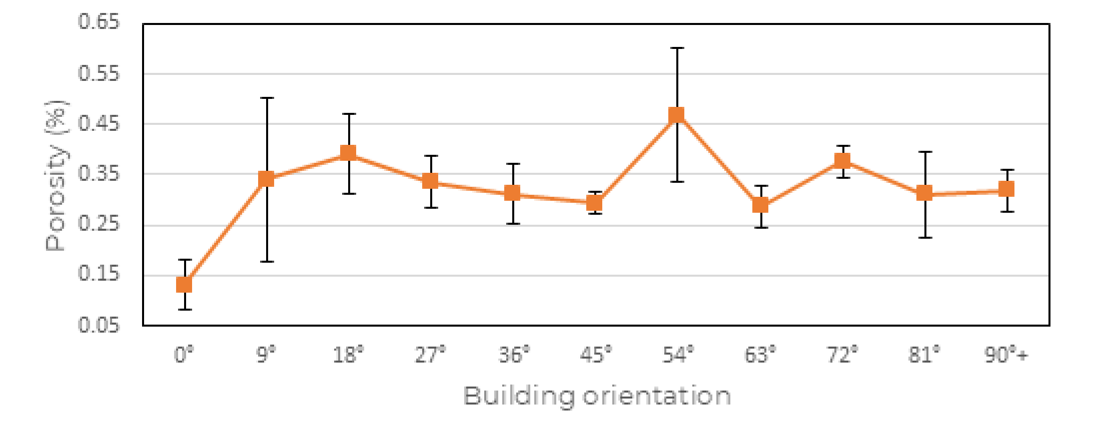

Case Studie 2

- Utilisation of XCT for surface measurement of metal additive manufacturing components

Co-funded by
the European Union

XCT for surface texture measurement

- Benchmark by focus variation - IUK: 3-in-1 X-ray CT inspection (partners: Nikon Metrology, Synopsys, HiETA, MTC, UoH)

Select ROI

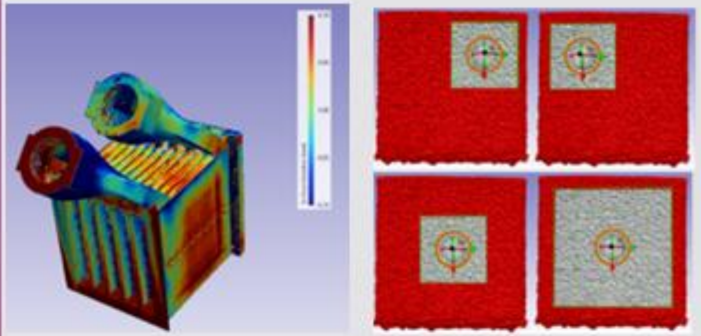

Two-stage surface registration: coarse alignment + fine alignment

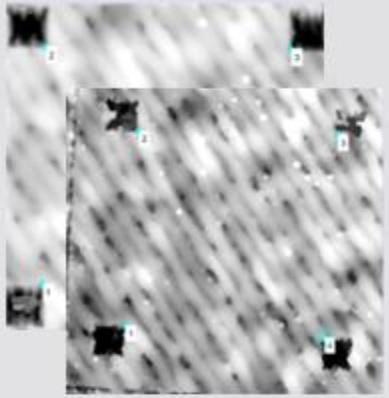

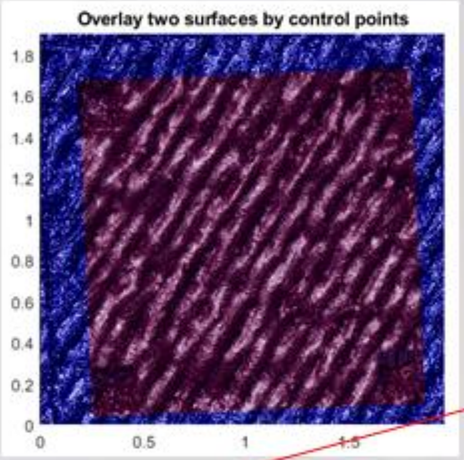

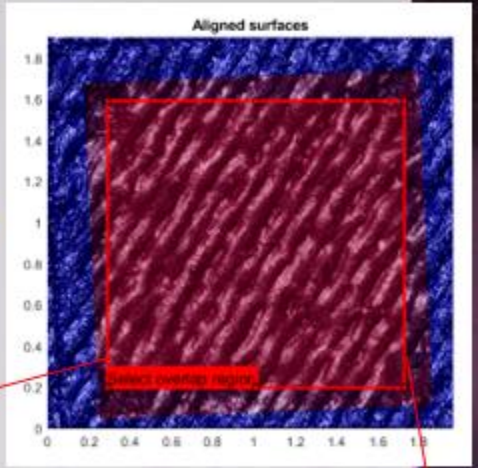

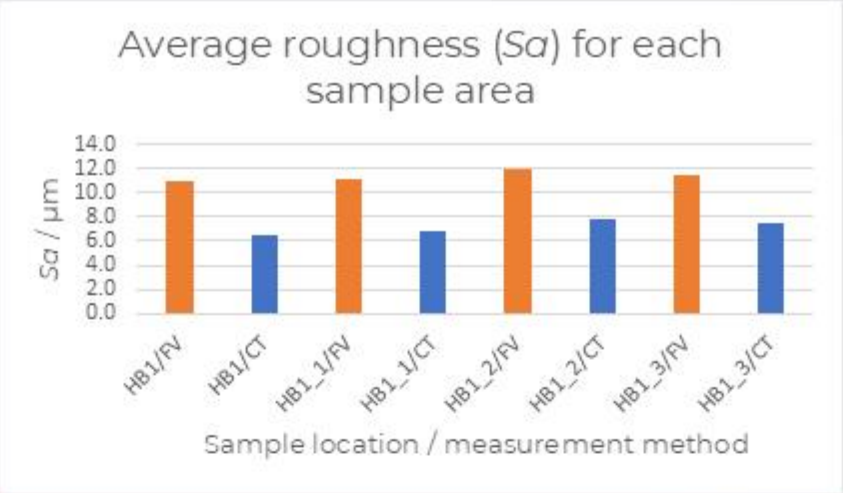

Surface texture parameters (L-filter cut-off: 0.25 mm)

Sa	8.2 µm
Sq	10.2 µm
Ssk	-0.273
Sku	3.047

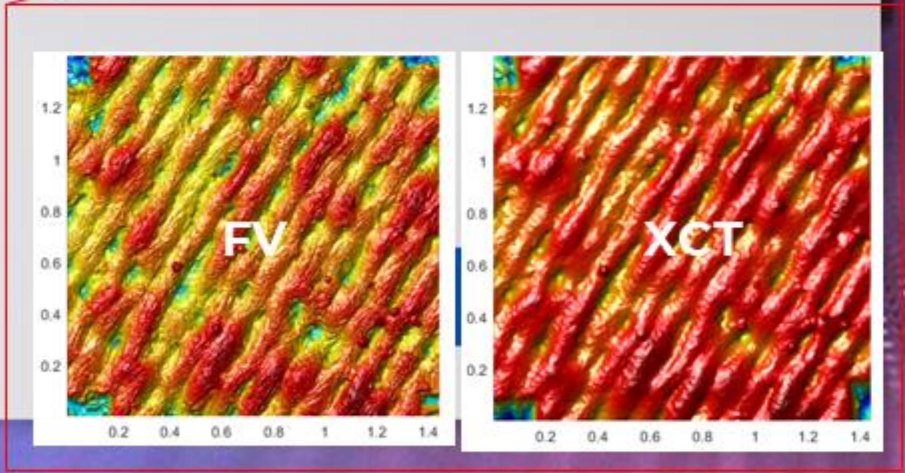

XCT for surface texture measurement

- Spatial resolution & blurring

Spatial resolution
- 1. Voxel resolution — Detector pixel size; Magnification factor
- 2. Point spread function (PSF) — X-ray focus size and drift; Detecting system PSF; Mechanical alignment; Sample movement
- 3. Contrast, signal-to-noise ratio, artifacts

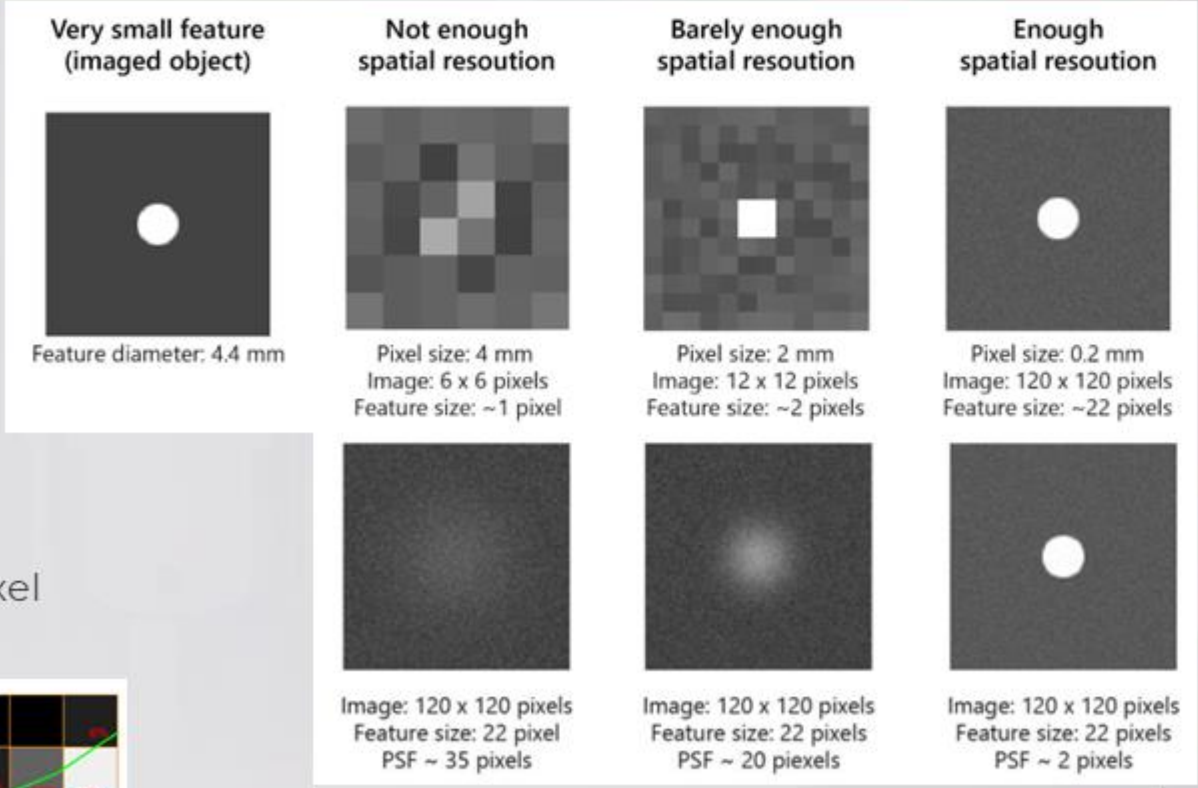

- Focal spot blur - penumbra effect

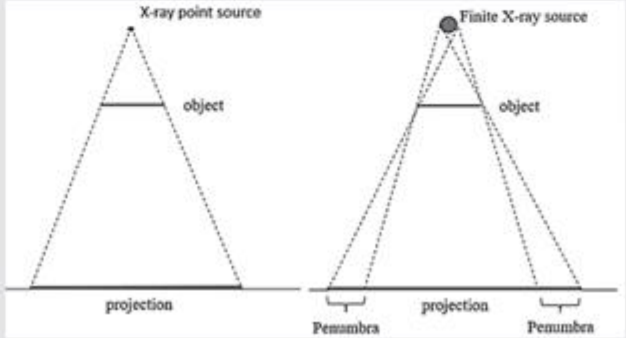

- Finite size of detector pixel - partial volume effect

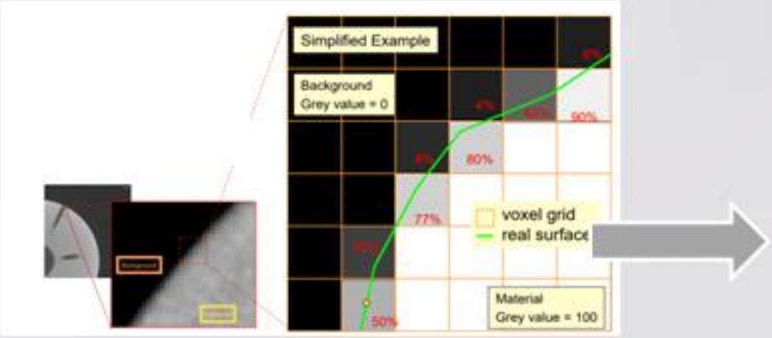

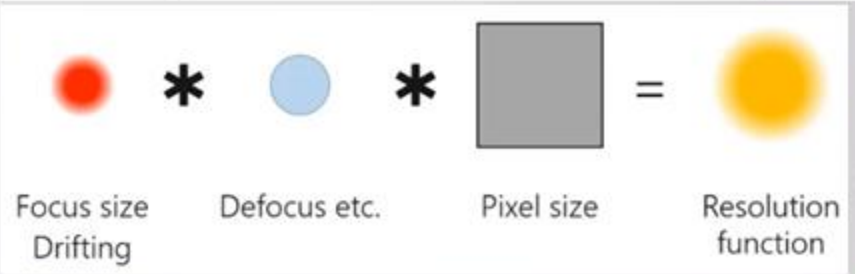

XCT for surface texture measurement

Lateral Resolution	
AM surface requirement	Below 10 µm
Optical instruments	Around 1 µm
XCT for metal AM sample	High X-ray power (>20 watt), Focal spot size ∝ power Voxel size >10 µm

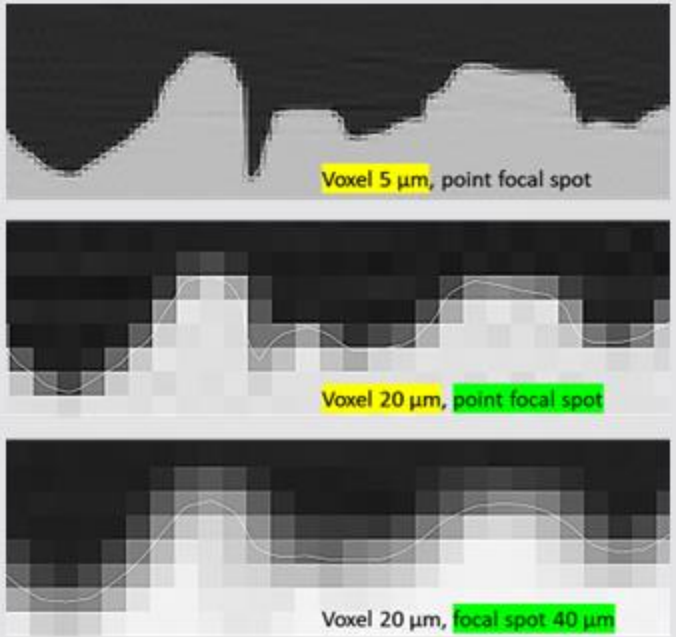

- Blurring assessment: System Modulation Transfer Function (MTF_{system}) – Smoothing effect over spatial wavelength

$$MTF_{sys} = \frac{A_{measured}}{A_{ture/reference}} = \frac{|\mathcal{F}\{\text{measured surface}\}|}{|\mathcal{F}\{\text{ture/reference surface}\}|}$$

$$MTF_{sys} = \exp\left(-\ln(2) \cdot \left(\frac{\sqrt{(u^2+v^2)}}{k_c}\right)^n\right)$$

u, v: surface wavelengths

n: fitted order 1~2 µm

k_c: fitted frequency to the 0.5

$\lambda_c = 1/k_c$

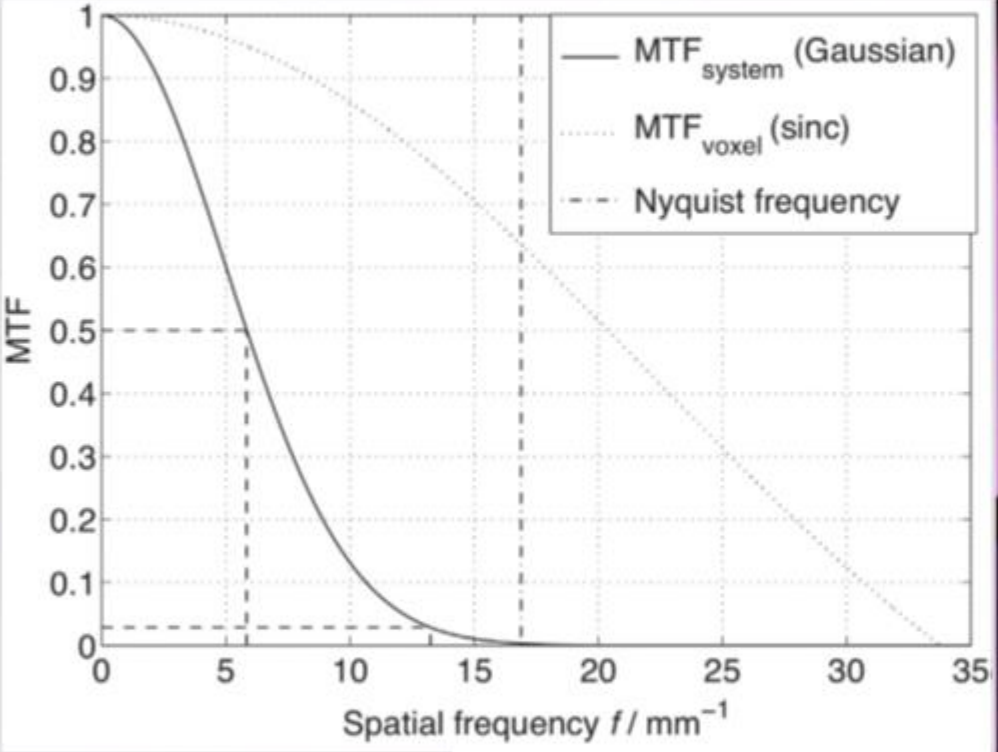

Ref: Hiller, J. and Hornberger, P., 2016

the European Union

XCT for surface texture measurement

- XCT limitation: structural resolution

Focal spot size

Focal spot size: 15 - 80 µm
Voxel size: 20 µm (fixed)

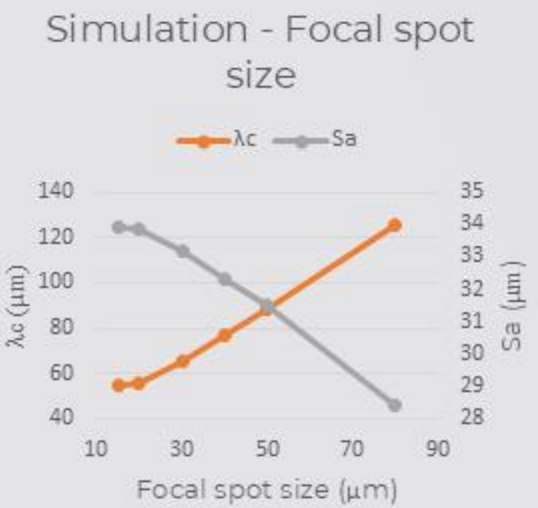

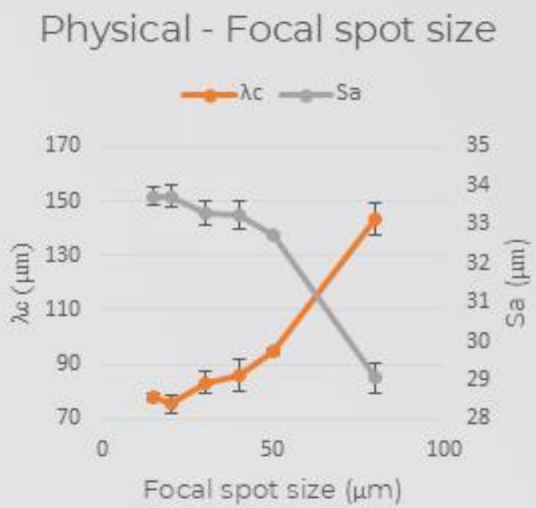

- A positive relationship between focal spot size & λ_c
- Simulation: linear relationship
- Physical: non-linear relationship

Voxel size

Focal spot size: point
Voxel size: 5 - 20 µm

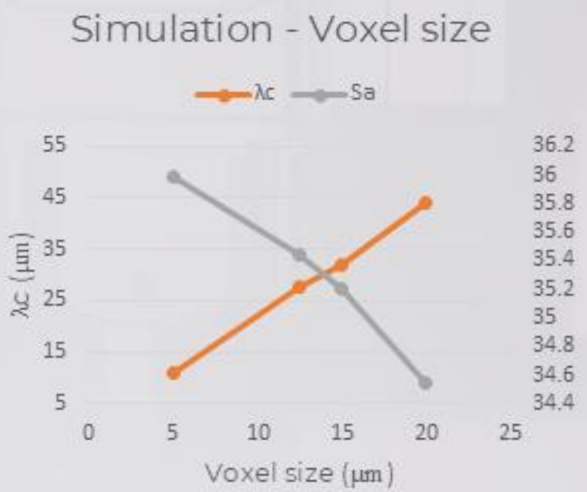

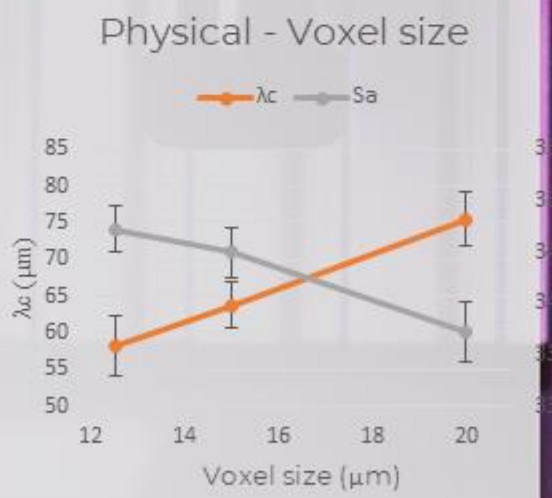

- A positive relationship between voxel size & λ_c
- Simulation: linear relationship
- Physical: linear relationship

XCT for surface texture measurement - Resolution enhancement

- Focal spot reconstruction using a star pattern artefact

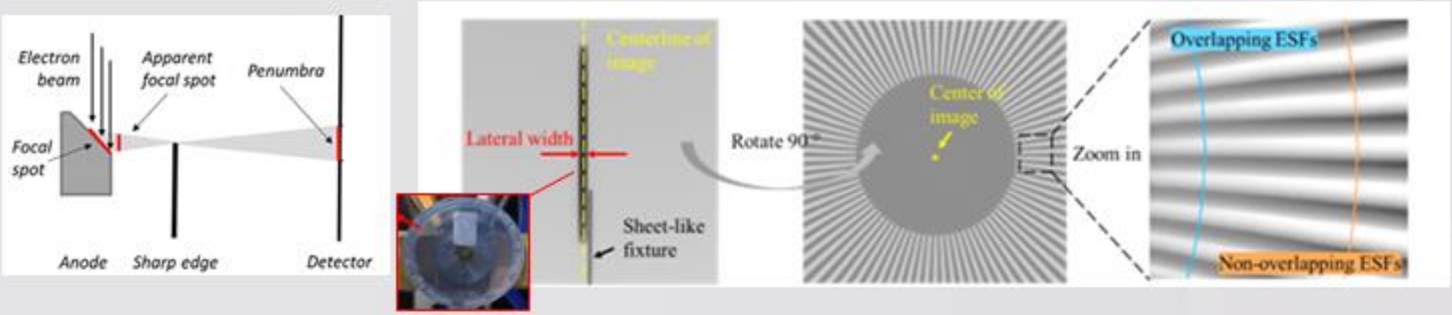

Ref. Probst et al. CIRP 2020

Reconstruction of effective focal spot

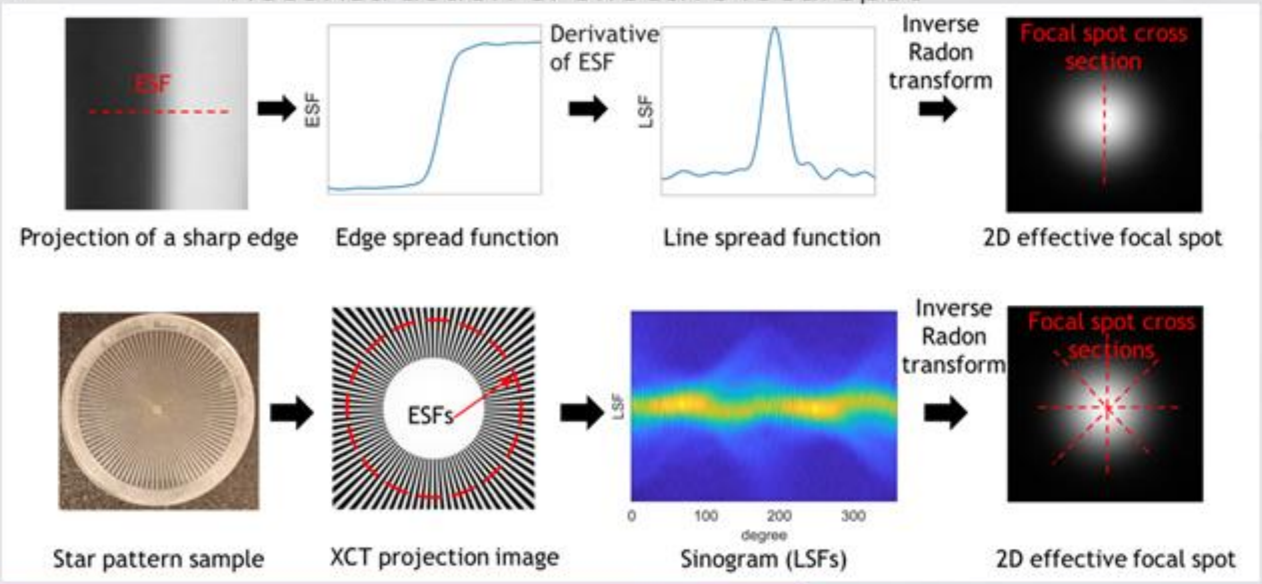

- Focal spot deblurring using deconvolution

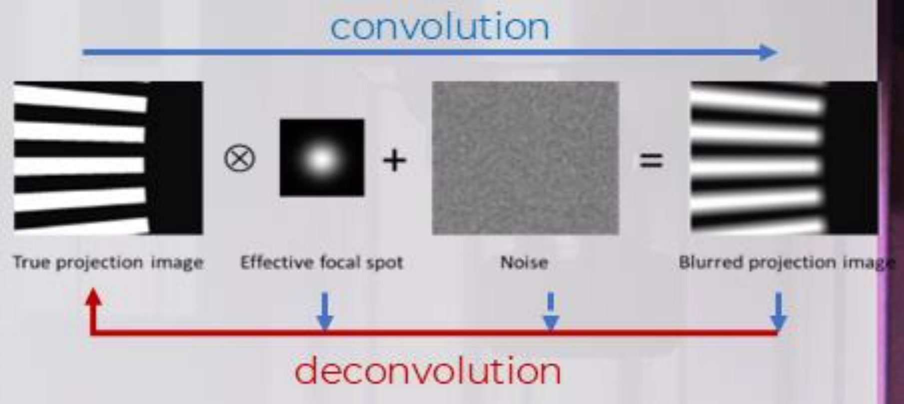

Spatial domain: $g = f * h + n$

Frequency domain: $G = F \cdot H + N$

Solution: $Y = \frac{1}{H}, \quad \hat{F} = Y \cdot G = F + \frac{N}{H}$

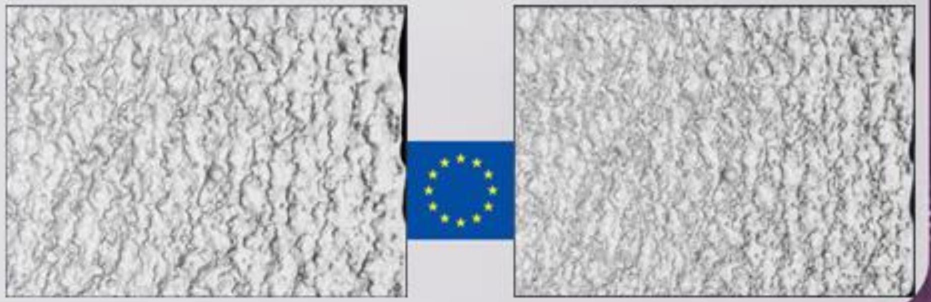

Characterisation of high speed sintering surface topography with re-entrant open surface pores

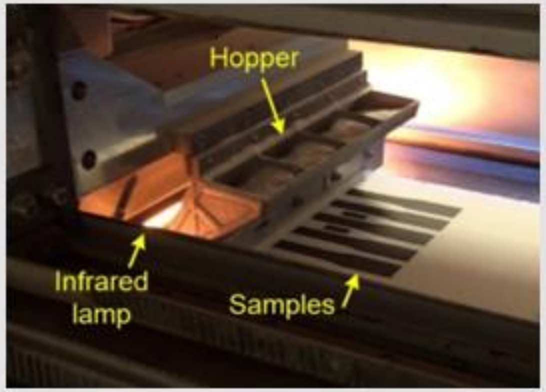

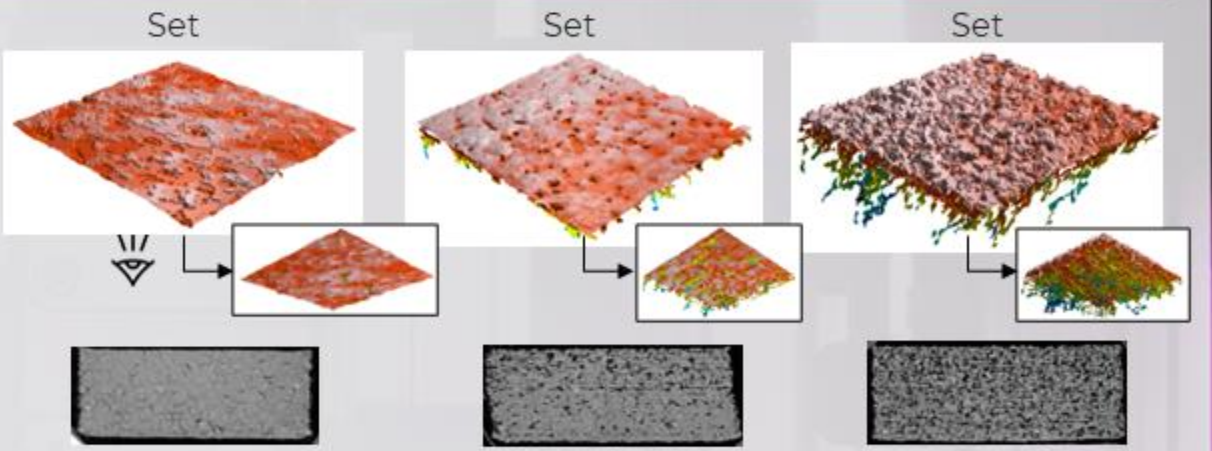

3D height parameters

Set No.	Set 1	Set 2	Set 3
Areal Sa (µm)	10.5	16.0	18.6
3D Sa (µm)	10.4	65.0	114.6
Porosity (%)	6.9	15.3	34.5

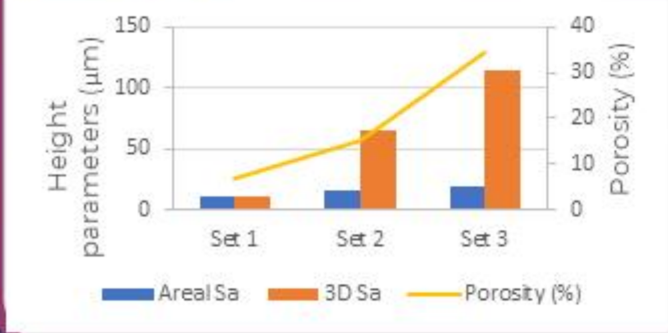

3D spatial parameters

Set No.	Set 1	Set 2	Set 3
Sdq	2.4	4.5	4.9
Sdr (%)	8.9	61.3	130.9
Srf (%)	0.5	12.9	57.4

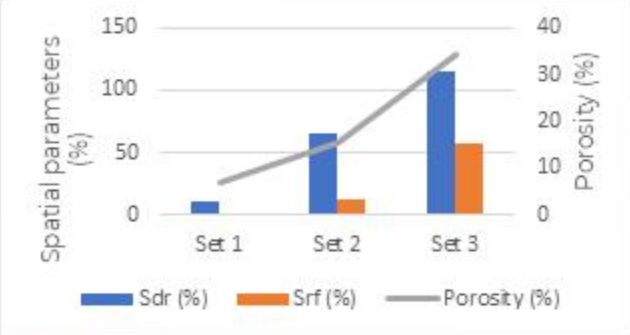

3D volume parameters – re-entrant open surface pores

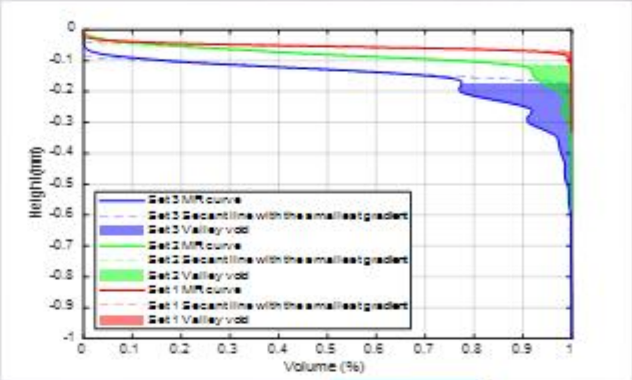

Set No.	Set 1	Set 2	Set 3
*Mr*2 (%)	90.1%	90.2%	77.4%
Vvv (mm³/mm)	2.2x10⁻⁷	3.8 x10⁻⁶	7.5x10⁻⁵

Surface measurement and characterisation of acetabular cup

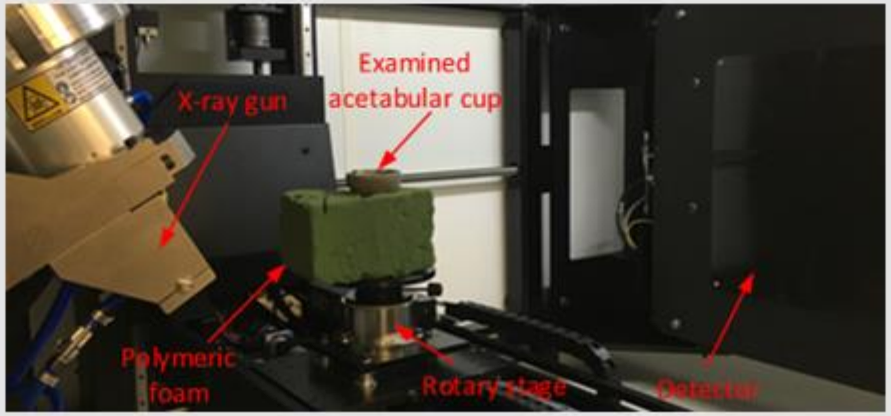

3D hight parameters

Patch No.	1	2	3	4	Mean	STD
Sa (µm)	5.94	5.71	5.61	5.73	5.75	0.14
Sq (µm)	10.77	10.33	9.94	11.62	10.67	0.72
Ssk	4.29	4.22	3.84	6.99	4.84	1.45
Sku	32.26	31.89	24.92	94.83	45.98	32.74

3D feature parameters

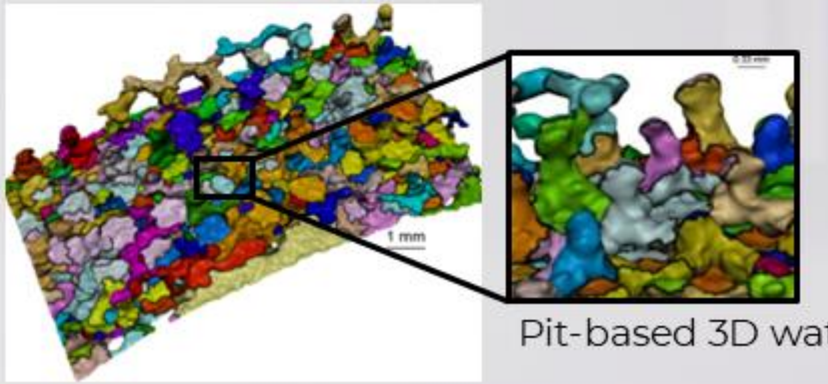

$$Spd = \frac{\#\ peaks}{A}$$

$$Svd = \frac{\#\ valleys}{A}$$

Pit-based 3D watershed segmentation

Patch No.	1	2	3	4	Mean	STD
Spd ($1/mm^2$)	0.22	0.24	0.23	0.23	0.23	0.01
Svd ($1/mm^2$)	0.97	1.18	1.08	1.10	1.08	0.09

FLASH

Flexible Laser-Based Manufacturing

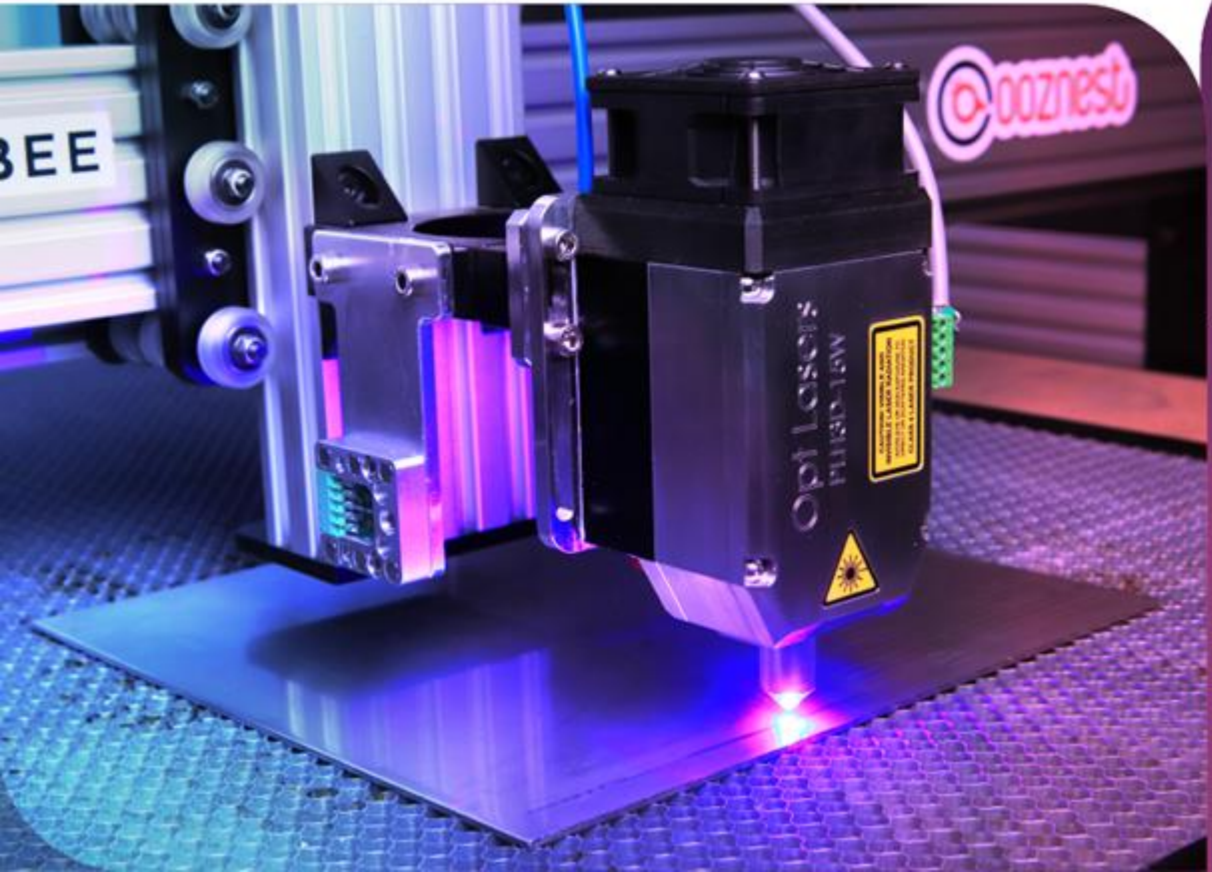

Thanks & Question

Contact me: Dr Shan Lou, s.lou@hud.ac.uk

Acknowledgement: Thanks to colleagues at CPT for providing some of the research slides.

Co-funded by the European Union

Funded by the European Union. Views and opinions expressed are however those of the author(s) only and do not necessarily reflect those of the European Union or the European Health and Digital Executive Agency. Neither the European Union nor the granting authority can be held responsible for them. **HORIZON-CL4-2023-TWIN-TRANSITION-01-02.**